NASA CONTRACTOR REPORT


NASA CR-2472

NASA CR-2472

# CASCADE TESTS OF SERRATED LEADING EDGE BLADING AT HIGH SUBSONIC SPEEDS

*by E. G. Smith and H. D. Sowers*

*Prepared by*
GENERAL ELECTRIC COMPANY
Cincinnati, Ohio 45215
*for Ames Research Center*


NATIONAL AERONAUTICS AND SPACE ADMINISTRATION • WASHINGTON, D. C. • DECEMBER 1974

| 1. Report No. | 2. Government Accession No. | 3. Recipient's Catalog No. |
|---|---|---|
| NASA CR-2472 | | |

| 4. Title and Subtitle | 5. Report Date |
|---|---|
| CASCADE TESTS OF SERRATED LEADING EDGE BLADING AT HIGH SUBSONIC SPEEDS | December 1974 |
| | 6. Performing Organization Code |
| 7. Author(s) | 8. Performing Organization Report No. |
| E. G. Smith and H. D. Sowers | |
| | 10. Work Unit No. |
| 9. Performing Organization Name and Address | 11. Contract or Grant No. |
| General Electric Company<br>Cincinnati, Ohio 45215 | NAS 2-5462 |
| | 13. Type of Report and Period Covered |
| 12. Sponsoring Agency Name and Address | Contractor Report |
| National Aeronautics and Space Administration<br>Washington, D.C. 20546 | 14. Sponsoring Agency Code |

15. Supplementary Notes

16. Abstract

Cascade tests of two-dimensional fan rotor blade rows were performed to investigate the effects of leading edge serration on acoustic and aerodynamic performance. The test configurations covered a range of serration tooth geometries. Tests were performed to investigate effects of inlet air angle and velocity on performance. Aerodynamic performance was determined by flow surveys at the mid-span of the blade exit. Acoustic performance was determined by wake turbulence surveys and sound measurements in the semi-reverberent exhaust chamber.

Measured acoustic and aerodynamic performance was comparable and indicated that a serration length of about six percent blade chord yields minimum noise generation and minimum total pressure losses.

| 17. Key Words (Suggested by Author(s)) | 18. Distribution Statement |
|---|---|
| Serrated Leading Edges, Noise Reduction, Turbotip Lift Fans, Exit Turbulence, Rotor Blade Cascade | Unclassified - Unlimited<br>CAT. 01 |

| 19. Security Classif. (of this report) | 20. Security Classif. (of this page) | 21. No. of Pages | 22. Price* |
|---|---|---|---|
| Unclassified | Unclassified | 92 | $4.75 |

*For sale by the National Technical Information Service, Springfield, Virginia 22151

TABLE OF CONTENTS

## TABLES

ILLUSTRATIONS

ILLUSTRATIONS

ILLUSTRATIONS

# CASCADE TESTS OF SERRATED LEADING EDGE BLADING AT HIGH SUBSONIC SPEEDS

By E. G. Smith and H. D. Sowers

## SUMMARY

A two-dimensional cascade test program was performed to investigate the effects of serrations on the acoustic and aerodynamic performance of blade contours representative of those employed in the LF336/E statorless lift fan. The test airfoils had a two inch (5.08 cm) chord and blade shapes equivalent to the meanline plane of the actual rotor blading. Two unserrated and six serrated blade configurations were tested. The serration geometry covered a range of serration lengths between four and eight percent of the airfoil chord. Serration tooth spacing ranged between 1.3 and 2.0 times the serration length. The test program included a range of blade inlet Mach numbers and inlet air angles which encompassed the blade design flow conditions of 0.85 Mach number and 57 degrees inlet air angle. During the test program, aerodynamic performance was obtained through measurements of the cascade exit flowfield. Acoustic performance was obtained by measurement of the exhaust turbulence levels and through measurement of the overall sound levels in the semi-reverberant exhaust section of the test facility.

Analysis and evaluation of the aerodynamic and acoustic measurements indicated that improvements in aerodynamic performance and reductions of noise generation can be obtained by serrating the airfoil leading edges. The most substantial improvements in performance and noise generation of the serrated configuration were observed in those areas where the inherent performance of the unserrated blading was poor. Serrating the blade leading edges appeared to broaden the operating range of the airfoils over which low losses and low noise generation will occur.

Comparison of the performance and acoustic data for the various

serration geometries, indicated that the most desirable serration geometry should have serration lengths of about six percent blade chord with spacings of about twice the serration length.

## INTRODUCTION

The use of V/STOL aircraft for commercial, low noise applications has received considerable attention in recent years. The propulsion systems for this type of low noise commercial vehicle will be required to meet stringent noise certification requirements. These requirements will, in turn, impose severe penalties in total system weight, cost and performance through the application of acoustic treatment. Because of this, methods of noise reduction which can be applied with minimum penalties must be continually sought and investigated for possible application in advanced low noise propulsion systems.

One concept suggested to reduce the noise generated by turbomachinery is serration of the blade leading edges (References 1, 2 and 3). This program studies the aerodynamic and acoustic performance of fan rotor blade airfoil sections with serrated leading edges in a cascade windtunnel. The program is part of an overall development plan to design, test and evaluate the performance and noise characteristics of a statorless (rotor only) turbotip lift fan with a 36 inch (91.44 cm) tip diameter. The overall program plan includes modification, through serration of the leading edge, of the full-scale rotor blading. Acoustic tests will be performed for verification of the results observed during the static cascade tests.

The statorless derivative of the LF336 fan family is identified as the LF336/E fan. Tests of the LF336/E fan represent a continuation of an extensive acoustic program based on the LF336 derivatives (References 4 and 5).

## EXPERIMENTAL FACILITIES AND TEST TECHNIQUES

### Cascade Test Facility

The cascade tests were performed in the Transonic Cascade Tunnel (TCT) facility of the General Electric Company. This facility has been developed for testing a wide variety of fan, compressor, turbine and strut cascades. The tunnel working section is a 4 by 12 inch (10.2 by 30.5 cm) rectangular area with inlet speed capability covering both the subsonic and transonic Mach number regions. Sidewall bleed can be employed for boundary layer removal to provide simulation of two dimensional flow into the cascade test section.

The general arrangement of the test facility is shown in Figure 1. A block diagram of the facility air supply is shown in Figure 2. The system employs a closed loop air supply driven by a test facility compressor system. Exhaust air from the test tank is compressed and returned to the test tank inlet. Recuperative air is drawn from the atmosphere and passes through a dryer prior to entering the inlet plenum chamber. The inlet chamber is a five foot (1.524 meter) diameter section with turbulence reducing screens and terminates in a rectangular nozzle which transitions to the test section. The test cascade is supported by two semi-circular rotating drums which provide variation of the cascade inlet air angle. The sides of these drums plus the tunnel upper and lower wall provide a constant test section height of 12 inches (30.48 cm).

Boundary layer bleed control is provided on the sidewalls of both the test section and the rotating drum. Bleed air is drawn through the porous walls into a separate suction manifold and plenum system. The bleed flow levels can be remotely controlled during the conduct of the test.

The complete test section is enclosed in a 10 foot (3.048 m) diameter pressure vessel tank. The pressure level in this tank establishes the

cascade exhaust conditions and is controlled by a hydraulically-operated valve in the ducting between the test tank and the inlet to the compressor air supply.

A photograph of the test facility looking into the exhaust enclosure is shown in Figure 3. Significant facility components are identified.

## Test Cascades and Serrations

The purpose of this test program was to develop a leading edge serration for the LF336/E statorless fan. Reference 6 is a summary of the mechanical and aerodynamic design of this fan system. For these tests, the airfoil section was selected based on the fan design and the airfoil geometry at the 50 percent flow streamline. Multiple circular arc airfoil meanline distributions were used in the blading development and produced the blade profile as shown in Figure 4. The airfoil chord selected for the cascades was 2.0 inches (5.08 cm) and thus the blade aspect ratio was set at 2.0 based on the four inch (10.16 cm) wide test section. The airfoil design includes a leading edge extension for addition of the serrations without disturbing the basic as-designed airfoil contour. In the full-scale configuration, the two inch (5.08 cm) chord of the cascade airfoil is equivalent to a 3.25 inch (8.255 cm) chord. In reference to a design airfoil chord of 3.0 inches (7.62 cm), the additional 0.25 inches (0.635 cm) was added through a simple extension of the basic as-designed airfoil. The procedure for development of this addition was to linearily extend the leading edge at the original leading edge meanline angle. The leading edge nose extension was developed using a 4-to-1 elliptical shape with a 0.75 percent chord maximum thickness. The remainder of the airfoil was developed by constructing surfaces tangent to the leading edge ellipse and the surfaces of the basic airfoil design. Figure 5 presents a sketch showing the design procedure employed in development of this leading edge extension.

The length of the serration extension was selected as the maximum

probable serration height based on experience from similar tests of other airfoils described in Reference 4. Using this design approach of adding airfoil chord length for serrations versus cutting serrations into the basic airfoil, relieves the problem of thick airfoil leading edges at the root of the serrations. For this add-on approach, the serrated root airfoil would be equivalent to the chord of the as-designed airfoil, thus the leading edge thickness is only slightly greater than the 0.75 percent design. The basic airfoil chord to the leading edge of the serrations is then variable depending on the height of the serration teeth. This variance in total chord is evident in the description of the test configuration as described later.

A summary of the airfoil geometry selected for the cascade test program is given in Table I. In addition, the airfoil coordinates for the as-designed airfoil are given in Table II.

The test serration configurations were selected to cover a range of serration heights and spacings. Table III gives the significant dimensions of the six serration configurations which were tested. Two unserrated cascades were also tested to establish baseline conditions and performance. One unserrated configuration was a blade contour equivalent to the as-designed airfoil and had a blade chord of 1.848 inches (4.694 cm). The second unserrated configuration had a chord of 1.962 inches (4.983 cm) and thus was representative of airfoils modified by the leading edge extension but prior to serrating the leading edges.

Each cascade configuration consisted of 15 blades installed in parallel plexiglass walls. The airfoil leading edge was located one chord downstream of the leading edge of the cascade walls.

## Instrumentation and Data Systems

The Transonic Cascade Tunnel incorporates conventional flow measurements

required for most cascade tests. These measurements include the following:

- Total pressure and total temperature in the inlet plenum section.
- Wall static pressures in a plane 1/4 inch (0.635 cm) upstream of the cascade sidewalls.
- Remotely controlled actuators for traversing the inlet flow conditions 2-3/4 inches (6.985 cm) upstream of the cascade inlet plane.
- Remotely controlled actuators for traversing the cascade exit flow. The traverse incorporated a cascade centerline traverse using a hot wire probe and a three element flow directional probe. The two probes were spaced two vane spacings apart to minimize probe interaction while traversing near the middle of the test section. A detailed description of the hot wire and directional probes will be presented later.

The test facility includes a digital recording system which converts all pressure and temperature readings into a digital format and records the data on punched paper tape. A computer program is then used to reconvert all data to engineering units using appropriate calibrations of the instrumentation systems.

Cascade Exit Flow Traverse Probe - The exit flow conditions of the cascade were surveyed using a three parameter directional probe. Photographs of this probe are shown in Figure 6. The probe axis was located on the centerline of the cascade exit and traversed in a plane parallel to the vane trailing edges. The probe traverse covered the wakes of about three blades near the center of the cascade, thus the flow variations near the end walls were avoided as much as possible. The axial location of the traverse probe was a test variable, with most of the surveys taken at a station about one chord downstream of the vane trailing edges.

The directional probe was calibrated prior to operation in this test program. The calibration was performed in the cascade test facility, with the probe installed near the center of the test section. Probe calibration data were obtained for a range of Mach numbers and flow incidence angles. The calibration data were converted into a coefficient format and used to show that the probe calibrations were insensitive to a reasonable range of Mach numbers. The coefficients used to present the calibration data are defined in Figure 7.

During the cascade tests, the probe axis was oriented at a 20 degree angle relative to the plane of the vane trailing edges. The test data obtained during the vane exit traverses were then processed to obtain flow parameters as described in the following discussion:

During the traverse of the cascade exit flow, the measured parameters were the three individual pressures of the directional probe. At selected locations spanning one blade row, the probe pressures and associated fixed instrumentation readings were recorded. For each probe position, the probe pressures were converted into local total pressure, static pressure and flow angle using the appropriate coefficients and calibration curves.

The complete exhaust flow survey of total pressure, static pressure and flow angle was then used to obtain average performance. The measured data were integrated across one blade span to obtain mass-flow weighted values of total pressure, static pressure and exit flow angle. These integrated flow measurements were then used to obtain the appropriate cascade performance parameters such as total pressure loss coefficient, static pressure rise coefficient and exit deviation angle.

Cascade Exit Hot Film Traverse Probe - Cascade exit flow conditions were also surveyed using a hot film probe. The hot film sensors are an improved version of the hot wire in that they are more rigidly constructed. The hot film sensor consists of a thin film of metal deposited onto a ceramic

substrate held by needle shaped supports. These supports are in turn attached to the stem of the probe. Photographs of the sensor X-array and the probe assembly are shown in Figure 8.

In operation, each sensor is part of a Wheatstone bridge. The sensors are kept at constant temperature by the anemometers, shown in the block diagram of Figure 9. They instantaneously measure fluid flow parameters by sensing the heat transfer rate between the electrically heated sensor and the flow. When the flow velocity changes, compensation is provided to maintain a temperature difference. Since the resistances in the Wheatstone bridge are kept constant, through a feedback control in the circuitry, the voltage across the bridge is directly proportional to the current, I, through the sensor and the power, P, is equal to the product of the square of the current and the resistance, R. Therefore, the square of the voltage, measured on top of the bridge is directly proportional to the instantaneous heat transfer between the sensor and its environment. This heat transfer is proportional to the fluid velocity. The output of the sensor amplified by the bridge is not linear for flow changes, therefore, a linearizer is incorporated in the system for convenience.

Sound Measurements - Sound measurements were made within the cascade plenum on the downstream side of the cascade. Location of the microphone is shown on Figure 3. The tank walls are metal, thus the microphone is essentially located in a semi-reverberant room. Noise data obtained were used on a comparative basis only, with no attempt to evaluate the absolute levels. A Bruel and Kjaer (B&K) microphone system with attendant cathode followers and power supply was used in conjunction with a Lockheed 411B, four-channel, AM tape recorder. A bypass filter was used ahead of the recorder to eliminate low frequency facility noise, less than 2000 Hertz.

The total system was level calibrated prior to each test series using a B&K pistonphone and was initially checked for frequency response out to 20 KHz. System response was flat beyond 10 KHz.

## *EXPERIMENTAL RESULTS*

The cascade test program was conducted to observe the effects of leading edge serrations on the aerodynamic and acoustic performance of a cascade representative of the LF336/E statorless fan blading. The aerodynamic performance was obtained by exit flow surveys using a three-element directional pressure probe. Acoustic performance was obtained by hot film probe surveys in the exit flowfields and through sound measurements in the exhaust plenum chamber.

The total program included testing over a range of inlet flow conditions, velocity and air angle, for a total of six serrated and two unserrated cascade configurations.

The range of flow Mach numbers was from about 0.75 to 0.97 and the range of inlet air angles was varied between 51 and 60 degrees. The aerodynamic design inlet flow condition for the blade section at the 50 percent flow streamline is summarized in Table IV. Other significant performance parameters are listed, such as blade loading and exit deviation angles. The estimated inlet flow condition at the aerodynamic design speed is an inlet Mach number of 0.97 at an airflow angle of 57 degrees. This flow condition corresponds to operation at the design speed or thrust levels. A second operating condition which is of interest for fan systems employed in V/STOL aircraft is the "Noise Rating" or "Nominal Rated" operating point. This operating point is defined as 80 percent of design thrust and is a typical thrust level required for hovering the aircraft system at its design gross weight. The noise generation characteristics of lift fan systems are usually evaluated at this partial thrust level. The remaining 20 percent thrust increment is then available to provide control forces for maneuvering of the aircraft.

The inlet airflow condition at the "Noise Rating" point was estimated using off-design cycle calculations and is an inlet Mach number of 0.85 at

the design air angle of 57 degrees. Since this operating condition is of prime interest for noise generation where the noise estimates are performed, the major portion of the test program was directed towards an investigation of performance at these flow conditions. Only selected configurations were employed in extended tests covering a wider range of flow velocities and inlet air angles.

## Test Summary

The complete test program is summarized in Table V. The table presents a listing of each blade configuration and the test values of inlet air velocity and air angle. The initial phase of the test program was performed without utilization of sidewall bleed system. Analysis of these data showed abnormal performance of the blade rows because of boundary layer interaction in the vicinity of the blade juncture with the cascade sidewalls. The most significant performance parameter indicative of this boundary layer interaction is the measured static pressure rise coefficients. Without boundary layer bleed, Test Runs 3 and 5, the pressure rise coefficients were between 0.09 and 0.15 for the range of inlet flow conditions. This compares to a pressure coefficient of 0.33 at the blade design conditions. This low measured value of pressure rise is indicative of a large area contraction through the blade row which is traceable to the blockage developed by the boundary layer interaction. Observation of the flowfield using a Schlieren system also indicated the same effect. The flowfield representation showed that a strong normal shock existed within the blade row near the blade trailing edge. This type of shock pattern indicates a minimum area or throat forward of this point. Based on the blading geometry, the only way a throat could occur at this location is for a large flow blockage due to the interaction of the boundary layer and the juncture of the cascade vanes and the sidewalls. The data, without boundary layer bleed, are being presented for informative purposes only and will not be used during the analysis of the effects of serrations on blading performance.

All remaining tests were performed using the sidewall boundary layer bleed system. The bleed system was used to minimize the boundary layer thickness at the leading edge of the cascade row. The boundary layer growth was measured by a total pressure survey about 2-3/4 inches (6.985 cm) upstream of the cascade inlet. The inlet flow conditions were measured without bleed and showed a boundary layer thickness of about 0.5 inches (1.27 cm). A typical velocity profile as measured during the tests without bleed is shown in Figure 10. For the case with sidewall bleed, the traverse probe was positioned at 0.08 inches (0.203 cm) from the tunnel wall and the bleed flow was adjusted until the probe total pressure was equal to the total pressure of the tunnel core flow. Thus, with bleed, the boundary layer thickness was controlled to about 0.08 inches (0.203 cm) maximum thickness.

This procedure for sidewall bleed was employed throughout the remainder of the test program and appeared to yield cascade pressure rise coefficients consistent with the design values.

## Aerodynamic Performance

The prime measurements for determination of the cascade aerodynamic performance were obtained from the three-element directional probe located in the cascade mid-span exit flowfield. Detailed probe data were taken across at least one blade spacing near the center of the test section. The measured data were converted into total pressure, static pressure and flow angles. Table VI is a listing of the significant averaged performance parameters as measured for each test configuration.

The blade exit profiles of total pressure, static pressure and flow angle are presented in Figure 11 for each blade configuration at the design air angle of 57 degrees and at an inlet Mach number of about 0.87. This inlet velocity level is indicative of operation at the fan "Noise Rating" point. Each profile covers one blade passage with the blade wake located at the zero blade location. The sections of the profiles identified as the

positive direction are located adjacent to the blade serration surface.

In each of the profiles, particularly for the unserrated or baseline configurations, a region of high pressure loss is located adjacent to the blade suction surface. This loss can be attributed to shock losses due to acceleration of the flow over the blade leading edge. These shock patterns were also observed through the Schlieren system. It is interesting to note that the serrated configurations exhibited a lower loss in this area of the flow. For example, comparing BL1 and SR6, the losses within blade space between wakes has vanished completely. This is one of the interesting effects due to serrations which will be discussed later.

Two configurations, BL2 and SR6, were tested to investigate the effects of inlet flow angle both with and without serrated leading edges. Pressure and exit angle profiles from tests of the unserrated configuration are shown in Figure 12. For these tests, the nominal inlet Mach number was 0.85. Comparable profiles for the serrated configuration are shown in Figure 13. The effects of angle of attack variations, associated with this range of inlet air angles, will be discussed and compared in detail in the discussion section of this report.

During the test program, numerous configurations were tested to determine the sensitivity of performance to variations of inlet velocity or Mach number. The range of inlet Mach numbers approached unity, which was comparable to design speed operation of the airfoil section. Test data for the two baseline configurations and serrated configuration, SR6, are presented in Figures 14 through 16. For these tests, the blade inlet flow angle was held constant at 57 degrees.

Flow surveys were taken at three different downstream locations during tests of Configuration SR6. The measured profiles taken and 1/2, 1 and 2 chords downstream of the blade trailing edges are presented in Figure 17.

## Cascade Exit Turbulence Levels

Cascade exit turbulence levels were obtained during a traverse of the mid-span cascade exit flowfield. This survey was taken during the aerodynamic surveys and covered at least one blade row located in line with and two blade spacings below the aerodynamic survey. Least mean squared levels of the axial and normal turbulence levels were recorded coincident with the aerodynamic measurements. Probe data were not recorded at cascade inlet Mach numbers above 0.9 because of the low hot film life at this high velocity.

Table VII presents a summary of the exhaust turbulence measurements for all tests performed with tunnel sidewall bleed. The peak and area average turbulence levels, normal and axial, are tabulated. The variations of turbulence level within the blade exhaust are presented in Figures 18 through 24. Figure 18 presents the turbulence profiles for the six configurations at inlet flow conditions of 0.85 Mach number and 57 degrees flow angle. Each profile covers a blade spacing with the appropriate blade wake, as indicated by the aerodynamic data, located at the zero percent chord location. Figures 19 and 20 show the effects of angle of attack on the measured turbulence profiles for the baseline configuration, BL2, and one serration configuration, SR6. Effects of inlet velocity on turbulence for the two baseline configurations and the serrated configuration are presented in Figures 21 through 23. Figure 24 compares turbulence measurements at three locations downstream of the cascade exit plane.

These turbulence data will provide the basis for evaluating the effects of serrations in a later section of the report.

## Turbulence Frequency Spectrums

At selected positions in the blade exit, one position within the blade wake and the second in the mid-passage between blade wakes, the output of the hot film probe was recorded on magnetic tape. This data tape was then used

for further spectrum evaluation of the turbulence levels. Typical turbulence spectrums are shown in Figures 25 through 28.

Figure 25 shows the wake turbulence spectra of typical unserrated and serrated configurations. The spectra are of a general broadband nature and are free of any puretones or resonances characteristic of wake shedding. Comparison of the turbulence levels of the two configurations is representative of the influence of serrations, particularly with respect to the axial turbulence intensity.

Figures 26 and 27 show the effects of cascade inlet air angle on the turbulence spectra for a serrated and an unserrated configuration. Increases of turbulence levels, throughout the spectrum, are apparent for larger excursions of the inlet flow angle.

A comparison of the wake turbulence spectra at three locations downstream of the blading trailing edges is given in Figure 28. Comparable freestream measurements are shown in Figure 29. This comparison shows a general decrease in turbulence level as the measurement location is moved downstream of the cascade exit. The effects are most apparent in the blade wake regions as expected, based on the overall level measurements.

## Sound Measurements

Acoustic data were recorded for each configuration for a minimum of 30 seconds. The recorded data were then either processed through a six percent bandwidth filter or by a narrowband analyzer to obtain frequency spectrum plots from 2000 to 10,000 Hertz.

Figures 30 and 31 present typical sound spectra and compare serrated and unserrated configurations. Figure 30 represents measurements recorded during the initial phases of the test (Run 8), and Figure 31 is for the final tests (Run 14). All spectra are broadband in nature and are free of any

puretones or resonances which are characteristic of vortex wake shedding. These particular configurations were selected to show an apparent change of noise during the early and later phases of the test. The clean unserrated baseline configuration exhibited a lower noise level of about four decibels throughout the complete spectrum. This discrepancy in test data will be discussed later and its consequent influence when comparing different serration configurations will be described.

Since the general noise spectra, as obtained during the narrowband analyses, were broadband in nature, the acoustic data were evaluated at one particular frequency band. The frequency selected to be representative of the noise levels was 4000 Hertz. All data were evaluated at this frequency using a 20 Hertz bandwidth filter. The noise level within this band is tabulated in Table VIII. This overall level will provide the basis for the acoustic analysis and discussion which follows.

## DISCUSSION OF TEST RESULTS

### Blade Loading Parameters

The cascade test apparatus as used during these tests had parallel walls throughout the approach and cascade test sections. Early in the test program, the need for boundary layer bleed was established, based on the low static pressure rise across the cascade and the abnormal blade passage shock patterns. Inlet section sidewall bleed was employed to remove the boundary layer at the inlet to the cascade test section. For a particular set of inlet flow conditions, the blade loading levels were dependent on the performance of the particular airfoil test configuration, since the sidewalls within the cascade test section were neither variable nor bled. For a given set of inlet flow conditions, Mach number and air angle, the blade loading is established by the following performance parameters of the cascade:

- Average loss coefficient

- Average cascade exit flow angle
- Blockage due to the blade wake
- Blockage due to interaction of the blade with the cascade sidewalls within the blade row

As indicated in the performance summary given in Table VI, the blade loading, such as blade static pressure coefficient and diffusion factors, was not constant for all test configurations. This variation from configuration to configuration was one of the shortcomings of this particular test program. The most significant of the four parameters listed above which appeared to influence the blade loading was the sidewall interaction blockage. In order to show how each of the variables influence the blade static pressure rise coefficient, two nomographs were constructed as shown in Figures 32 and 33 for an inlet Mach number of 0.85 and flow angles of 57 and 60 degrees. The two blockage effects, wake and sidewall, cannot be separated in this discussion. Figure 32 is for the "Nominal Rated" flow conditions where the design point assumptions are shown. For a static pressure rise coefficient of 0.33, a loss coefficient of 0.045, and an exit air angle of 40.9 degrees, the blockage factor is 0.83 at design. Therefore, in order to achieve design conditions, the blockage of both the wake and interaction effects must total 17 percent.

Typical test measurements, as given in Table VI, were used to obtain the apparent blockage levels which occurred during the tests. Table IX lists the apparent blockage for each test configuration. From this data, it is apparent that the blockage levels for all serrated configurations were between 0.83 and 0.85, which is close to the convergence expected in the fan system. It is interesting that both of the unserrated configurations indicated a blockage factor of about six percent lower, and consequently the blade loading parameters are slightly higher than the design values. Apparently, this higher blockage for the serrated configurations is caused by

some change in blade sidewall interaction. It may be possible that the serrated blade, adjacent to the sidewall, produces a thicker boundary layer and thus a greater level of blockage due to the interactions.

## Blade Aerodynamic Performance with Serrations

The effects of serration geometry on blade aerodynamic performance will be evaluated based on test measurements taken at an inlet Mach number equivalent to the "Noise Operating Point". At these inlet air conditions, aerodynamic performance was obtained through measurement of the total pressure loss and exit deviation angles. The effects of the serration geometry on these two performance parameters are shown in Figure 34. The serration geometry is presented using the parameters of serration height, H, serration spacing, S, and blade chord, C.

These data show reductions in total pressure losses for all serration configurations. In addition, the minimum losses occur at serration heights of five to eight percent of the blade chord. The losses also appear to reduce as the serration spacing, S, approaches the height, H, of the serration. Lower blade deviation angles were measured for all serration geometries, with no apparent influence due to serration height-to-spacing ratio.

## *Effects of Serration on Blade Off-Design Aerodynamic Performance*

During the test program, blade off-design performance was obtained for a range of inlet Mach numbers and inlet air angles. Aerodynamic performance at these off-design conditions for both serrated and unserrated configurations is shown in Figures 35 and 36. The effect of the serrated leading edges is improved performance for both increased inlet Mach numbers and flow angles less than or greater than the design inlet flow angle of 57 degrees.

This trend of improved off-design performance is a significant test result. It appears that serrated leading edges exhibit the desired performance characteristics of a very sharp leading edge airfoil without the associated poor performance at off-design air angles. The desired sharp leading edge characteristic is indicated in Figure 35 as a very small increase in fan total pressure loss coefficient with increasing inlet Mach number. The good off-design performance is shown in Figure 36 as a broader tolerance for inlet air angle excursions without large increases in total pressure loss or exit air deviation angles.

A possible explanation of this trend in performance can be seen in Figure 37 which compares blade thickness distribution in the vicinity of the leading edges, both with and without serrations. A rounded leading edge is desirable for a reasonable tolerance to excursions of blade incidence angle. The LF336/E blading has a 0.75 percent radius leading edge thickness. This leading edge radius is a compromise between good high speed performance and incidence angle tolerance. In addition, the airfoils are designed to operate at a small positive incidence angle in order to provide choking margin with the design leading edge thickness. The ideal airfoil design would have a zero leading edge thickness for good transonic performance. Operation of this sharp leading edge airfoil would be very limited in the range of incidence angle changes. Leading edge serrations effectively produce this sharp leading edge on an average basis because of the triangular shaped geometry while still maintaining an aerodynamically-blunt leading edge by virtue of the triangular shape of the leading edge serration shape.

## Blade Wake Turbulence Levels with Serrations

In the previous discussion, the effects of serrations on aerodynamic performance were evaluated using two serration dimensional parameters, (H/C) and (H/S). A similar comparison of the measured exit turbulence levels is presented in Figures 38 and 39. The turbulence measurements show effects

of serrations which are similar to the aerodynamic performance. Turbulence levels, both axial and normal, decrease as the serration height (H) is increased. Serration heights of greater than six percent of the blade chord yield the lowest turbulence levels. Effects of serration spacing (H/S) are not as clearly identified as in the case of a similar comparison of the aerodynamic performance.

The effects of serrations on blade off-design performance are shown in Figures 40 and 41. Addition of serrations shows a reduction in turbulence levels both with increasing Mach number and at incidence angles above and below the design level. At low Mach numbers and at an inlet air angle equivalent to zero degrees incidence (54 degrees), the effects of serrations on blade turbulence levels appear to be negligable.

## Acoustic Performance

Two series of tests were used to evaluate the acoustic performance of the unserrated and serrated cascade configurations. The first series had a baseline test which used the unserrated blade with an extended leading edge of 0.116 inches (0.295 cm) into which the serrations were cut on the serrated configurations. These tests included the baseline plus Serrations 1, 2 and 3. A noise reduction was noted for each configuration over the entire spectrum as shown for SR3 on Figure 30. The second test series had a baseline test which used the unserrated blade without the extended leading edge. This represented the aerodynamic blade as it would be designed without any provision for serrations. In addition to the baseline, Configurations SR4, 5 and 6 were tested. These data also showed a noise reduction as exemplified by Figure 21. These latter results, however, were conflicting relative to the initial test due to a significant reduction in the baseline noise level and the serrated blade noise level.

After a review of the total test sequence, it was concluded that the cause of the variation in noise level was an inconsistency in the bleed

system effect on the cascade operation. This conclusion was based primarily on the data shown on Figure 42, which compares the noise of the two baseline configurations as a function of the measured turbulence at the cascade exit. The louder baseline also had higher turbulence levels. Turbulence levels of the serrated blade configurations were also found to be correspondingly higher for the initial baseline tests. In order to normalize the data to a common baseline level, the initial tests, unserrated and serrated, were adjusted downward in noise level by 4 dB. This resulted in the data of Figure 43, which show a reduction in noise with all serrated configurations at Mach numbers from 0.75 to 0.98.

The effect of cascade angle on noise is shown by Figure 44. At the design angle of 57 and 60 degrees, a reduction was obtained; however, at 54 and 51 degrees, little or no reduction is seen. This is also consistent with turbulence data which show significant changes at 57 and 60 degrees, but small or no change at 54 and 51 degrees.

An analysis of noise generated by a cascade and its relationship to the wake turbulence was presented in Reference 6. The analysis predicted a noise change proportional to 20 log u/U. Figure 45 shows a comparison of this theoretical reduction with results obtained during the cascade tests. A reasonable amount of agreement is obtained for both unserrated to serrated comparisons as well as a comparison of the baseline noise change presented previously on Figure 42. The exceptions to the agreement are Configurations SR1 at 60 degrees and SR5 at 57 degrees. These data result in the conclusion that the measured noise change is reasonable and that the change is due to reductions in the blade wake turbulence. This would then confirm that the changes in noise are comparable to changes in aerodynamic performance, i.e., the better blade performance is indicative of lower noise.

The effect of serration geometry on noise was consistent with results presented previously for aerodynamic performance. Figure 46 is a plot of noise versus H/C at constant values of H/S, which is comparable to Figure 79

in the Performance section of this report. At constant serration height (H/C), larger spacing is better and at constant geometry (H/S) the larger tooth height and spacing is better. The conclusion from Figures 34 and 46 is that improved performance (lower loss) results in lower noise.

## CONCLUSIONS

A test program employing static cascades was performed to evaluate the effects of serrated blade leading edges on both acoustic and aerodynamic performance. An evaluation of the test results provided the following conclusions concerning operation of airfoil cascades employing serrated leading edges:

1. Serration of the leading edges of a typical rotor airfoil design produced improvements in aerodynamic performance, reductions in wake turbulence levels and reductions in downstream noise levels.

2. The performance improvements, associated with the serrated leading edges, were largest during off-design operation of the airfoils and at high inlet Mach numbers approaching sonic speeds. Only small gains were observed when the inlet flow angle established zero incidence at flow Mach numbers below about 0.80. Note that at the blade design conditions of +2.1 degrees incidence and 0.97 Mach number, both aerodynamic and acoustic performance improvement should occur with the addition of serrated leading edge blading.

3. Based on a comparison of the aerodynamic and acoustic performance for the range of test serrations, the desired serration configuration should have a height greater than six percent of the blade chord, and height-to-spacing ratio (H/S) of 1.5 or less.

4. A comparison of the measured noise levels in the cascade facility and the wake turbulence levels shows a correlation as predicted by

20 times log of turbulence ratio.

5. The delta shape of the serrations adds the additional capability of permitting larger excursions of inlet flow angle without producing high velocities associated with turning the flow over the blade leading edge. Thus, in high speed flow, lower shock losses can be expected. These trends were demonstrated by the measured aerodynamic performance.

## NOMENCLATURE

| Symbol | Definition | Units |
|---|---|---|
| AM | Amplitude Modulated | |
| BL | Baseline Configuration | |
| C | Blade Chord | inch (cm) |
| $C_p$ | Pressure Coefficient, $(P-P_{T1})/(P_{T1}-P_{S1})$ | |
| $C_{p_S}$ | Static Pressure Rise Coefficient, $(P_S-P_{T1})/(P_{T1}-P_{S1})$ | |
| DC | Direct Current | |
| (D-F) | Cascade Diffusion Factor | |
| $(D-F)_T$ | Tunnel Plenum Exit Diffusion Factor | |
| H | Serration Height | inch (cm) |
| I | Electrical Current | ampere |
| KHz | Kilohertz | |
| $K_1$ | Aerodynamic Probe Total Pressure Coefficient | |
| $K_{12}, K_{13}$ | Aerodynamic Probe Static Pressure Coefficients | |
| $K\Psi$ | Aerodynamic Probe Angle Coefficient | |
| L | Peak-to-Peak Spacing of Serrations | inch (cm) |
| $M_1$ | Cascade Inlet Mach Number | |
| $M_2$ | Cascade Exit Mach Number | |
| $M_{2T}$ | Tunnel Plenum Exit Mach Number | |
| P | Electrical Power | watts |
| $P_{S1}$ | Cascade Inlet Static Pressure | $lb/in^2$ ($kN/m^2$) |
| $P_{S2}$ | Cascade Exit Static Pressure | $lb/in^2$ ($kN/m^2$) |
| $P_{S2T}$ | Tunnel Plenum Exit Static Pressure | $lb/in^2$ ($kN/m^2$) |
| $P_{T1}$ | Cascade Inlet Total Pressure | $lb/in^2$ ($kN/m^2$) |
| $P_{T2}$ | Cascade Exit Total Pressure | $lb/in^2$ ($kN/m^2$) |
| $P_1, P_2, P_3$ | Aerodynamic Probe Pressures | $lb/in^2$ ($kN/m^2$) |
| q | Cascade Inlet Dynamic Pressure | $lb/in^2$ ($kN/m^2$) |
| R | Electrical Resistance | ohms |
| R | Radius | inch (cm) |
| S | Serration Spacing | inch (cm) |
| SPL | Sound Pressure Level | dB |
| SR | Serrated Configuration | |

## NOMENCLATURE (Concluded)

| Symbol | Definition | Units |
|---|---|---|
| t | Blade Thickness | inch (cm) |
| TCT | Transonic Cascade Tunnel | |
| TRMS | True Root Mean Square | |
| $T_{T1}$ | Cascade Inlet Total Temperature | °R (°k) |
| (u'/U) | Axial Turbulence | |
| X | Distance from Blade Leading Edge | inch (cm) |
| $\beta$ | Blockage Factor, (Effective/Physical Flow Area) | |
| $\beta_1$ | Cascade Inlet Flow Angle | degrees |
| $\beta_2$ | Cascade Exit Flow Angle | degrees |
| $\delta$ | Deviation Angle | degrees |
| $\Psi$ | Flow Angle | degrees |
| $\bar{\omega}$ | Total Pressure Loss Coefficient, $(P_T-P_{T1})/(P_{T1}-P_{S1})$ | |

## REFERENCES


1. Soderman, Paul T.: Aerodynamic Effects of Leading Edge Serrations on a Two-Dimensional Airfoil, NASA TMX-2643, 1972.

2. Soderman, Paul T.: Leading Edge Serrations which Reduce the Noise of Low-Speed Rotors, NASA TND 7371, 1973.

3. Kazin, S.B.; Paas, J.E.; Minzner, W.R.: Acoustic Testing of a 1.5 Pressure Ratio Low Tip Speed with a Serrated Rotor (QEP Fan B Scale Model), NASA CR 120846, 1973.

4. Kazin, S.B.; Volk, L.J.: LF336 Lift Fan Modification and Acoustic Test Program, NASA CR 1934, General Electric Company, December, 1971.

5. Smith, E.G.: LF336/E Design Summary, General Electric Company, R72AEG293, December, 1972.

6. Benzakein, M.J., et al: Fan Compressor Noise Research, FAA-RD-71-85 I, General Electric Company, March, 1972.

Table I. Significant Airfoil Parameters.

| | |
|---|---|
| Chord | 2.0 inches* (5.08 cm) |
| Aspect Ratio | 2.0 |
| Solidity | 1.439 |
| Blade Leading Edge Angle | 54.9° |
| Blade Trailing Edge Angle | 36.7° |
| Design Incidence Angle | +2.1° |
| Design Deviation Angle | 4.2° |
| Blade Maximum Thickness | 5.5% |
| Blade Leading Edge Radius | 0.75% |

*Includes 0.152 inch (0.386 cm) leading edge extension for serrations

Table II. Casecade Airfoil Coordinates Without Serrated Leading Edge Extension.

| Upper Surface | | Lower Surface | |
|---|---|---|---|
| "X/C" | "Y/C" | "X/C" | "Y/C" |
| -0.5000 | 0.0000 | -0.5000 | 0.0000 |
| -0.4956 | 0.0050 | -0.4943 | -0.0032 |
| -0.4510 | 0.0166 | -0.4486 | 0.0000 |
| -0.4017 | 0.0255 | -0.3982 | 0.0028 |
| -0.3519 | 0.0392 | -0.3480 | 0.0048 |
| -0.3019 | 0.0483 | -0.2978 | 0.0069 |
| -0.2852 | 0.0556 | -0.2481 | 0.0080 |
| -0.2017 | 0.0614 | -0.1984 | 0.0092 |
| -0.1511 | 0.0654 | -0.1487 | 0.0103 |
| -0.1002 | 0.0677 | -0.0992 | 0.0112 |
| -0.0500 | 0.0679 | -0.0497 | 0.0121 |
| 0.0002 | 0.0672 | 0.0000 | 0.0127 |
| 0.0509 | 0.0655 | 0.0499 | 0.0127 |
| 0.1010 | 0.0626 | 0.0990 | 0.0126 |
| 0.1512 | 0.0586 | 0.1823 | 0.0121 |
| 0.2015 | 0.0536 | 0.1988 | 0.0113 |
| 0.2883 | 0.0474 | 0.2485 | 0.0101 |
| 0.3017 | 0.0403 | 0.2988 | 0.0084 |
| 0.3514 | 0.0327 | 0.3485 | 0.0062 |
| 0.4013 | 0.0273 | 0.3988 | 0.0036 |
| 0.4509 | 0.0173 | 0.4493 | 0.0003 |
| 0.4990 | 0.0046 | 0.4944 | -0.0034 |
| 0.5000 | 0.0000 | 0.5000 | 0.0000 |

Table III. Summary of Serrated Geometry.

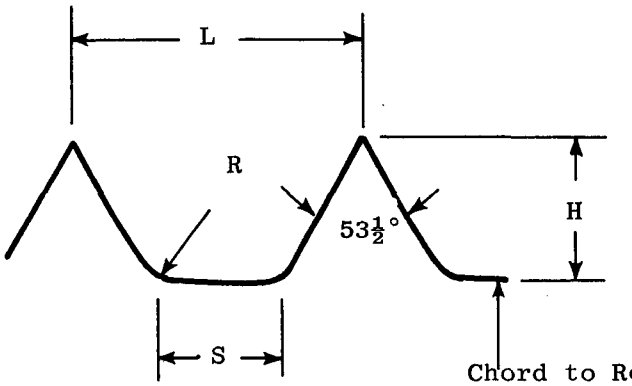


| | H | | H/C | S | | L | | R | | | |
|---|---|---|---|---|---|---|---|---|---|---|---|
| Serration | (in.) | (cm) | (in.) | (in.) | (cm) | (in.) | (cm) | (in.) | (cm) | H/S | L/H |
| BL1 | 0.116 | 0.295 | - | - | - | - | - | - | - | - | - |
| SR1 | 0.116 | 0.295 | 0.063 | 0.036 | 0.091 | 0.153 | 0.389 | 0.024 | 0.061 | 3.2 | 1.32 |
| SR2 | 0.077 | 0.196 | 0.042 | 0.024 | 0.061 | 0.102 | 0.259 | 0.016 | 0.041 | 3.2 | 1.32 |
| SR3 | 0.116 | 0.295 | 0.063 | 0.076 | 0.193 | 0.193 | 0.490 | 0.024 | 0.061 | 1.5 | 1.66 |
| SR4 | 0.152 | 0.386 | 0.083 | 0.100 | 0.254 | 0.253 | 0.643 | 0.031 | 0.079 | 1.5 | 1.66 |
| SR5 | 0.077 | 0.196 | 0.042 | 0.072 | 0.183 | 0.150 | 0.381 | 0.016 | 0.041 | 1.1 | 1.95 |
| SR6 | 0.116 | 0.295 | 0.063 | 0.076 | 0.193 | 0.193 | 0.490 | 0.061 | 0.155 | 1.5 | 1.66 |
| BL2 | 0.000 | 0.000 | - | - | - | - | - | - | - | - | - |

Table IV. Estimated Aerodynamic Design Point Operating Conditions for Serrated Airfoil Sections.

| | |
|---|---|
| Inlet Mach Number | 0.97 |
| Inlet Air Angle | 57° |
| Diffusion Factor | 0.36 |
| Static Pressure Rise Coefficient | 0.33 |
| Total Pressure Loss Coefficient | 0.045 |
| Blade Incidence Angle | +2.1° |
| Blade Deviation Angle | 4.2° |

Table V. Test Run Summary.

| Run No. | Test Date | Serration Configuration | Inlet Mach Number | Inlet Air Angle (Deg.) |
|---|---|---|---|---|
| 3 | 10/24/71 | BL1 | 0.75 | 60 (1) |
| | | | 0.85 | 60 (1) |
| | | | 0.97 | 60 (1) |
| | | | 0.75 | 57 (1) |
| | | | 0.85 | 57 (1) |
| | | | 0.97 | 57 (1) |
| 5 | 10/26/71 | SR1 | 0.75 | 60 (1) |
| | | | 0.85 | 60 (1) |
| | | | 0.97 | 60 (1) |
| | | | 0.85 | 57 (1) |
| | | | 0.97 | 57 (1) |
| 6 | 1/4/72 | SR1 | 0.74 | 60 (1) |
| | | | 0.88 | 60 |
| 7 | 1/6/72 | SR1 | 0.84 | 60 |
| 8 | 1/23/72 | BL1 | 0.84 | 57 |
| | | | 0.76 | 57 |
| | | SR2 | 0.75 | 57 |
| | | | 0.86 | 57 |
| | | SR3 | 0.76 | 57 |
| | | | 0.86 | 57 |
| 9 | 1/25/72 | SR1 | 0.75 | 57 |
| | | | 0.86 | 57 |
| | | | 0.86 | 60 |
| | | | 0.87 | 60 |

Table V. Test Run Summary (Concluded).

| Run No. | Test Date | Serration Configuration | Inlet Mach Number | Inlet Air Angle (Deg.) |
|---|---|---|---|---|
| 11 | 6/9/72 | BL1 | 0.99 | 57 |
| | | | 0.88 | 60 |
| | | SR3 | 0.87 | 60 |
| | | | 0.87 | 57 |
| | | SR4 | 0.86 | 57 |
| | | | 0.86 | 60 |
| 12 | 6/12/72 | SR5 | 0.88 | 57 |
| | | | 0.90 | 60 |
| | | SR6 | 0.89 | 60 |
| | | | 0.88 | 57 |
| 14 | 8/4/72 | BL2 | 0.87 | 57 |
| | | | 0.76 | 57 |
| | | | 1.01 | 57 |
| | | | 0.89 | 60 |
| | | | 0.83 | 54 |
| | | SR6 | 0.84 | 54 |
| | | | 0.87 | 57 |
| | | | 0.99 | 57 |
| | | | 0.77 | 57 |
| | | | 0.86 | 57 (2) |
| | | | 0.90 | 57 (3) |
| | | BL2 | 0.87 | 51 |
| | | SR6 | 0.82 | 51 |

(1) Tests without boundary layer bleed
(2) Instrumentation at 1/2 chord
(3) Instrumentation at 2 chords

Table VI. Aerodynamic Performance Summary.

| Conf | Run | $\beta_1$ (Deg) | $M_1$ | $P_{T1}$ (lb/in$^2$) | $P_{T1}$ (kN/m$^2$) | $T_{T1}$ (°R) | $T_{T1}$ (°K) | $P_{T2}/P_{T1}$ | $P_{S2}/P_{T1}$ | $P_{S2T}/P_{T1}$ | $\beta_2$ (Deg) | $\delta$ (Deg) | $\bar{\omega}$ | $C_{PT}$ | $C_P$ | $(D-F)_T$ | $(D-F)$ | $M_{2T}$ | $M_2$ | |
|---|---|---|---|---|---|---|---|---|---|---|---|---|---|---|---|---|---|---|---|---|
| BL1 | 3 | 60 | 0.759 | 11.40 | 78.55 | 534 | 299 | 0.982 | 0.727 | 0.743 | 41.6 | 4.90 | 0.054 | 0.190 | 0.141 | 0.240 | 0.205 | 0.645 | 0.670 | (1) |
| | | 60 | 0.842 | 11.25 | 77.51 | 534 | 299 | 0.977 | 0.676 | 0.692 | 41.9 | 5.18 | 0.062 | 0.171 | 0.130 | 0.230 | 0.201 | 0.719 | 0.743 | (1) |
| | | 60 | 0.962 | 11.08 | 76.34 | 534 | 299 | 0.952 | 0.609 | 0.616 | 43.6 | 6.93 | 0.106 | 0.143 | 0.130 | 0.228 | 0.219 | 0.815 | 0.824 | (1) |
| | | 57 | 0.752 | 11.45 | 78.89 | 533 | 298 | 0.983 | 0.721 | 0.735 | 41.7 | 5.05 | 0.055 | 0.154 | 0.108 | 0.202 | 0.169 | 0.658 | 0.681 | (1) |
| | | 57 | 0.858 | 11.22 | 77.31 | 533 | 298 | 0.963 | 0.653 | 0.666 | 43.7 | 7.03 | 0.096 | 0.124 | 0.093 | 0.196 | 0.173 | 0.747 | 0.765 | (1) |
| | | 57 | 0.972 | 11.03 | 76.00 | 533 | 298 | 0.924 | 0.587 | 0.583 | 47.9 | 11.15 | 0.168 | 0.081 | 0.092 | 0.183 | 0.196 | 0.839 | 0.830 | (1) |
| SR1 | 5 | 60 | 0.753 | 11.37 | 78.34 | 528 | 296 | 0.988 | 0.726 | 0.742 | 41.4 | 4.68 | 0.039 | 0.180 | 0.125 | 0.223 | 0.184 | 0.651 | 0.679 | (1) |
| | | 60 | 0.846 | 11.21 | 77.24 | 532 | 298 | 0.977 | 0.680 | 0.690 | 41.2 | 4.51 | 0.064 | 0.171 | 0.145 | 0.234 | 0.216 | 0.722 | 0.738 | (1) |
| | | 60 | 0.963 | 11.08 | 76.34 | 531 | 297 | 0.957 | 0.610 | 0.617 | 43.2 | 6.48 | 0.096 | 0.147 | 0.131 | 0.226 | 0.216 | 0.817 | 0.828 | (1) |
| | | 57 | 0.749 | 10.98 | 75.65 | 531 | 297 | 0.988 | 0.719 | 0.737 | 41.0 | 4.30 | 0.039 | 0.151 | 0.095 | 0.194 | 0.153 | 0.662 | 0.690 | (1) |
| | | 57 | 0.850 | 10.87 | 74.89 | 531 | 297 | 0.974 | 0.656 | 0.671 | 42.2 | 5.45 | 0.070 | 0.126 | 0.086 | 0.189 | 0.160 | 0.750 | 0.773 | (1) |
| SR1 | 6 | 60 | 0.738 | 11.70 | 80.61 | 513 | 287 | 0.989 | 0.743 | 0.748 | 40.1 | 3.36 | 0.040 | 0.168 | 0.152 | 0.220 | 0.209 | 0.644 | 0.652 | (1) |
| | | 60 | 0.879 | 11.38 | 78.41 | 512 | 287 | 0.976 | 0.726 | 0.728 | 41.0 | 4.31 | 0.063 | 0.311 | 0.305 | 0.350 | 0.346 | 0.660 | 0.664 | |
| SR1 | 7 | 60 | 0.843 | 11.11 | 76.55 | 511 | 286 | 0.986 | 0.735 | 0.741 | 41.1 | 4.42 | 0.039 | 0.302 | 0.288 | 0.326 | 0.315 | 0.652 | 0.661 | |
| BL1 | 8 | 57 | 0.817 | 10.94 | 76.38 | 518 | 290 | 0.971 | 0.749 | 0.762 | 45.1 | 8.43 | 0.083 | 0.332 | 0.295 | 0.355 | 0.324 | 0.597 | 0.619 | |
| | | 57 | 0.752 | 11.08 | 76.34 | 515 | 288 | 0.985 | 0.776 | 0.790 | 44.7 | 8.01 | 0.049 | 0.329 | 0.285 | 0.328 | 0.293 | 0.570 | 0.593 | |
| SR2 | | 57 | 0.737 | 11.14 | 76.75 | 515 | 288 | 0.981 | 0.779 | 0.791 | 43.7 | 6.96 | 0.061 | 0.309 | 0.273 | 0.322 | 0.295 | 0.565 | 0.583 | |
| | | 57 | 0.851 | 11.03 | 76.00 | 515 | 288 | 0.978 | 0.724 | 0.743 | 43.2 | 6.48 | 0.057 | 0.318 | 0.271 | 0.334 | 0.296 | 0.640 | 0.669 | |
| SR3 | | 57 | 0.746 | 11.16 | 76.89 | 514 | 288 | 0.987 | 0.773 | 0.784 | 42.9 | 6.23 | 0.044 | 0.304 | 0.264 | 0.310 | 0.280 | 0.580 | 0.600 | |
| | | 57 | 0.844 | 11.06 | 76.20 | 514 | 288 | 0.976 | 0.727 | 0.743 | 43.1 | 6.36 | 0.059 | 0.313 | 0.268 | 0.331 | 0.296 | 0.638 | 0.664 | |
| SR1 | 9 | 57 | 0.742 | 11.15 | 76.82 | 517 | 290 | 0.979 | 0.778 | 0.789 | 43.0 | 6.28 | 0.065 | 0.311 | 0.276 | 0.328 | 0.303 | 0.565 | 0.583 | |
| | | 57 | 0.847 | 11.14 | 76.75 | 520 | 291 | 0.978 | 0.728 | 0.741 | 42.8 | 6.11 | 0.058 | 0.309 | 0.275 | 0.328 | 0.302 | 0.642 | 0.662 | |
| BL1 | | 60 | 0.837 | 11.17 | 76.96 | 518 | 290 | 0.945 | 0.743 | 0.748 | 45.9 | 9.22 | 0.148 | 0.317 | 0.302 | 0.395 | 0.384 | 0.587 | 0.596 | |
| SR2 | | 60 | 0.847 | 11.18 | 77.03 | 518 | 290 | 0.966 | 0.716 | 0.731 | 44.0 | 7.26 | 0.089 | 0.282 | 0.243 | 0.330 | 0.299 | 0.645 | 0.668 | |

## Table VI. Aerodynamic Performance Summary (Concluded).

| Conf | Run | $\beta_1$ (Deg) | $M_1$ | $P_{T1}$ (lb/in$^2$) | $P_{T1}$ (kN/m$^2$) | $T_{T1}$ (°R) | $T_{T1}$ (°K) | $P_{T2}/P_{T1}$ | $P_{S2}/P_{T1}$ | $P_{S2T}/P_{T1}$ | $\beta_2$ (Deg) | $\delta$ (Deg) | $\bar{\omega}$ | $C_{PT}$ | $C_P$ | $(D\text{-}F)_T$ | $(D\text{-}F)$ | $M_{2T}$ | $M_2$ | |
|---|---|---|---|---|---|---|---|---|---|---|---|---|---|---|---|---|---|---|---|---|
| BL1 | 11 | 57 | 0.874 | 11.07 | 76.27 | 530 | 297 | 0.969 | 0.740 | 0.742 | 43.8 | 7.12 | 0.079 | 0.341 | 0.336 | 0.367 | 0.364 | 0.630 | 0.634 | |
| | | 57 | 0.994 | 11.04 | 76.07 | 534 | 299 | 0.944 | 0.678 | 0.678 | 45.8 | 9.12 | 0.121 | 0.312 | 0.310 | 0.368 | 0.369 | 0.704 | 0.705 | |
| | | 60 | 0.883 | 11.07 | 76.27 | 535 | 300 | 0.943 | 0.733 | 0.734 | 44.9 | 8.18 | 0.144 | 0.332 | 0.329 | 0.411 | 0.410 | 0.609 | 0.610 | |
| SR3 | | 60 | 0.873 | 11.06 | 76.20 | 533 | 298 | 0.966 | 0.725 | 0.731 | 43.6 | 6.92 | 0.088 | 0.315 | 0.298 | 0.360 | 0.347 | 0.642 | 0.653 | |
| | | 57 | 0.872 | 11.02 | 75.93 | 532 | 298 | 0.984 | 0.734 | 0.741 | 43.1 | 6.44 | 0.043 | 0.338 | 0.318 | 0.343 | 0.329 | 0.648 | 0.661 | |
| SR4 | | 57 | 0.859 | 11.06 | 76.20 | 530 | 297 | 0.985 | 0.731 | 0.735 | 43.0 | 6.31 | 0.041 | 0.308 | 0.296 | 0.316 | 0.308 | 0.659 | 0.666 | |
| | | 60 | 0.861 | 11.01 | 75.86 | 530 | 297 | 0.964 | 0.727 | 0.730 | 43.8 | 7.09 | 0.094 | 0.300 | 0.288 | 0.350 | 0.343 | 0.641 | 0.648 | |
| SR5 | 12 | 57 | 0.876 | 11.21 | 77.24 | 532 | 298 | 0.984 | 0.723 | 0.730 | 43.4 | 6.68 | 0.039 | 0.313 | 0.295 | 0.319 | 0.306 | 0.668 | 0.679 | |
| | | 60 | 0.895 | 11.17 | 76.96 | 533 | 298 | 0.974 | 0.713 | 0.719 | 43.2 | 6.46 | 0.063 | 0.307 | 0.293 | 0.340 | 0.329 | 0.674 | 0.683 | |
| SR6 | | 60 | 0.889 | 11.15 | 76.82 | 537 | 301 | 0.975 | 0.721 | 0.727 | 43.3 | 6.58 | 0.063 | 0.322 | 0.306 | 0.352 | 0.341 | 0.660 | 0.670 | |
| | | 57 | 0.884 | 11.18 | 77.03 | 537 | 301 | 0.982 | 0.732 | 0.733 | 43.0 | 6.28 | 0.046 | 0.332 | 0.328 | 0.341 | 0.336 | 0.659 | 0.661 | |
| BL2 | 14 | 57 | 0.870 | 10.77 | 74.21 | 529 | 296 | 0.964 | 0.749 | 0.750 | 44.6 | 7.93 | 0.093 | 0.359 | 0.356 | 0.390 | 0.391 | 0.609 | 0.611 | |
| | | 57 | 0.756 | 11.26 | 77.58 | 534 | 299 | 0.991 | 0.788 | 0.791 | 43.0 | 6.30 | 0.029 | 0.338 | 0.326 | 0.328 | 0.319 | 0.576 | 0.583 | |
| | | 57 | 1.014 | 11.02 | 75.93 | 533 | 298 | 0.962 | 0.681 | 0.691 | 43.2 | 6.50 | 0.080 | 0.356 | 0.336 | 0.391 | 0.375 | 0.704 | 0.720 | |
| | | 60 | 0.895 | 11.07 | 76.27 | 531 | 297 | 0.965 | 0.726 | 0.734 | 44.2 | 7.46 | 0.087 | 0.341 | 0.323 | 0.382 | 0.368 | 0.639 | 0.651 | |
| | | 54 | 0.825 | 11.18 | 77.03 | 530 | 297 | 0.985 | 0.742 | 0.752 | 43.3 | 6.59 | 0.043 | 0.312 | 0.282 | 0.308 | 0.384 | 0.632 | 0.650 | |
| SR6 | | 54 | 0.845 | 11.12 | 76.62 | 531 | 297 | 0.987 | 0.737 | 0.744 | 43.1 | 6.36 | 0.039 | 0.312 | 0.292 | 0.307 | 0.292 | 0.648 | 0.660 | |
| | | 57 | 0.874 | 11.11 | 76.55 | 531 | 297 | 0.986 | 0.732 | 0.739 | 42.8 | 6.13 | 0.037 | 0.333 | 0.315 | 0.337 | 0.323 | 0.655 | 0.667 | |
| | | 57 | 0.985 | 11.06 | 76.20 | 531 | 297 | 0.972 | 0.683 | 0.690 | 42.4 | 5.65 | 0.059 | 0.330 | 0.315 | 0.356 | 0.345 | 0.718 | 0.729 | |
| | | 57 | 0.771 | 11.24 | 77.44 | 530 | 297 | 0.985 | 0.778 | 0.784 | 42.8 | 6.08 | 0.046 | 0.337 | 0.319 | 0.340 | 0.327 | 0.580 | 0.590 | |
| | | 57 | 0.857 | 11.10 | 76.48 | 526 | 295 | 0.989 | 0.743 | 0.746 | 40.2 | 3.40 | 0.029 | 0.334 | 0.326 | 0.340 | 0.318 | 0.642 | 0.652 | (2) |
| | | 57 | 0.895 | 10.78 | 74.27 | 536 | 300 | 0.986 | 0.724 | 0.730 | 43.2 | 6.45 | 0.035 | 0.337 | 0.318 | 0.339 | 0.323 | 0.668 | 0.680 | (3) |
| BL2 | | 51 | 0.870 | 10.72 | 73.86 | 533 | 298 | 0.946 | 0.642 | 0.634 | 47.9 | 11.16 | 0.138 | 0.061 | 0.082 | 0.131 | 0.150 | 0.778 | 0.765 | |
| SR6 | | 51 | 0.815 | 10.72 | 73.86 | 532 | 298 | 0.958 | 0.701 | 0.715 | 46.1 | 9.39 | 0.117 | 0.194 | 0.157 | 0.235 | 0.207 | 0.661 | 0.683 | |

(1) No boundary layer bleed

(2) Traverse plane at 1/2 chord

(3) Traverse Plane at 2 chords

Table VII. Summary of Exhaust Turbulence Measurements.

| Configuration | Run | $\beta_1$ | $M_1$ | Peak (u'/U) | Peak (v'/U) | Avg ($\bar{u}$'/U) | Avg ($\bar{v}$'/U) |
|---|---|---|---|---|---|---|---|
| SR1 | 7 | 60 | 0.843 | 0.045 | 0.032 | 0.031 | 0.022 |
| BL1 | 8 | 57 | 0.817 | 0.104 | 0.080 | 0.090 | 0.078 |
| | | 57 | 0.752 | 0.050 | 0.048 | 0.038 | 0.035 |
| SR2 | | 57 | 0.737 | 0.066 | 0.073 | 0.036 | 0.038 |
| | | 57 | 0.851 | 0.055 | 0.057 | 0.036 | 0.033 |
| SR3 | | 57 | 0.746 | 0.057 | 0.060 | 0.038 | 0.035 |
| | | 57 | 0.844 | 0.060 | 0.060 | 0.040 | 0.037 |
| SR1 | 9 | 57 | 0.742 | 0.073 | 0.088 | 0.038 | 0.039 |
| | | 57 | 0.847 | 0.071 | 0.080 | 0.031 | 0.036 |
| BL1 | | 60 | 0.837 | 0.120 | 0.097 | 0.111 | 0.088 |
| SR2 | | 60 | 0.847 | 0.080 | 0.049 | 0.050 | 0.030 |
| BL1 | 11 | 57 | 0.874 | 0.079 | 0.039 | 0.060 | 0.032 |
| | | 60 | 0.883 | 0.205 | 0.065 | 0.190 | 0.061 |
| SR3 | | 60 | 0.873 | 0.119 | 0.051 | 0.078 | 0.028 |
| | | 57 | 0.872 | 0.042 | 0.023 | 0.026 | 0.018 |
| SR4 | | 57 | 0.859 | 0.027 | 0.017 | 0.016 | 0.014 |
| | | 60 | 0.861 | 0.074 | 0.026 | 0.043 | 0.021 |
| SR5 | 12 | 57 | 0.876 | 0.038 | 0.031 | 0.020 | 0.020 |
| | | 60 | 0.895 | 0.043 | 0.031 | 0.026 | 0.032 |
| SR6 | | 60 | 0.889 | No Data -- Probe Failed | | | |
| | | 57 | 0.884 | 0.024 | 0.020 | 0.018 | 0.018 |
| BL2 | 14 | 57 | 0.870 | 0.050 | 0.051 | 0.043 | 0.045 |
| | | 57 | 0.756 | 0.052 | 0.041 | 0.032 | 0.026 |
| | | 60 | 0.895 | 0.170 | 0.130 | 0.161 | 0.106 |
| | | 54 | 0.825 | 0.027 | 0.027 | 0.022 | 0.023 |
| SR6 | | 54 | 0.845 | 0.029 | 0.028 | 0.020 | 0.022 |
| | | 57 | 0.874 | 0.038 | 0.031 | 0.026 | 0.026 |
| | | 57 | 0.771 | 0.042 | 0.027 | 0.026 | 0.022 |
| | | 57 | 0.857 | 0.058 | 0.058 | 0.035 | 0.032* |
| | | 57 | 0.895 | 0.036 | 0.040 | 0.028 | 0.026** |
| BL2 | | 51 | 0.870 | 0.150 | 0.143 | 0.110 | 0.102 |
| SR6 | | 51 | 0.815 | 0.092 | 0.082 | 0.058 | 0.050 |

* Probe at $\frac{1}{2}$ Chord
** Probe at 2 Chord

Table VIII. Summary of Acoustic and Turbulence Data.

- Turbulence Level is Area Weighted Average Behind One Blade from Midpoint to Midpoint
- Noise Level is at 4000 Hertz with 20 Hertz Bandwidth

| Configuration | | | Turbulence | Noise |
|---|---|---|---|---|
| Blade | $\beta_1$ | $M_1$ | $\bar{u}'/U\%$ | SPL,dB |
| BL1 | 57 | 0.817 | 9.0 | 105.2 |
| | 57 | 0.752 | 3.8 | 102.5 |
| | 60 | 0.837 | 11.1 | 107 |
| BL2 | 57 | 0.870 | 4.3 | 100.5 |
| | 57 | 0.756 | 3.2 | 98.5 |
| | 57 | 0.97 | - | 102.5 |
| | 60 | 0.895 | 16.1 | 103.5 |
| | 54 | 0.825 | 2.2 | 100.5 |
| | 51 | 0.870 | 11.0 | 99 |
| SR1 | 57 | 0.860 | 3.1 | 97 |
| | 57 | 0.742 | 3.8 | 98 |
| | 60 | 0.843 | 3.1 | 101.5 |
| | 57 | 0.970 | - | 97.5 |
| SR2 | 57 | 0.851 | 3.6 | 95 |
| | 57 | 0.737 | 3.6 | 95.5 |
| | 60 | 0.847 | 5.0 | 98.5 |
| | 57 | 0.970 | - | 96.5 |
| SR3 | 57 | 0.844 | 4.0 | 96.5 |
| | 57 | 0.746 | 3.8 | 95.0 |
| | 57 | 0.970 | - | 97.5 |
| SR4 | 57 | 0.859 | 1.6 | 90.5 |
| SR5 | 57 | 0.876 | 2.0 | 88 |
| SR6 | 57 | 0.874 | 2.6 | 93 |
| | 57 | 0.771 | 2.6 | 90.5 |
| | 57 | 0.985 | - | 92.5 |
| | 54 | 0.845 | 2.0 | 100 |
| | 51 | 0.815 | 5.8 | 98 |

Table IX. Cascade Exit Blockage Comparison at $M_1 = 0.85$, $\beta_1 = 57$ Degrees.

| Configuration | $\bar{\omega}$ | $\beta_2$ | $C_p$ | Blkg |
|---|---|---|---|---|
| BL1 | 0.079 | 43.8 | 0.34 | 0.88 |
| BL2 | 0.093 | 44.6 | 0.36 | 0.92 |
| SR1 | 0.058 | 42.8 | 0.31 | 0.85 |
| SR2 | 0.057 | 43.2 | 0.27 | 0.84 |
| SR3 | 0.043 | 43.1 | 0.32 | 0.85 |
| SR4 | 0.041 | 43.0 | 0.30 | 0.83 |
| SR5 | 0.039 | 43.4 | 0.30 | 0.84 |
| SR6 | 0.037 | 42.8 | 0.32 | 0.84 |

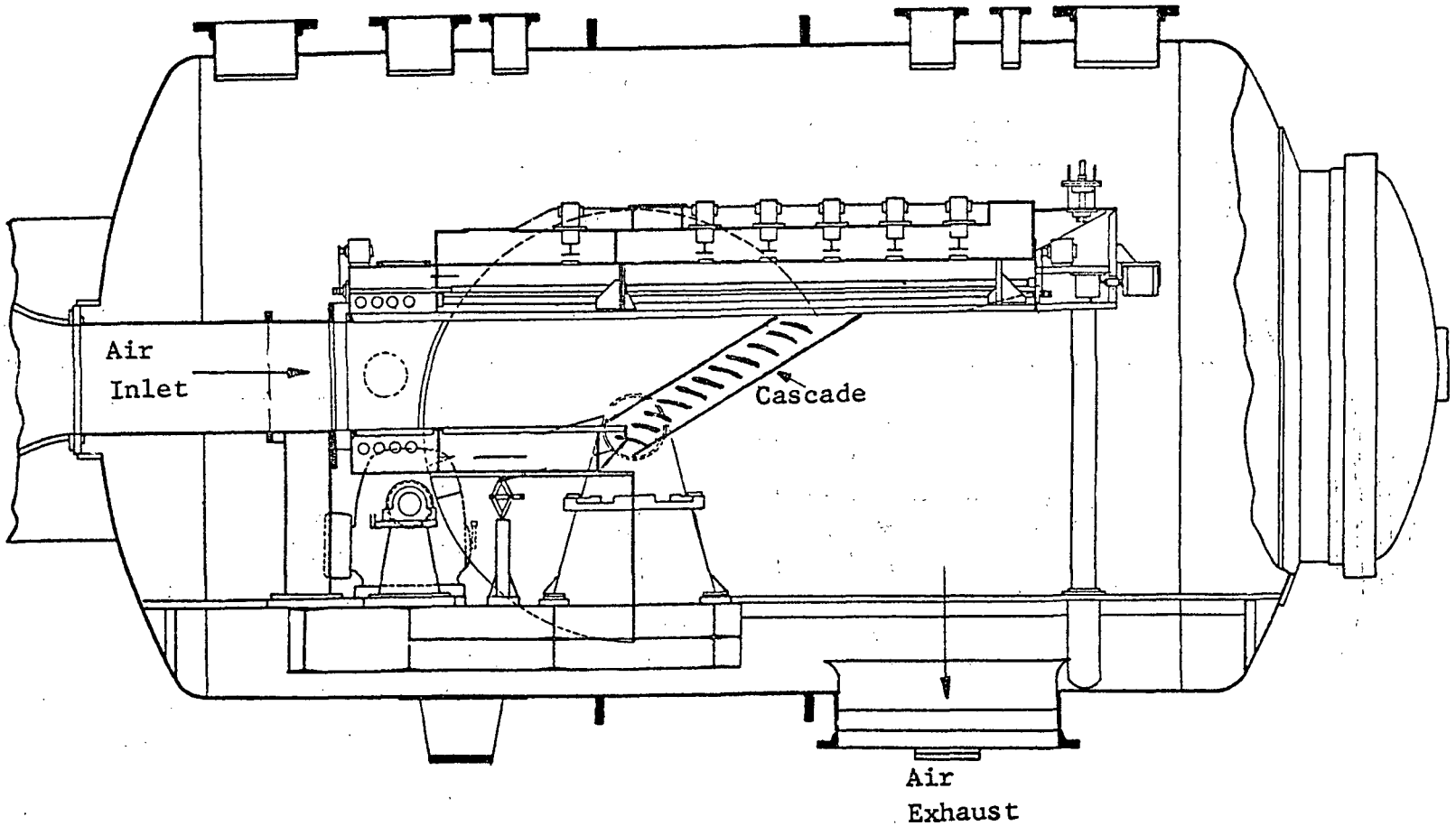


Figure 1. General Arangement of Transonic Cascade Facility.

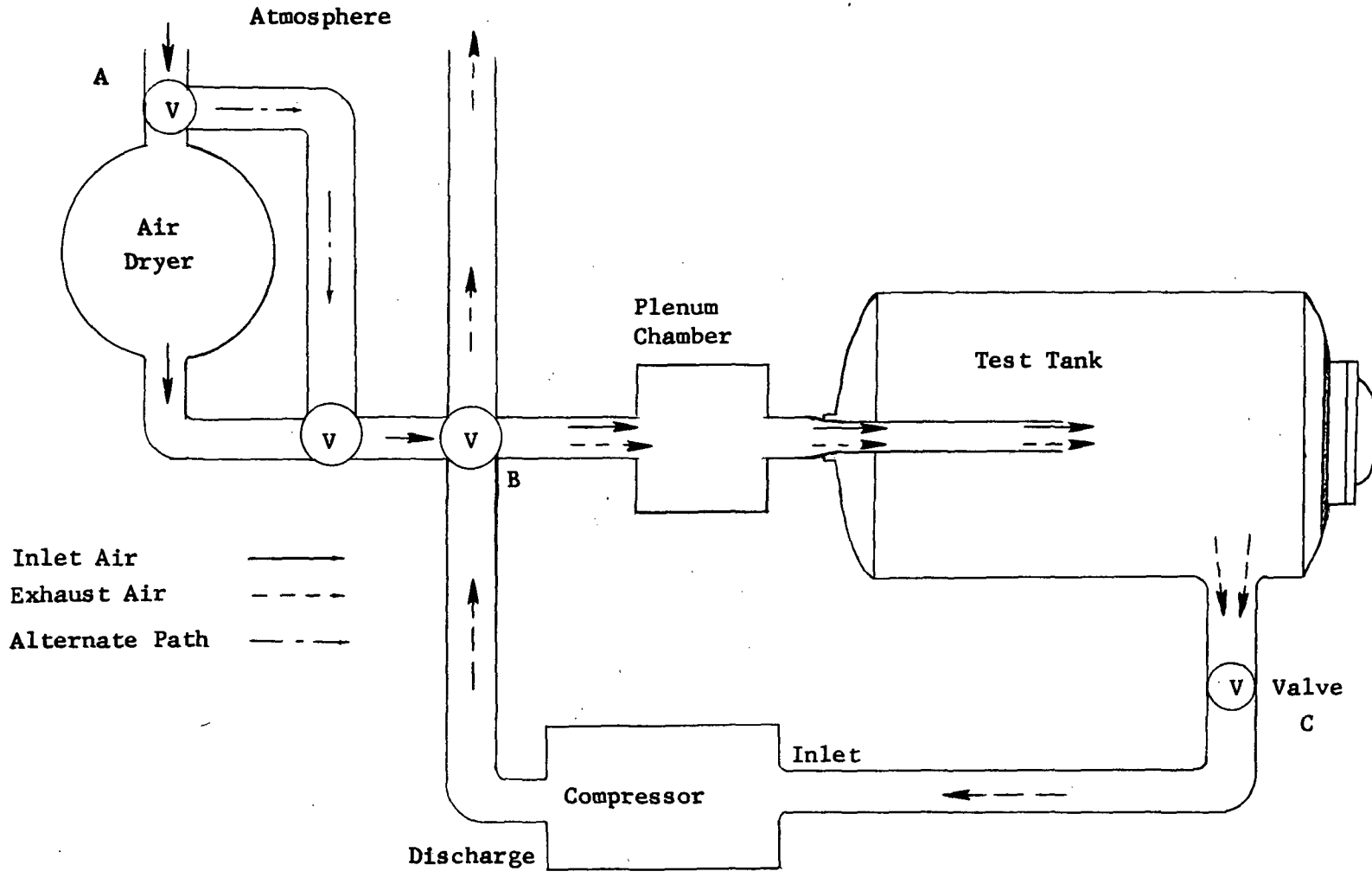


Figure 2. Flow Schematic for Transonic Cascade Test Facility.

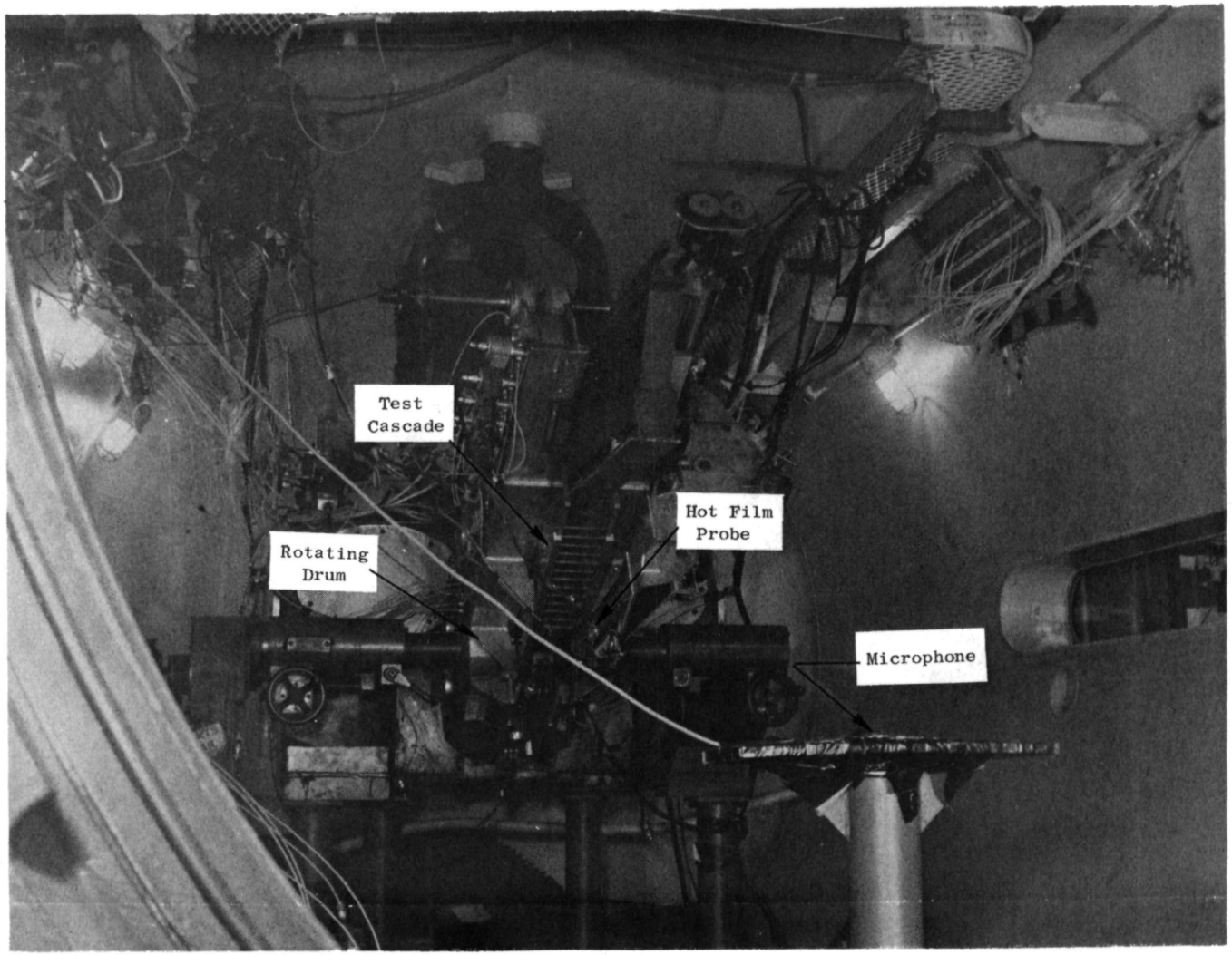


Figure 3. Photograph of Transonic Cascade Test Facility.

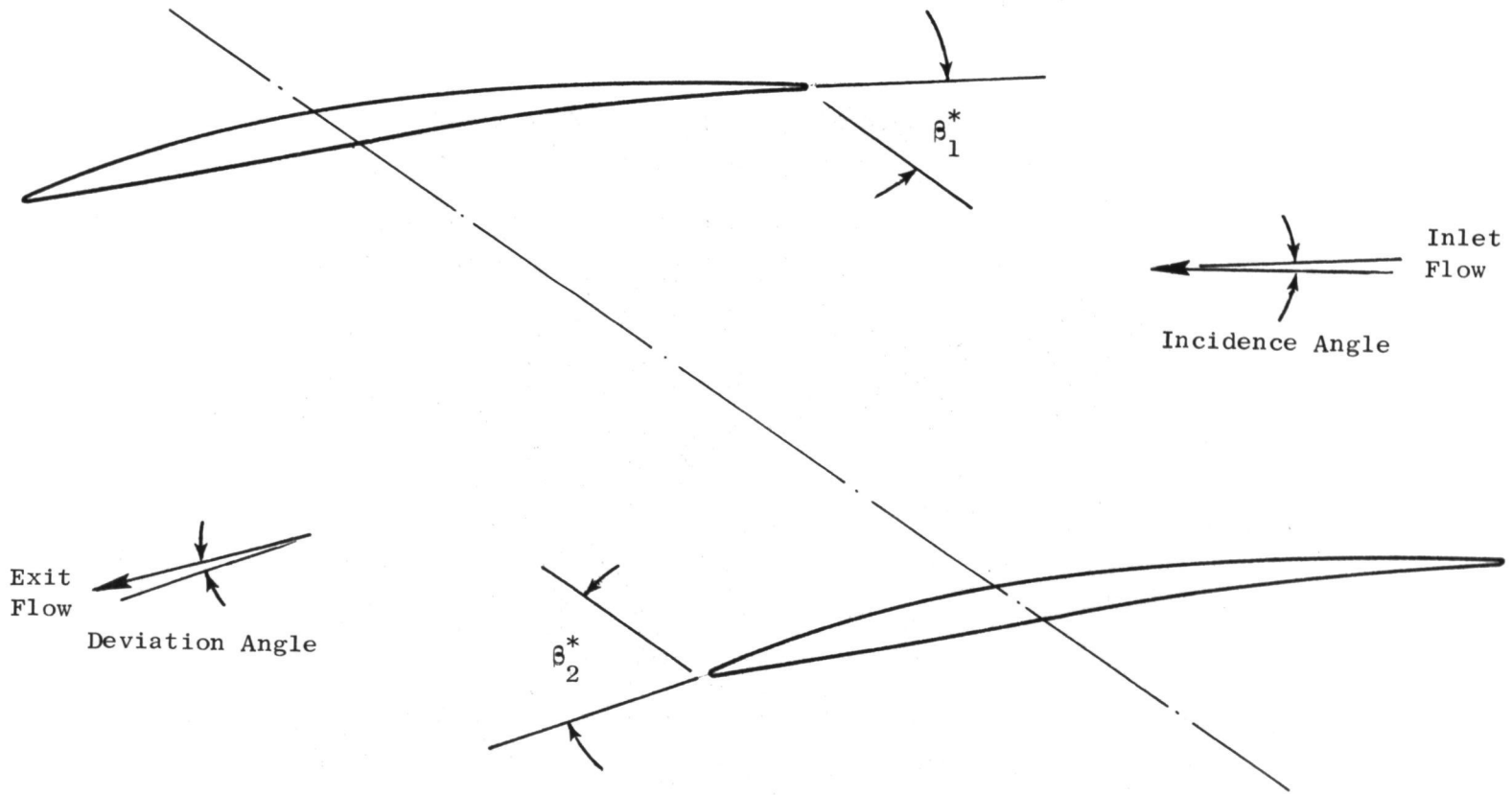


Figure 4. Test Section Airfoil Cross-Section.

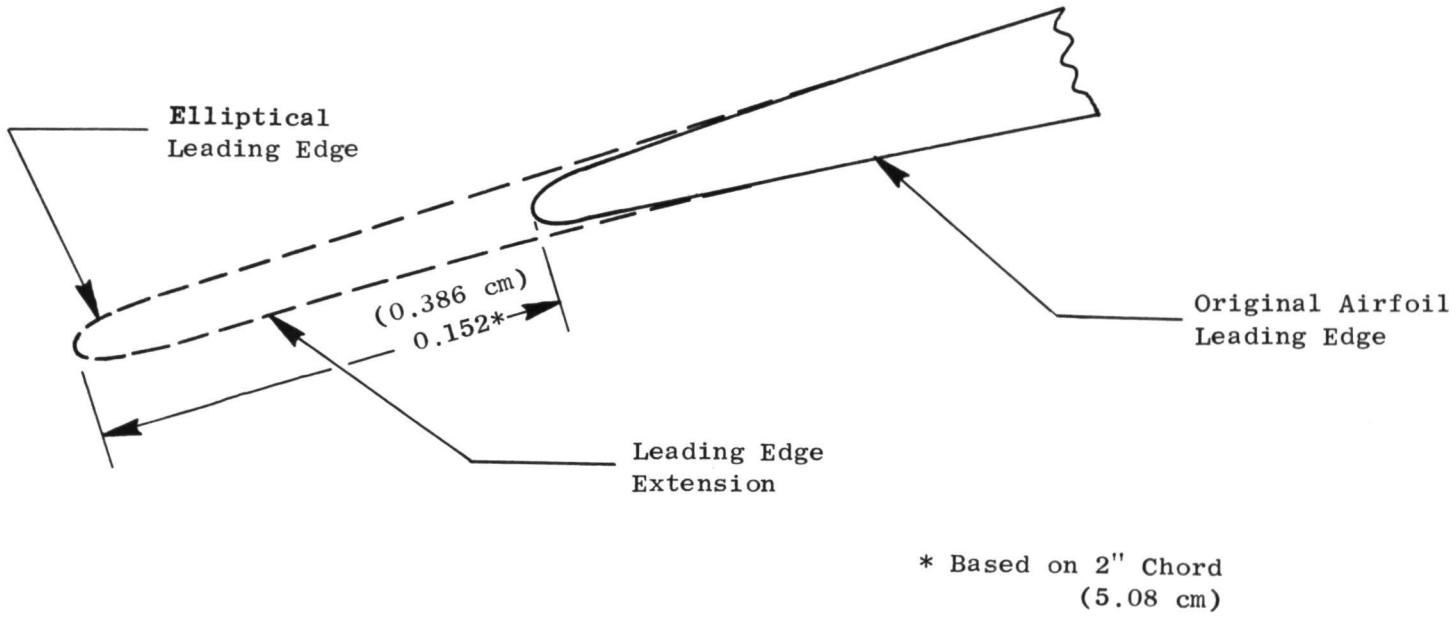


Figure 5. Airfoil Leading Edge Geometry.

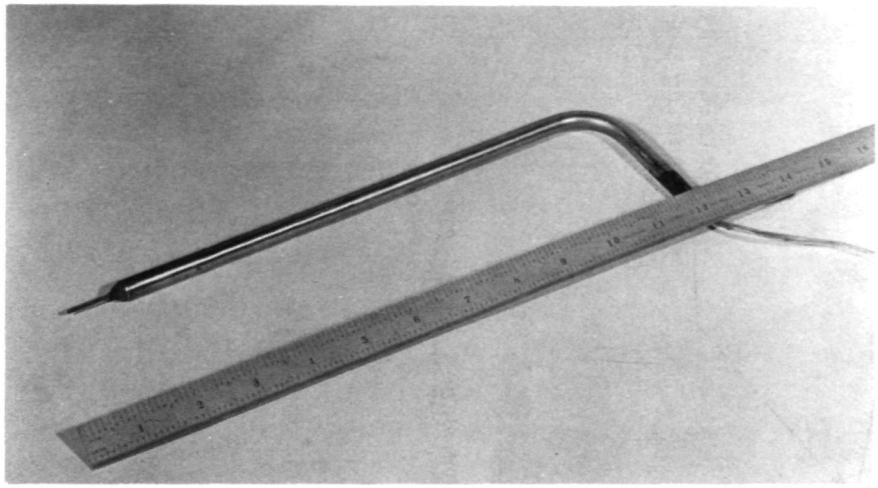

a) Overall View of Probe

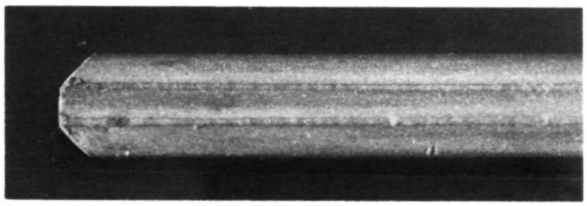

b) Close-up of Probe Sensors

Figure 6. Photographs of Three Parameter Survey Probe.

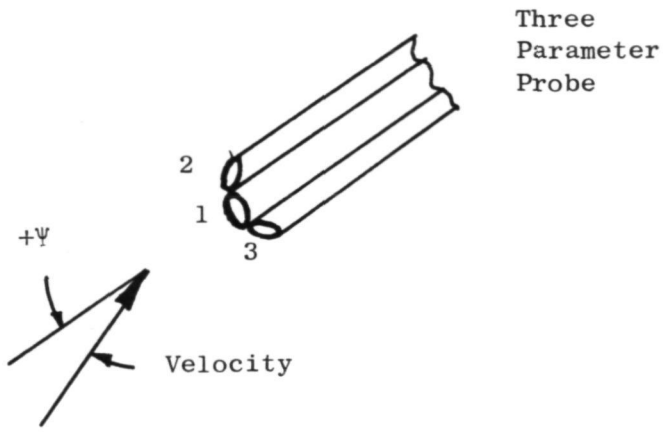


$$K_{\Psi} = (P_1 - P_2)/(P_1 - P_3)$$

$$K_1 = (P_1 - P_s)/q$$

$$K_{12} = (P_1 - P_2)/q$$

$$K_{13} = (P_1 - P_3)/q$$

Figure 7. Definition of Aerodynamic Probe Coefficients.

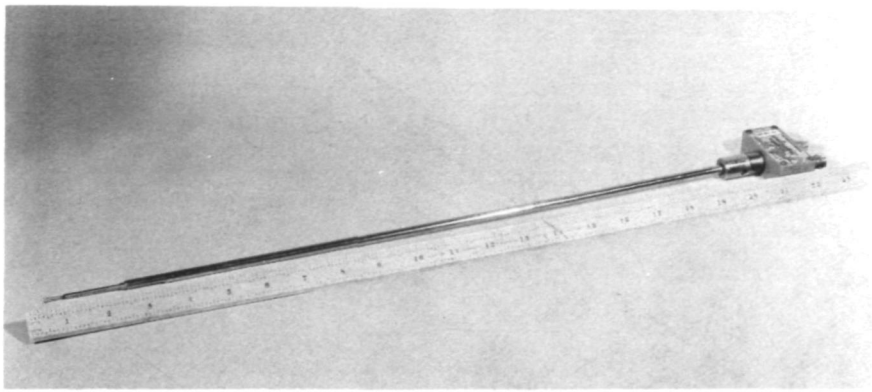

a) Overall View of Probe

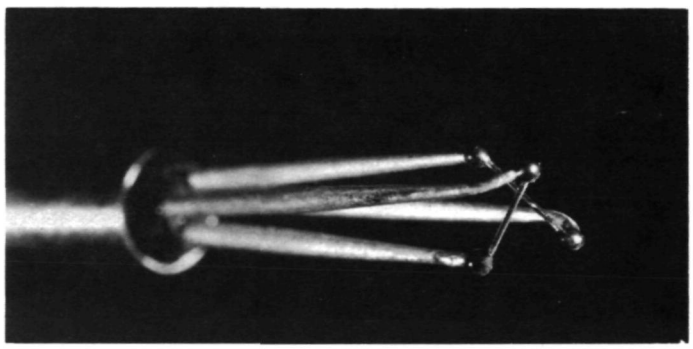

b) Close-up of Sensor X-Array

Figure 8. Photographs of Hot Film Probe.

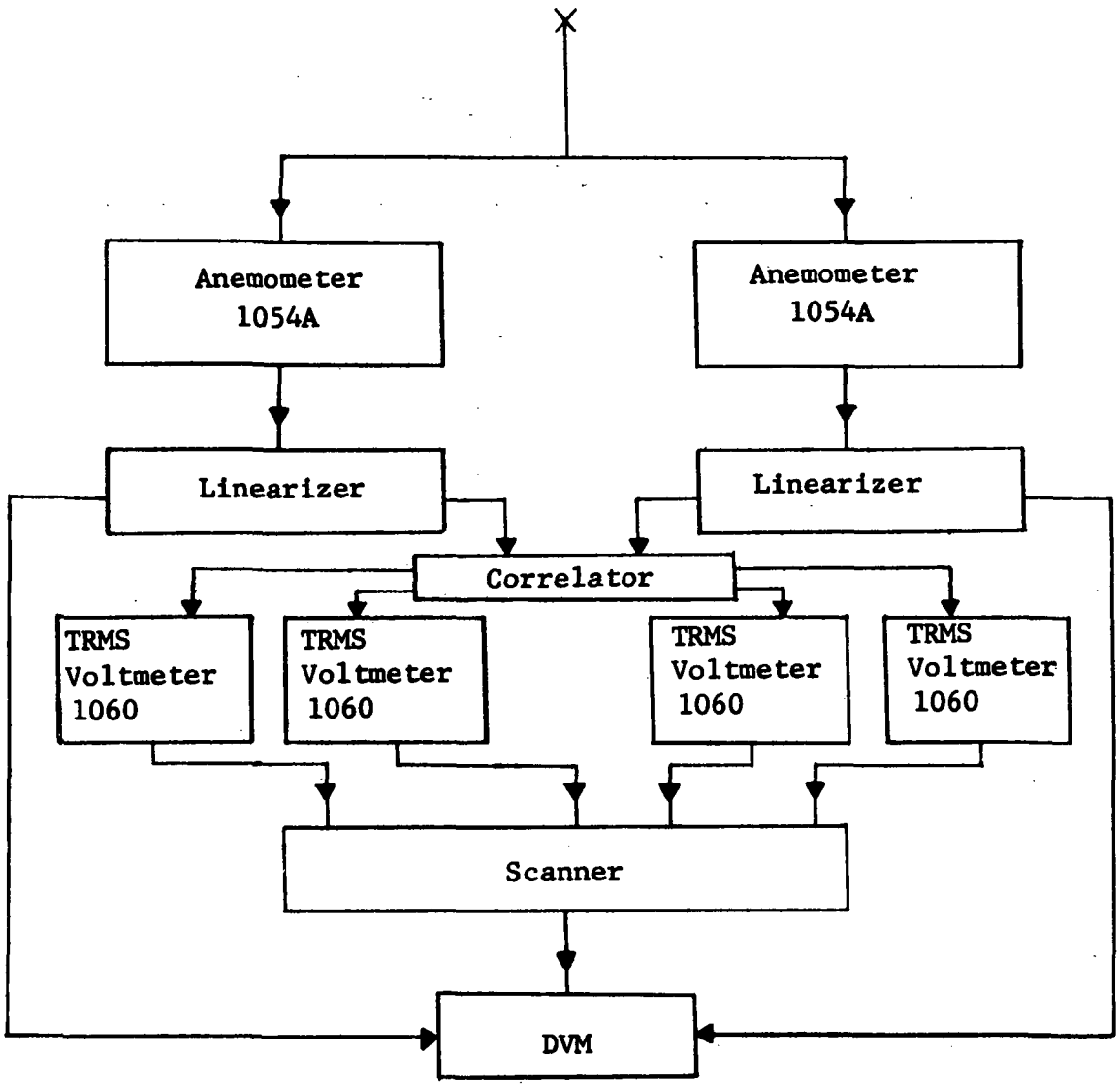


Figure 9. Block of Hot Film Data System.

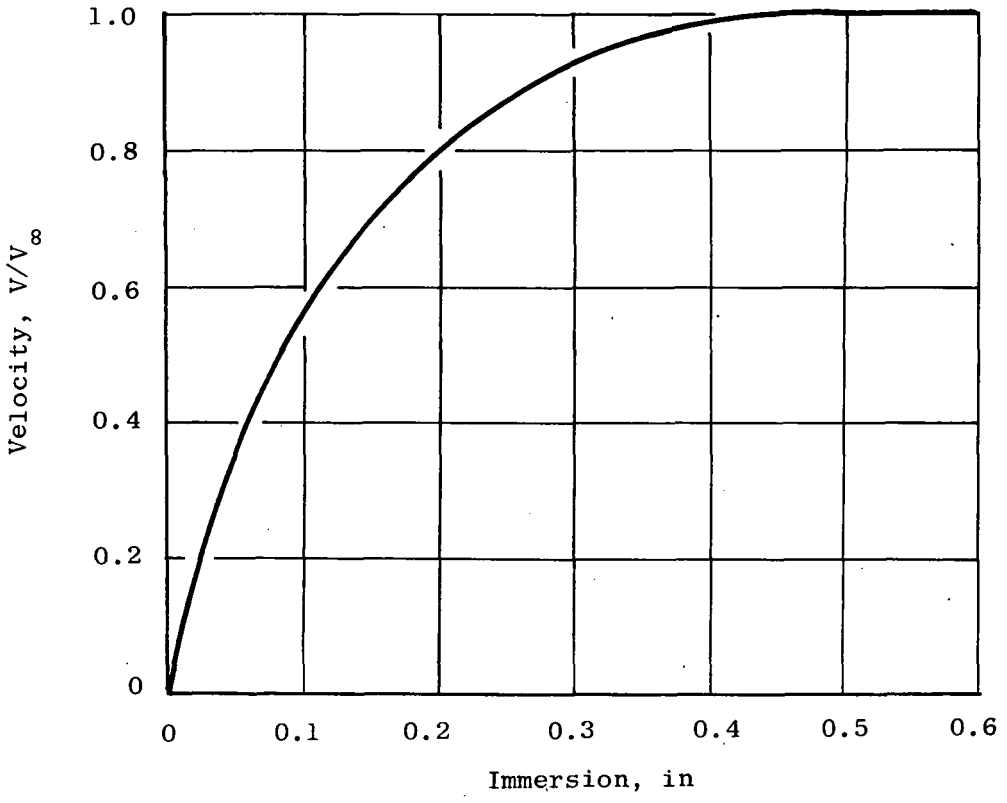


Figure 10. Cascade Inlet Boundary Layer.

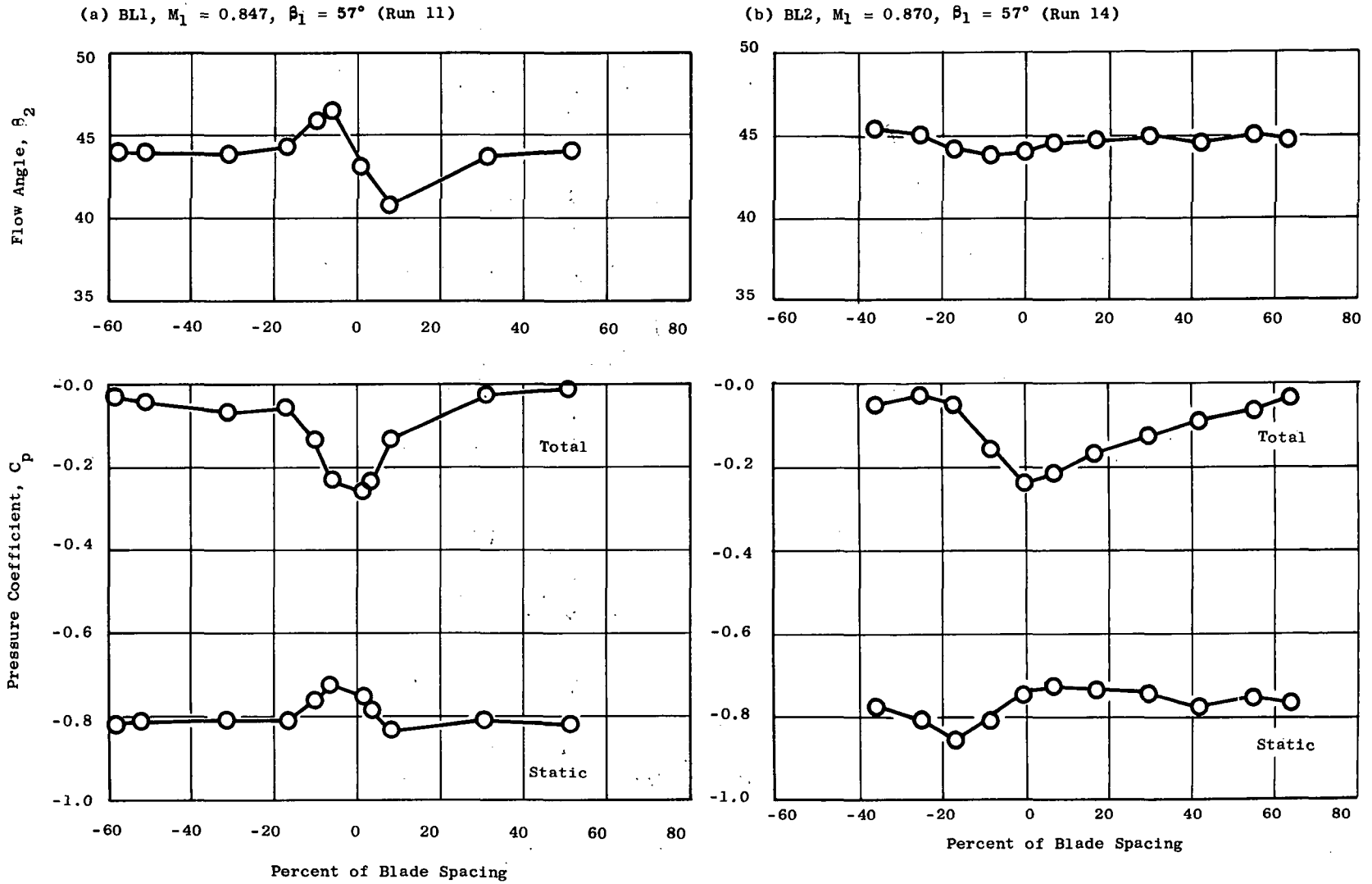


Figure 11. Effect of Serrations on Exit Flow Profiles at a Nominal Mach Number of 0.85 and an Inlet Air Angle of 57 Degrees.

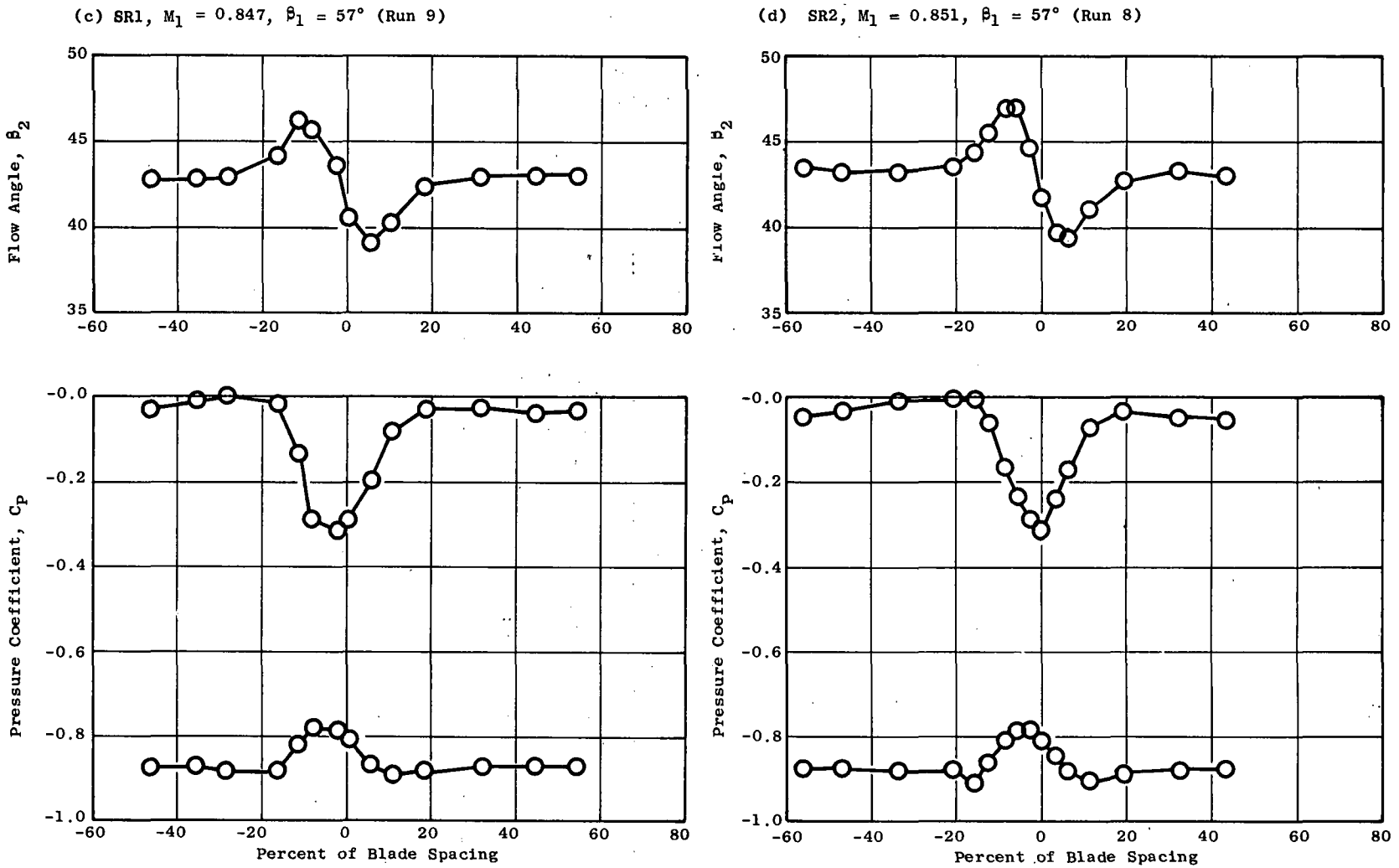


Figure 11. Effect of Serrations on Exit Flow Profiles at a Nominal Mach Number of 0.85 and an Inlet Air Angle of 57 Degrees (Continued).

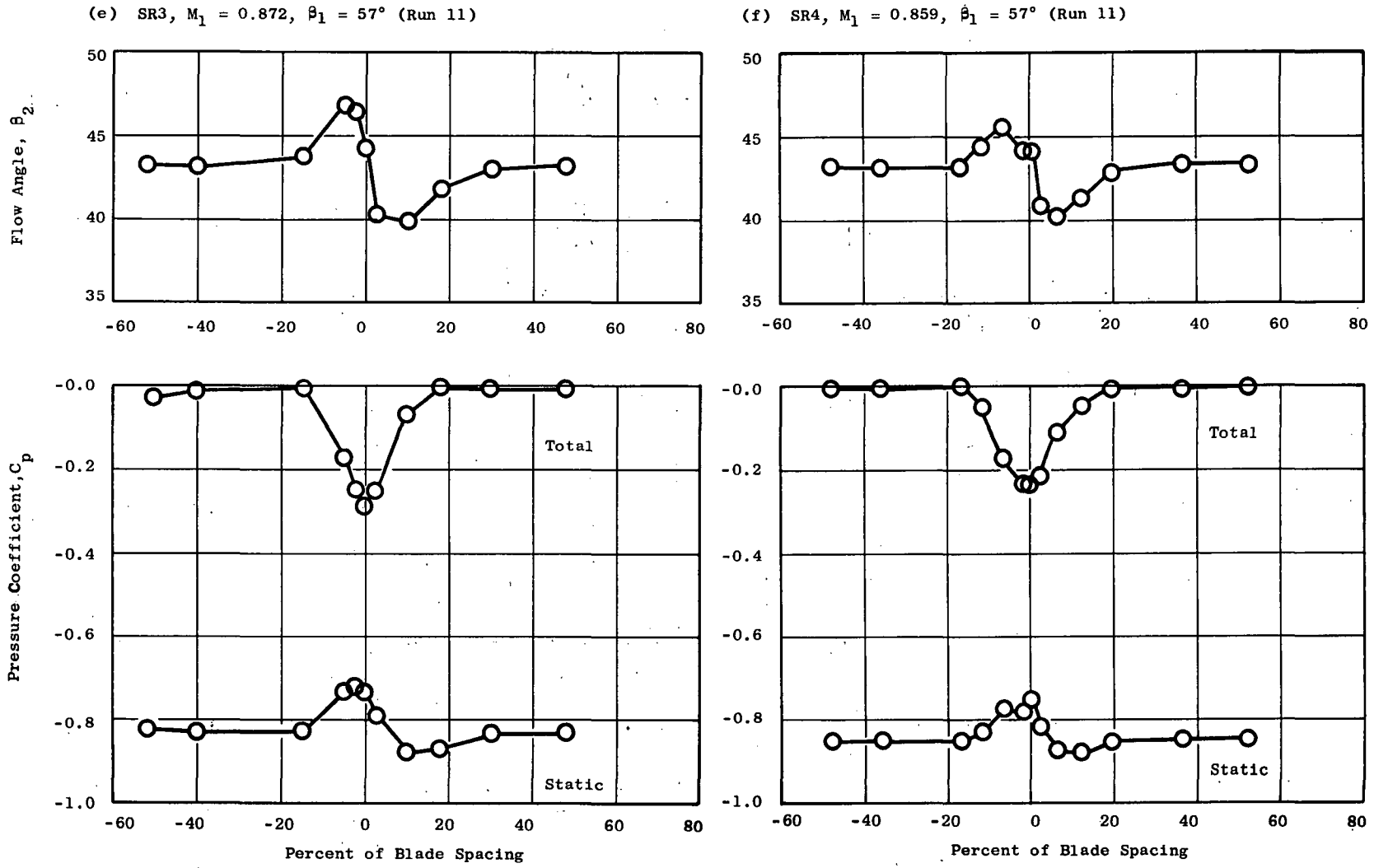


Figure 11. Effect of Serrations on Exit Flow Profiles at a Nominal Mach Number of 0.85 and an Inlet Air Angle of 57 Degrees (Continued).

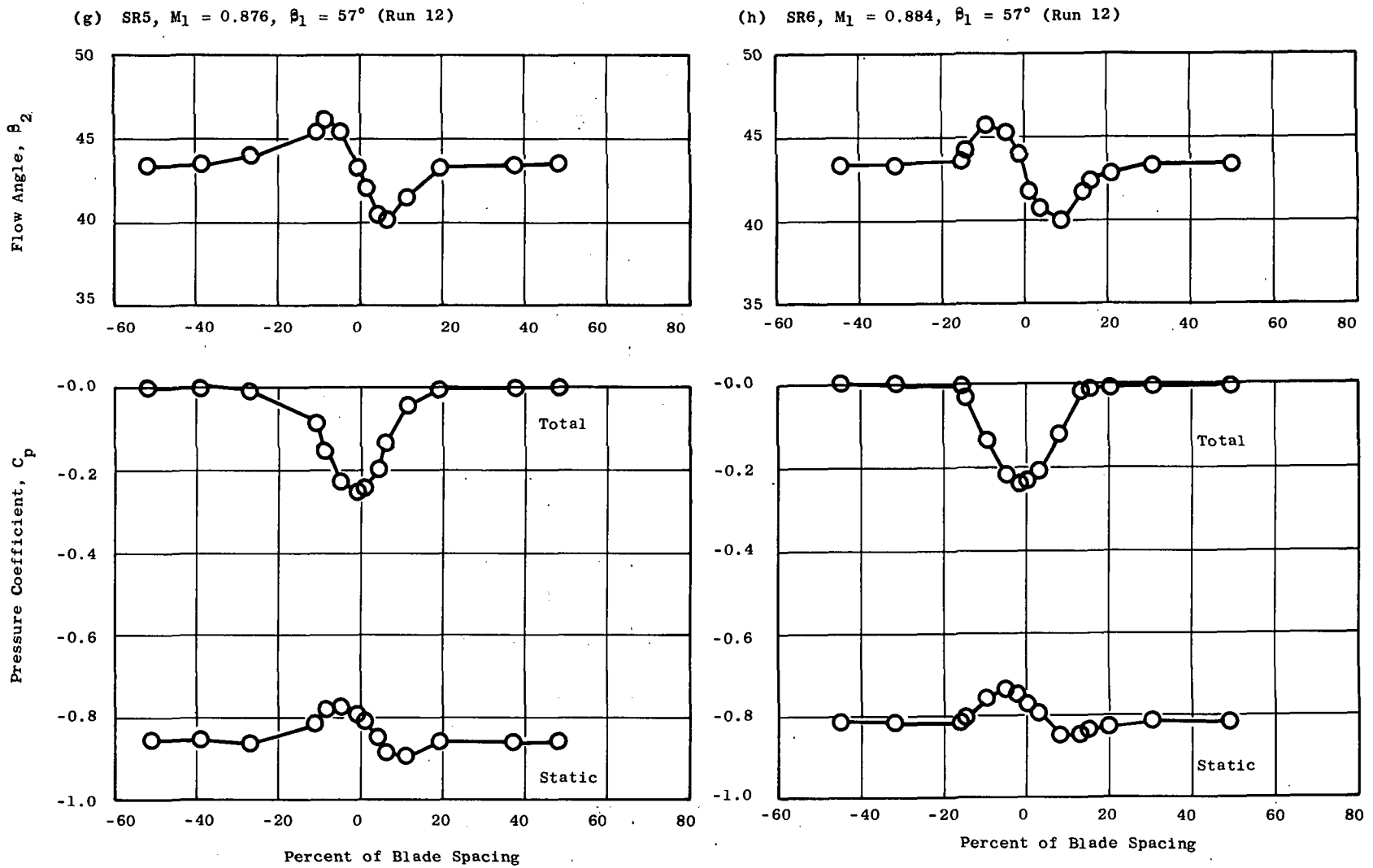


Figure 11. Effect of Serrations on Exit Flow Profiles at a Nominal Mach Number of 0.85 and an Inlet Air Angle of 57 Degrees (Concluded).

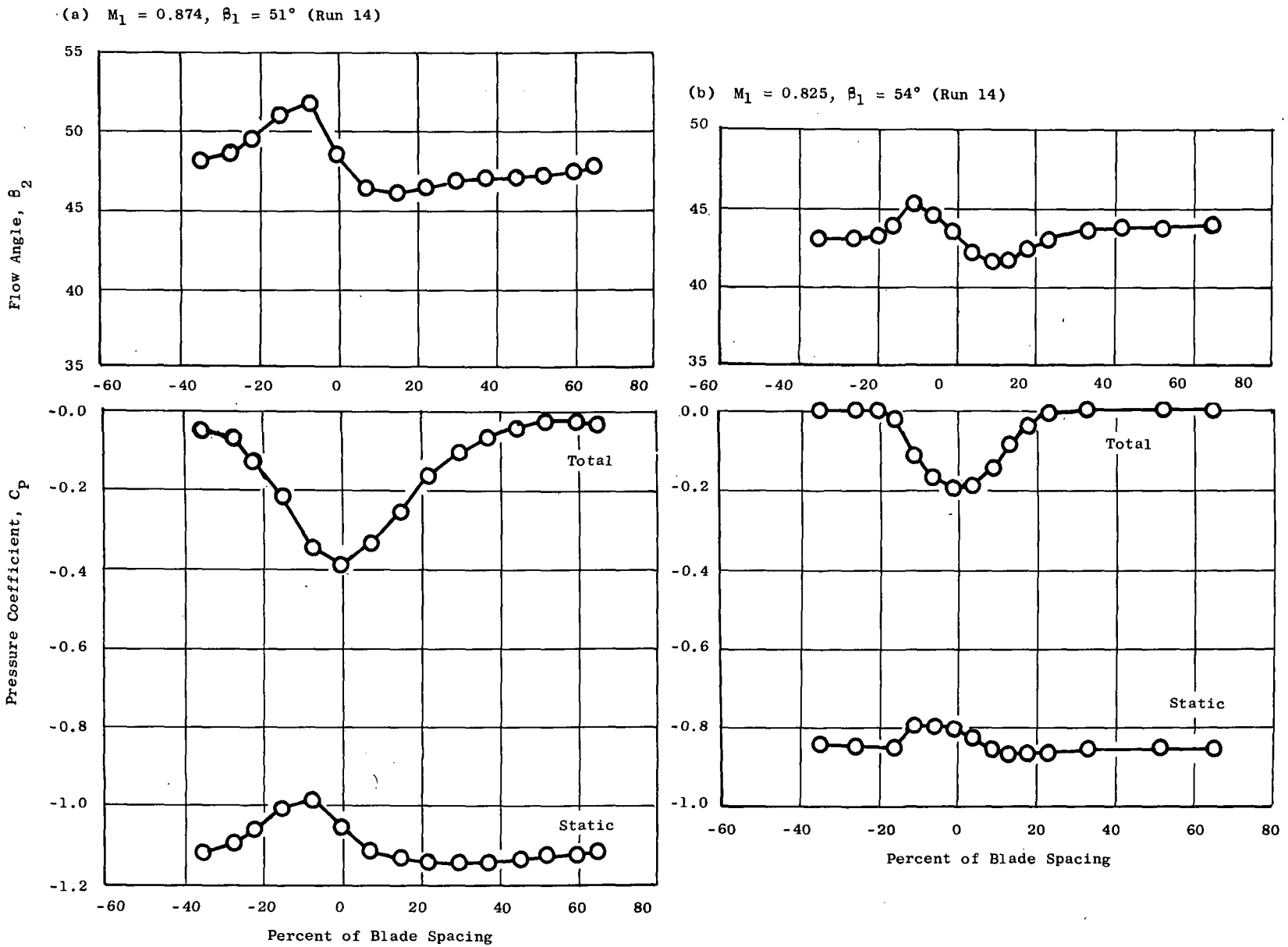


Figure 12. Effect of Inlet Air Angle on Exit Flow Profiles, Configuration BL2.

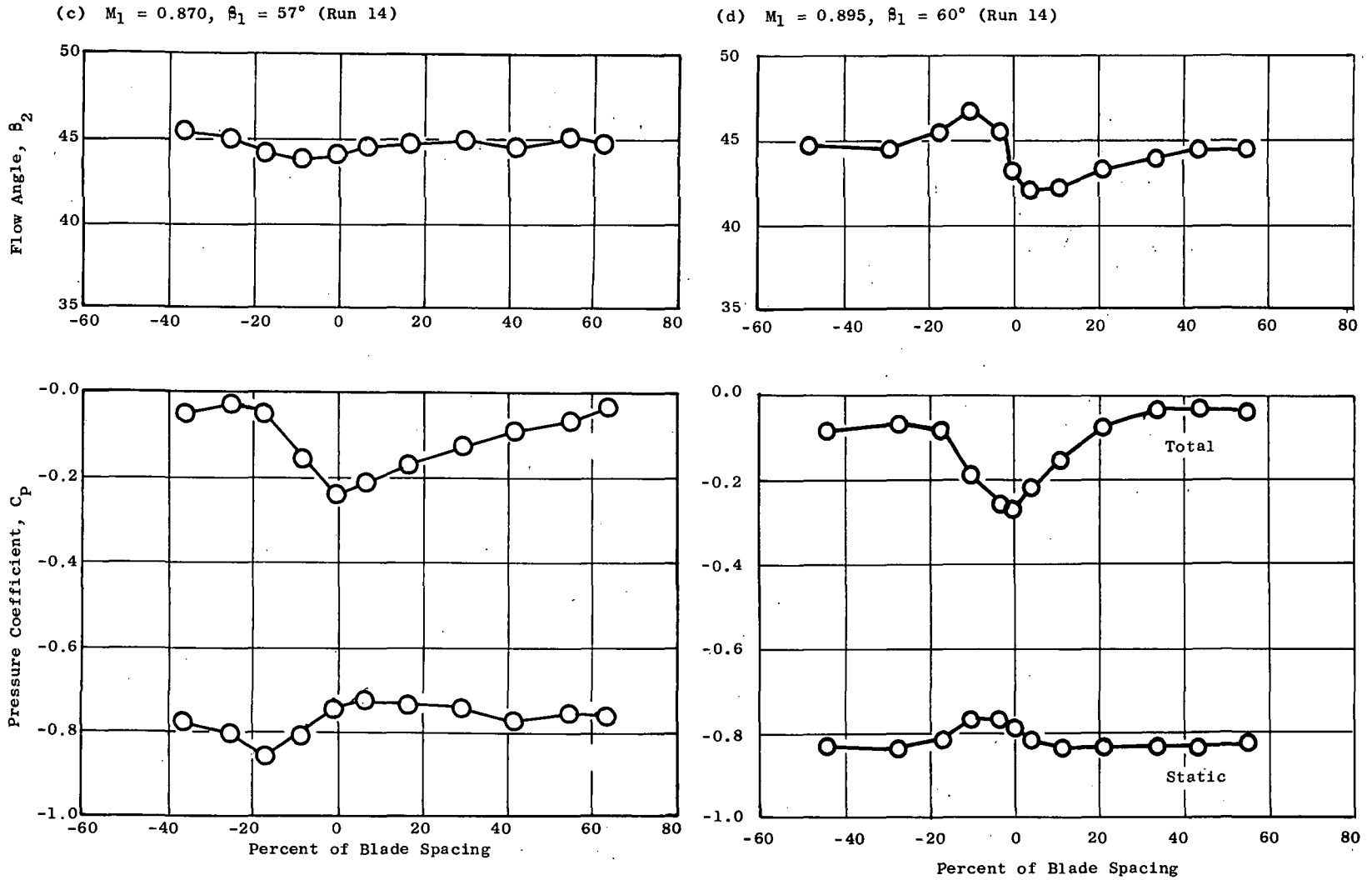


Figure 12. Effect of Inlet Air Angle on Exit Flow Profiles, Configuration BL2 (Concluded).

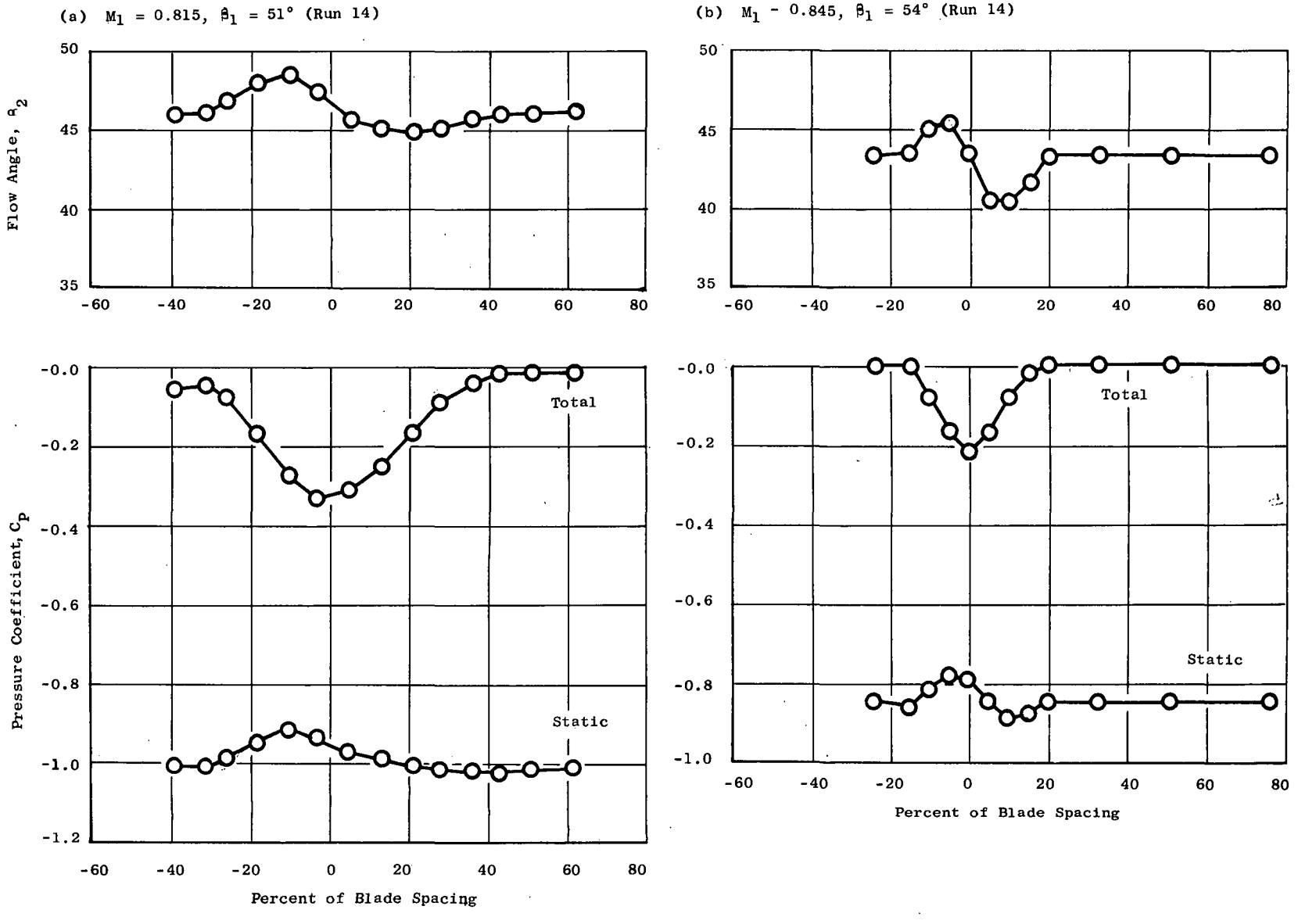


Figure 13. Effect of Inlet Air Angle on Exit Flow Profiles, Configuration SR6.

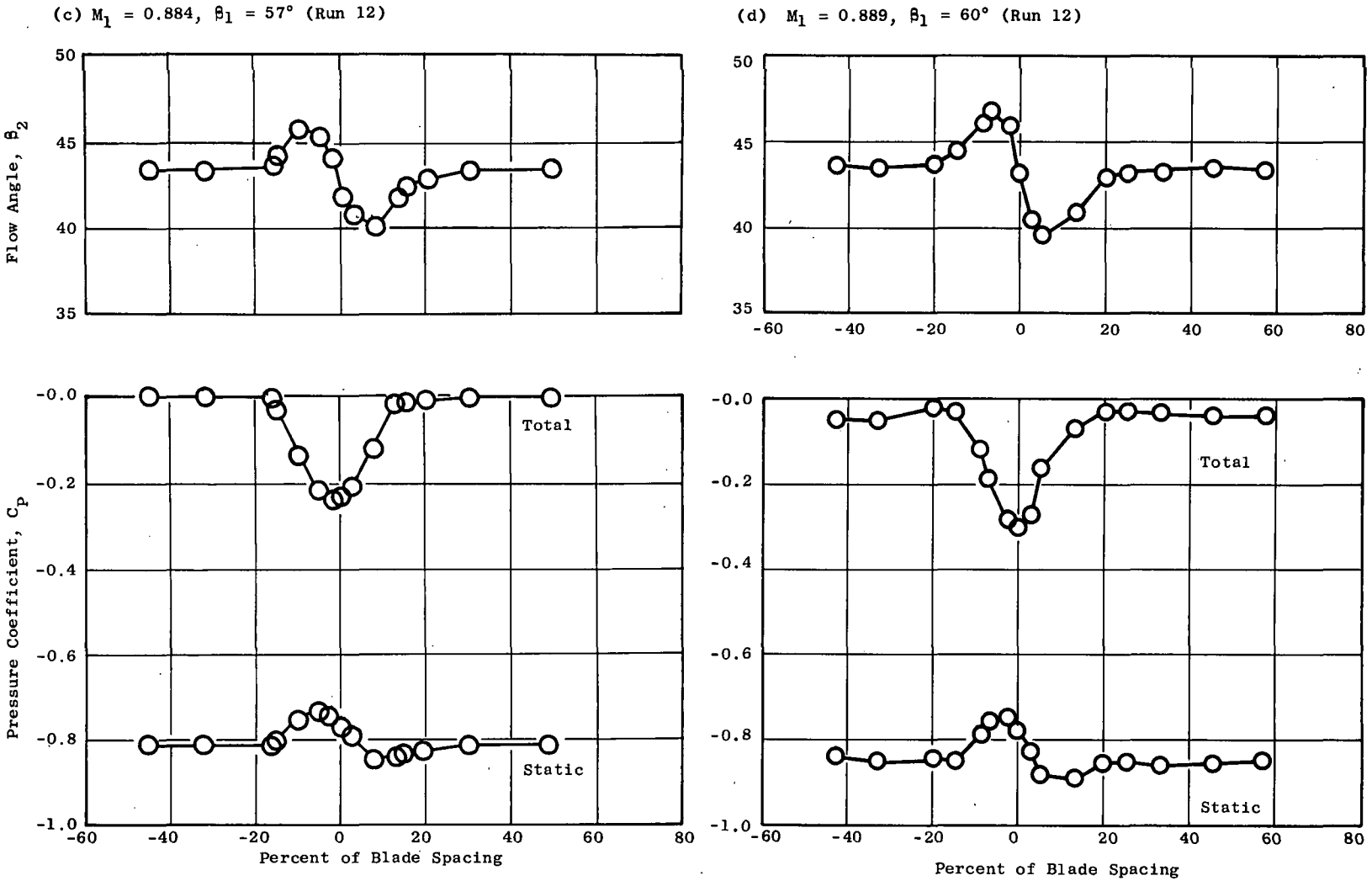


Figure 13. Effect of Inlet Air Angle on Exit Flow Profiles, Configuration SR6 (Concluded).

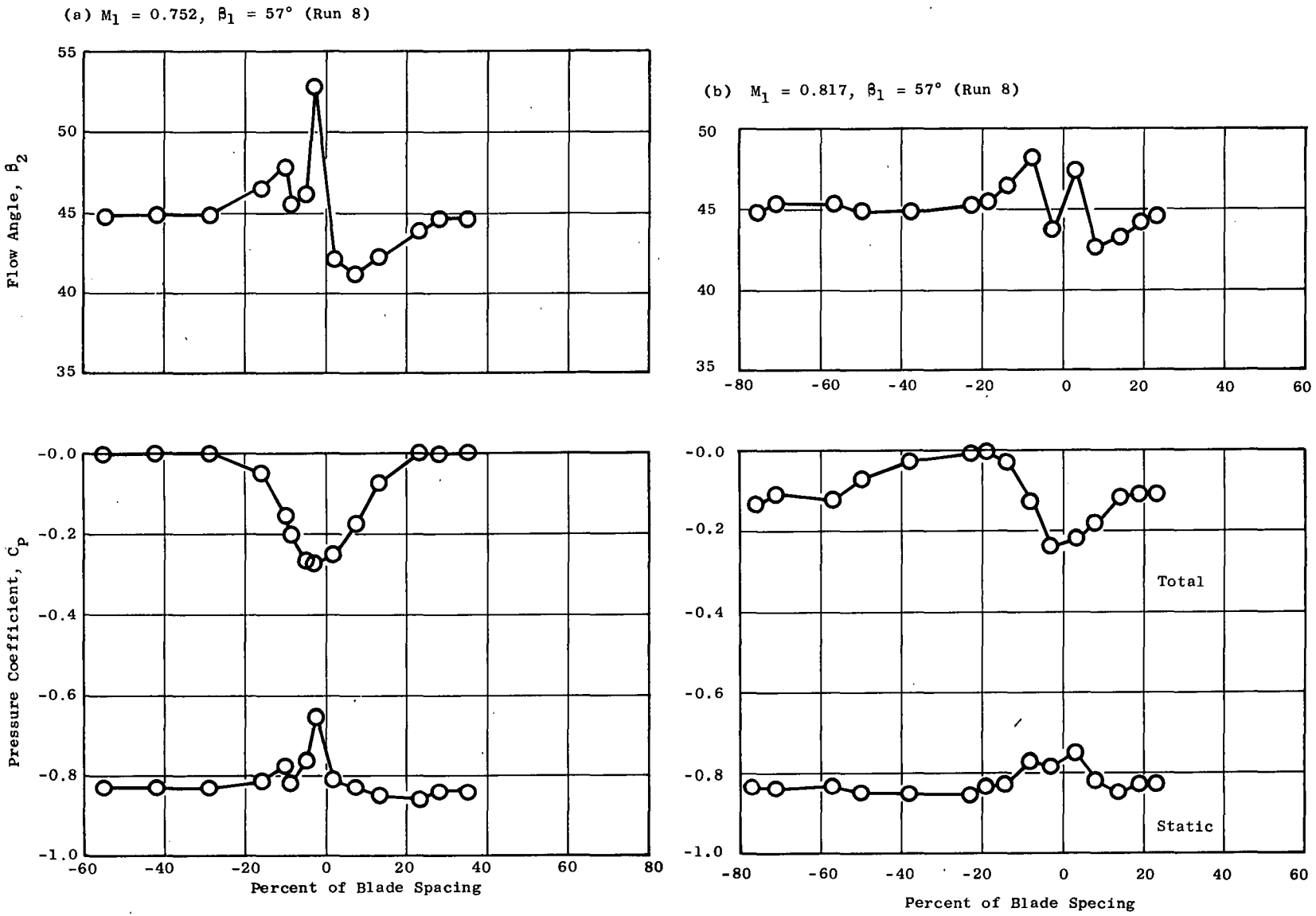


Figure 14. Effect of Inlet Mach Number on Exit Flow Profiles, Configuration BL1.

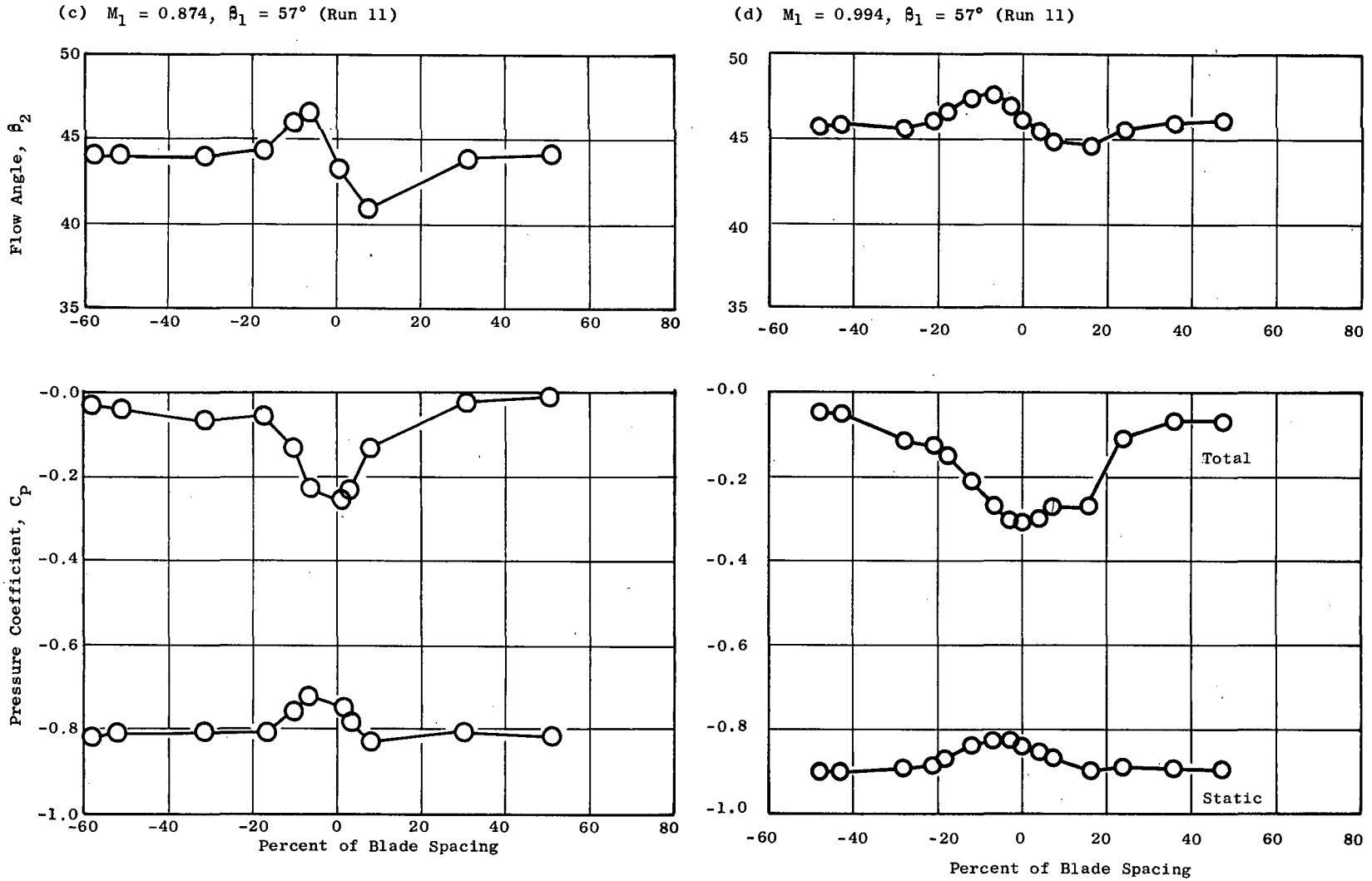


Figure 14. Effect of Inlet Mach Number on Exit Flow Profiles, Configuration BL1 (Concluded).

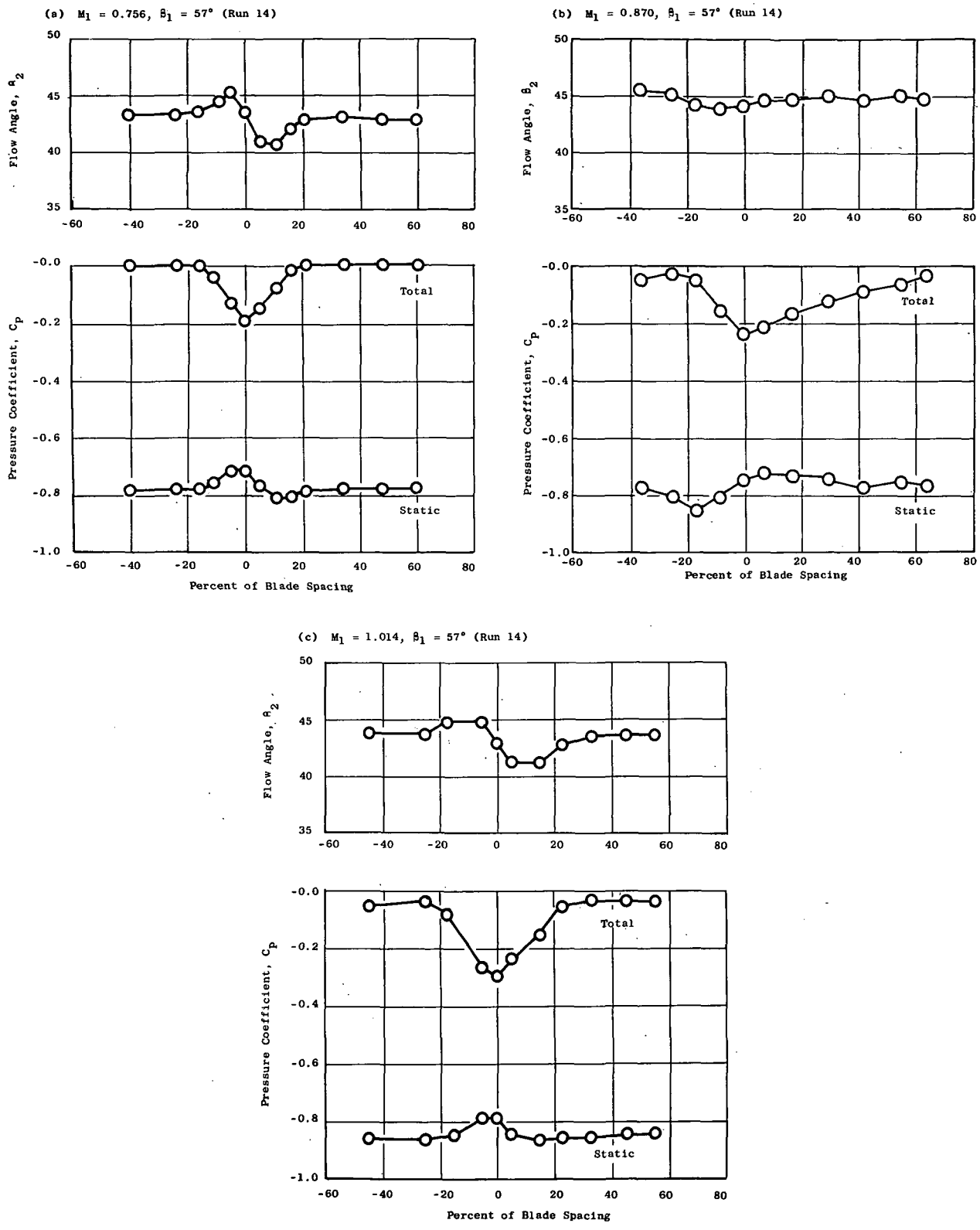


Figure 15. Effect of Inlet Mach Number on Exit Flow Profiles, Configuration BL2.

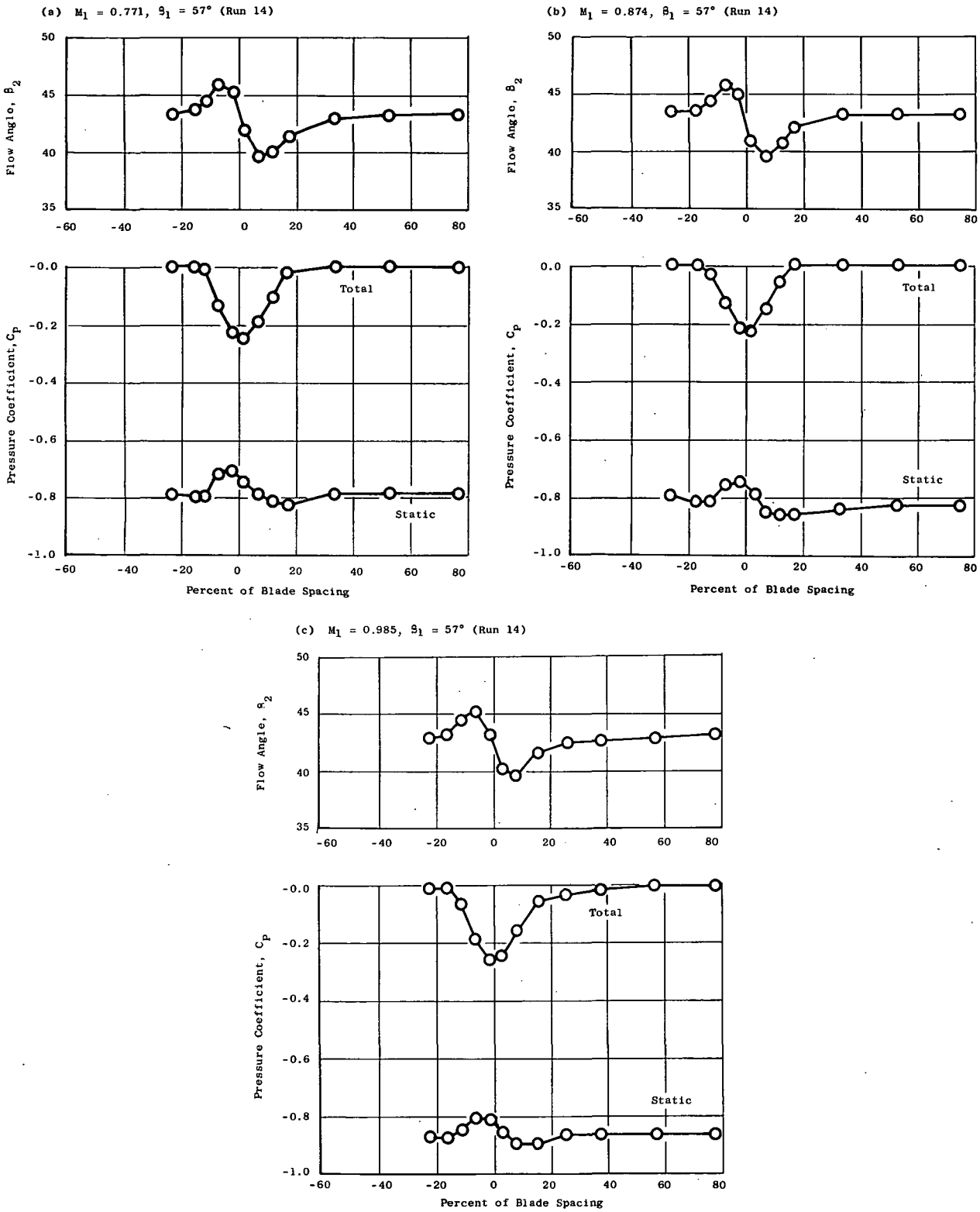


Figure 16. Effect of Inlet Mach Number on Exit Flow Profiles, Configuration SR6.

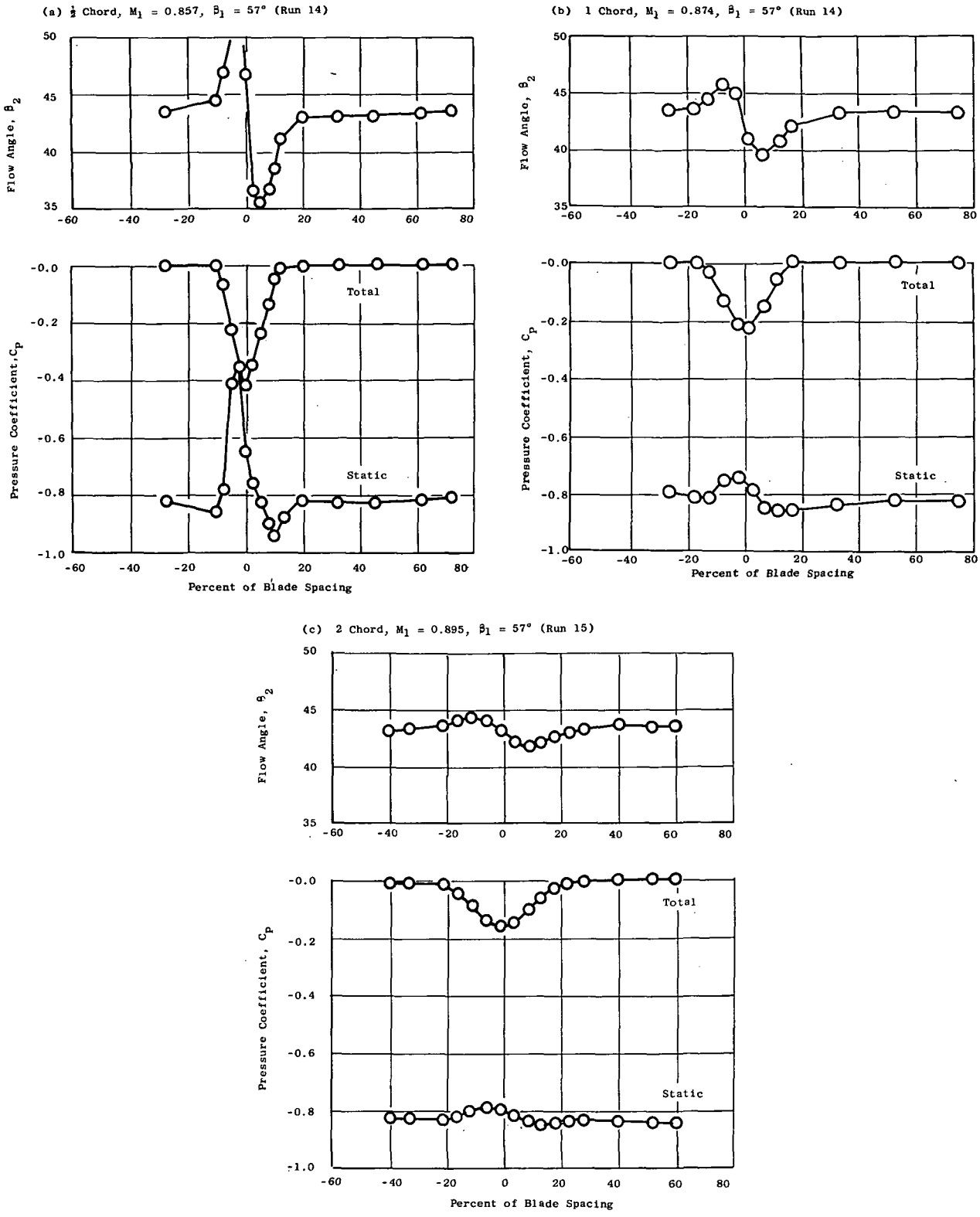


Figure 17. Effect of Traverse Location of Exit Flow Profiles, Configuration SR6.

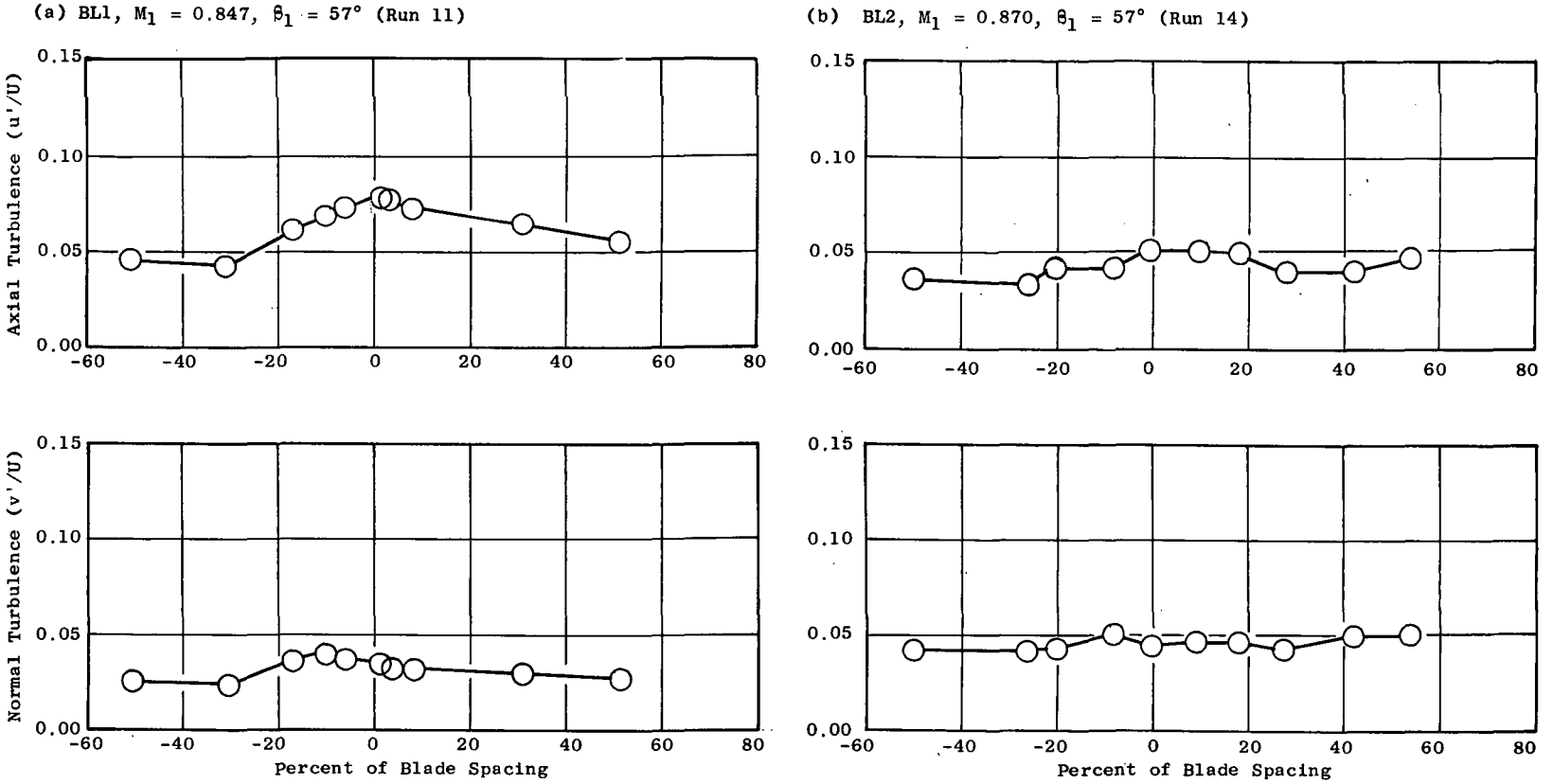


Figure 18. Effect of Serrations on Exit Turbulence Profiles at a Nominal Mach Number of 0.85 and an Inlet Air Angle of 57 Degrees.

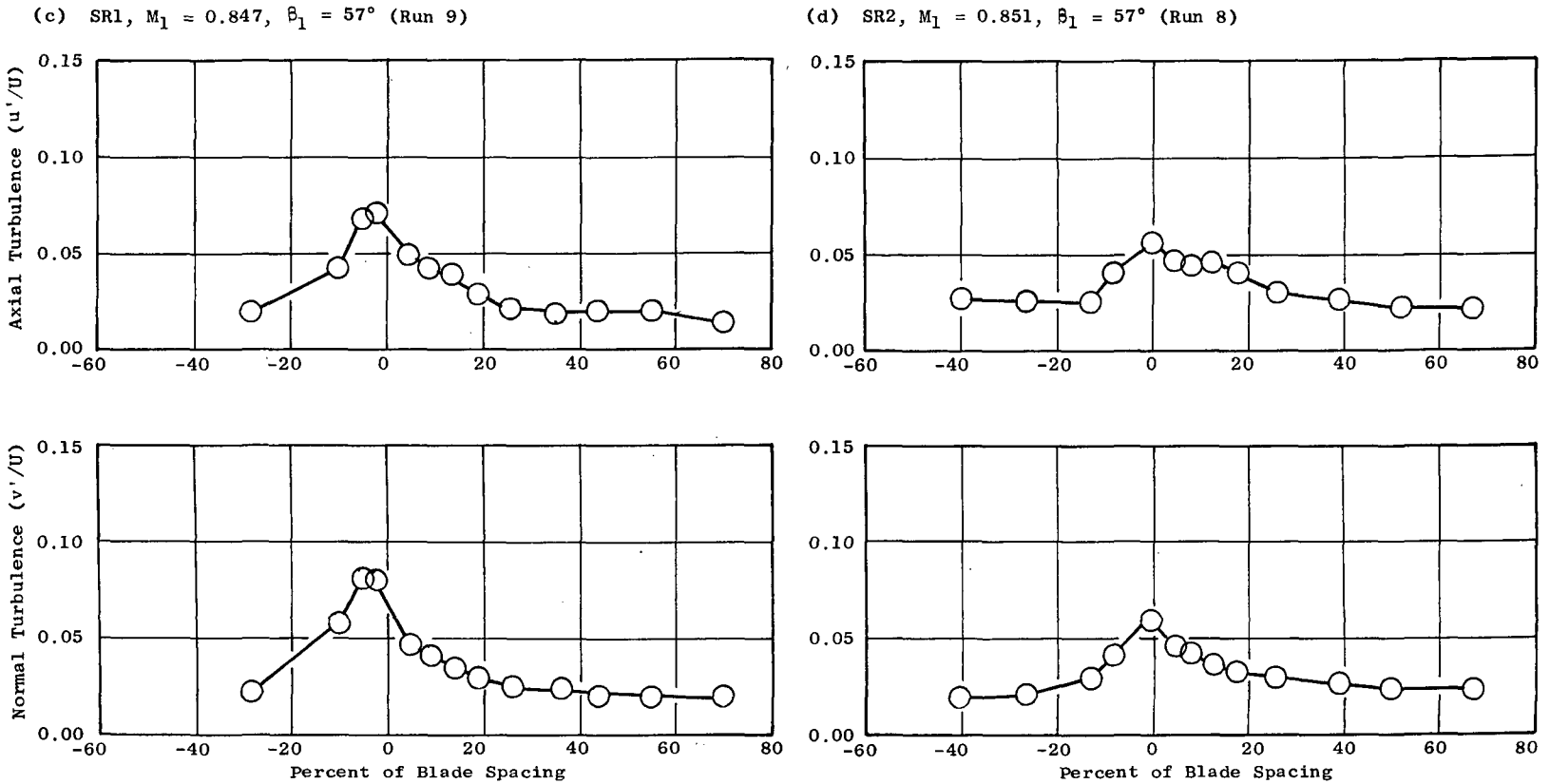


Figure 18. Effect of Serrations on Exit Turbulence Profiles at a Nominal Mach Number of 0.85 and an Inlet Air Angle of 57 Degrees (Continued).

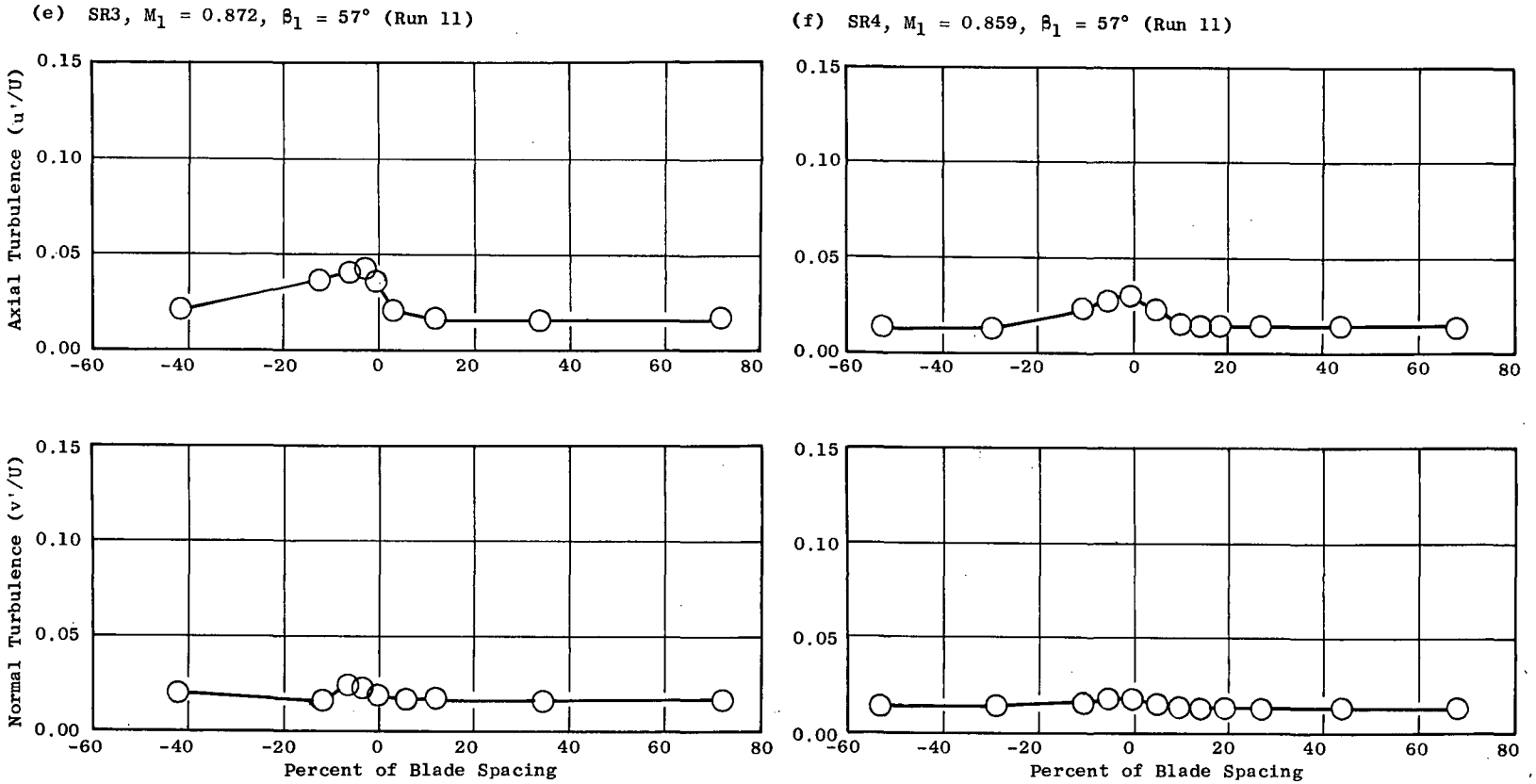


Figure 18. Effect of Serrations on Exit Turbulence Profiles at a Nominal Mach Number of 0.85 and an Inlet Air Angle of 57 Degrees (Continued).

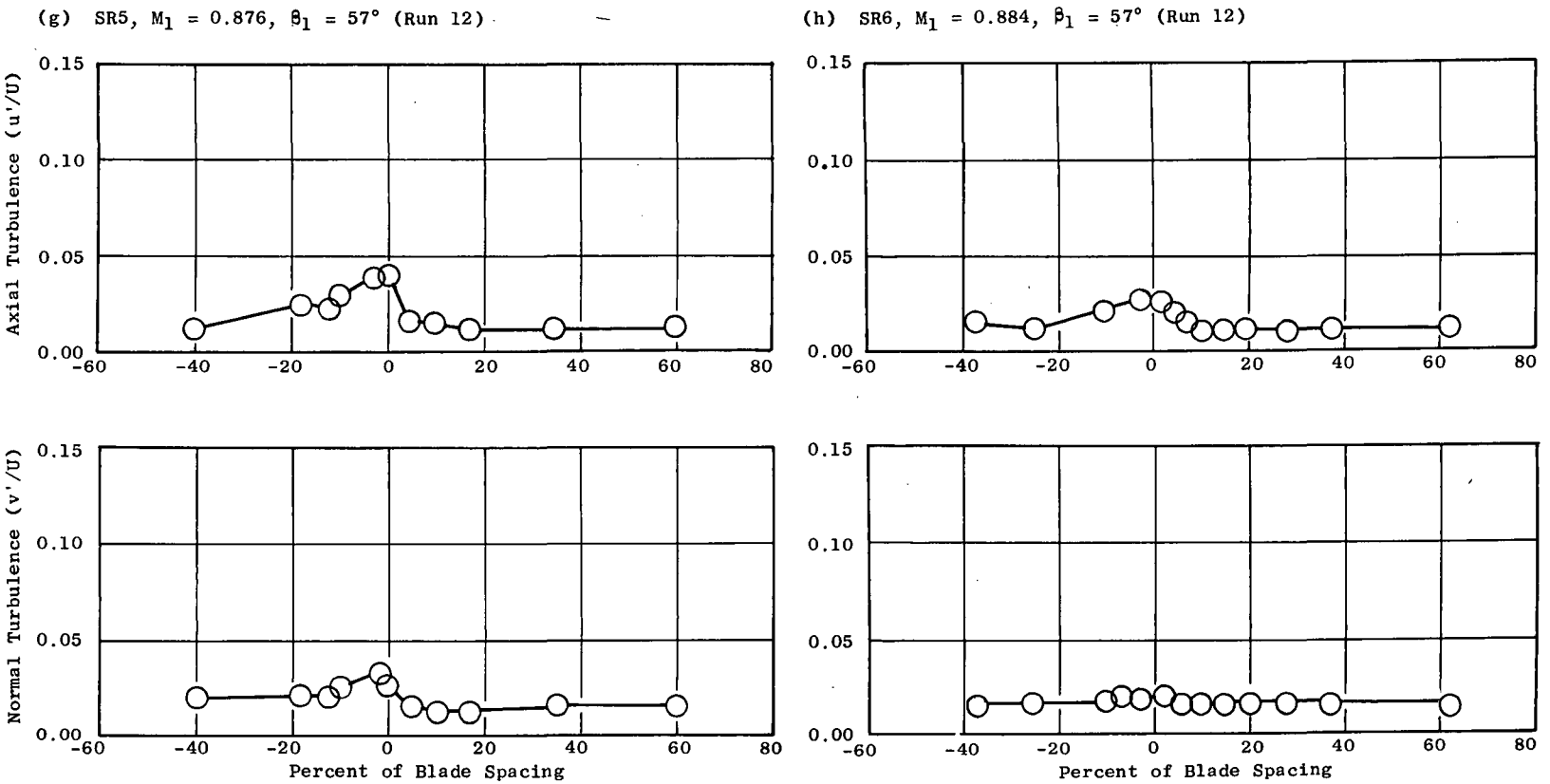


Figure 18. Effect of Serrations on Exit Turbulence Profiles at a Nominal Mach Number of 0.85 and an Inlet Air Angle of 57 Degrees (Concluded).

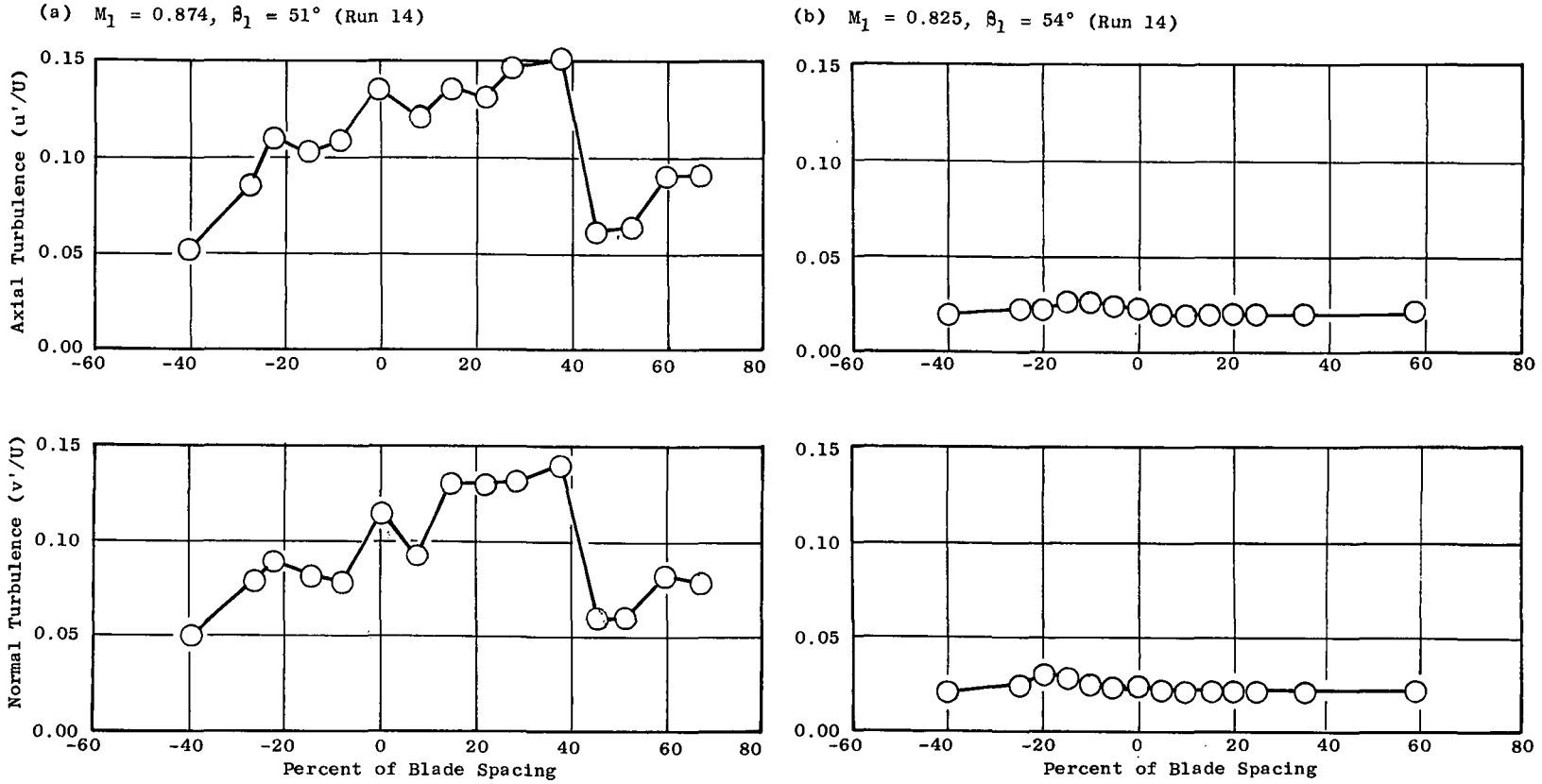


Figure 19. Effect of Inlet Air Angle on Exit Turbulence Profiles, Configuration BL2.

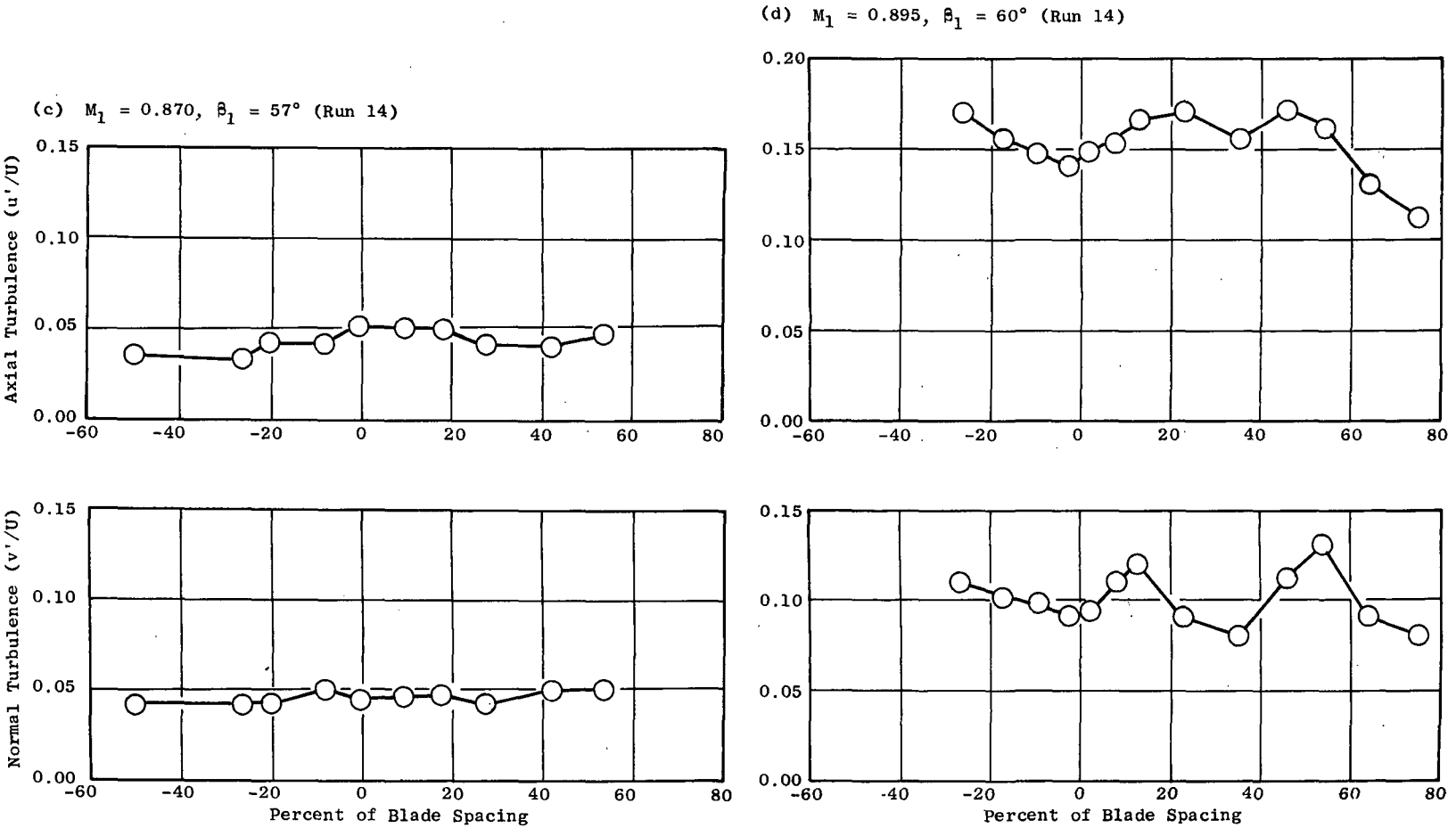


Figure 19. Effect of Inlet Air Angle on Exit Turbulence Profiles, Configuration BL2 (Concluded).

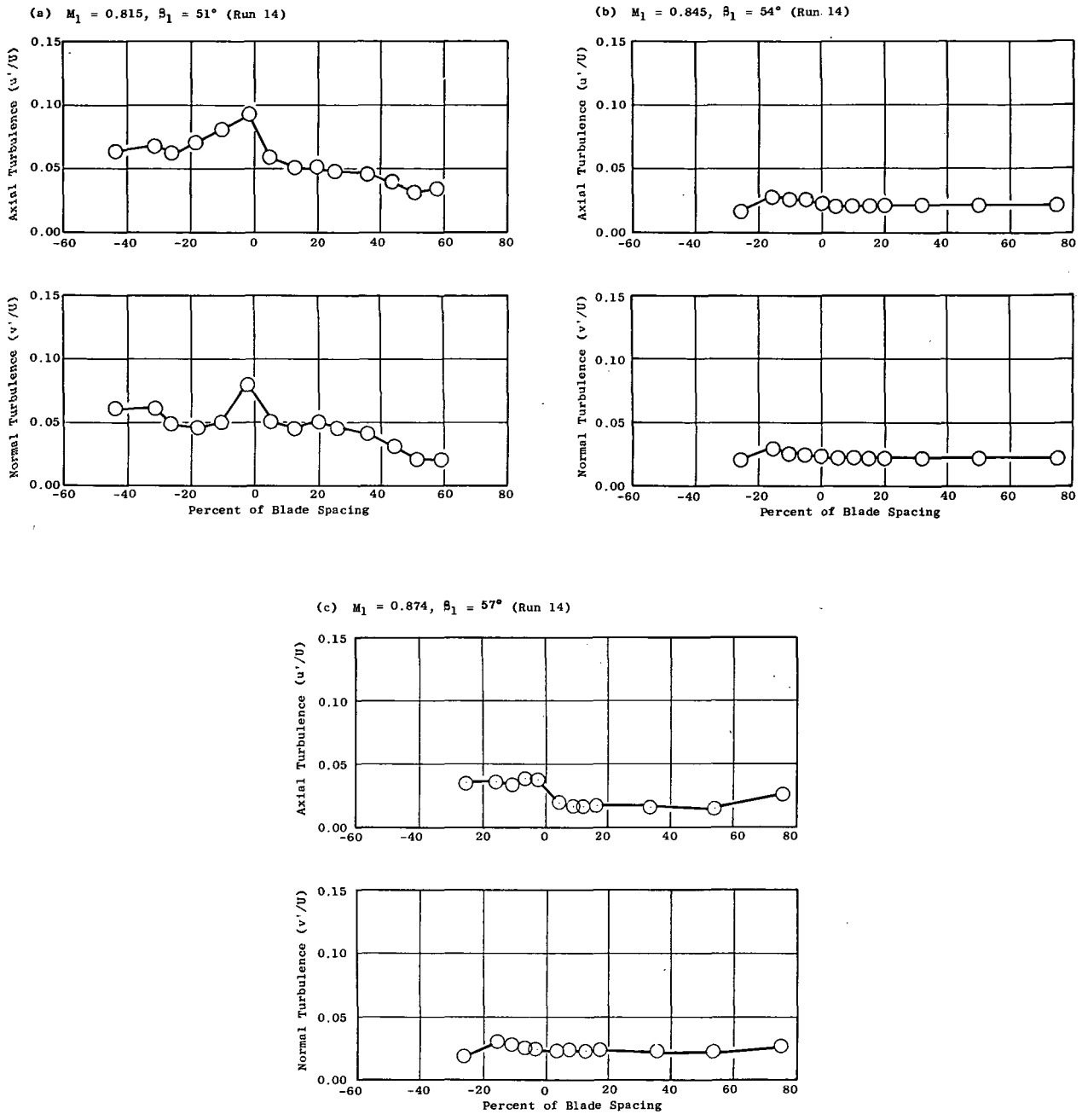


Figure 20. Effect of Inlet Air Angle on Exit Turbulence Profiles, Configuration SR6.

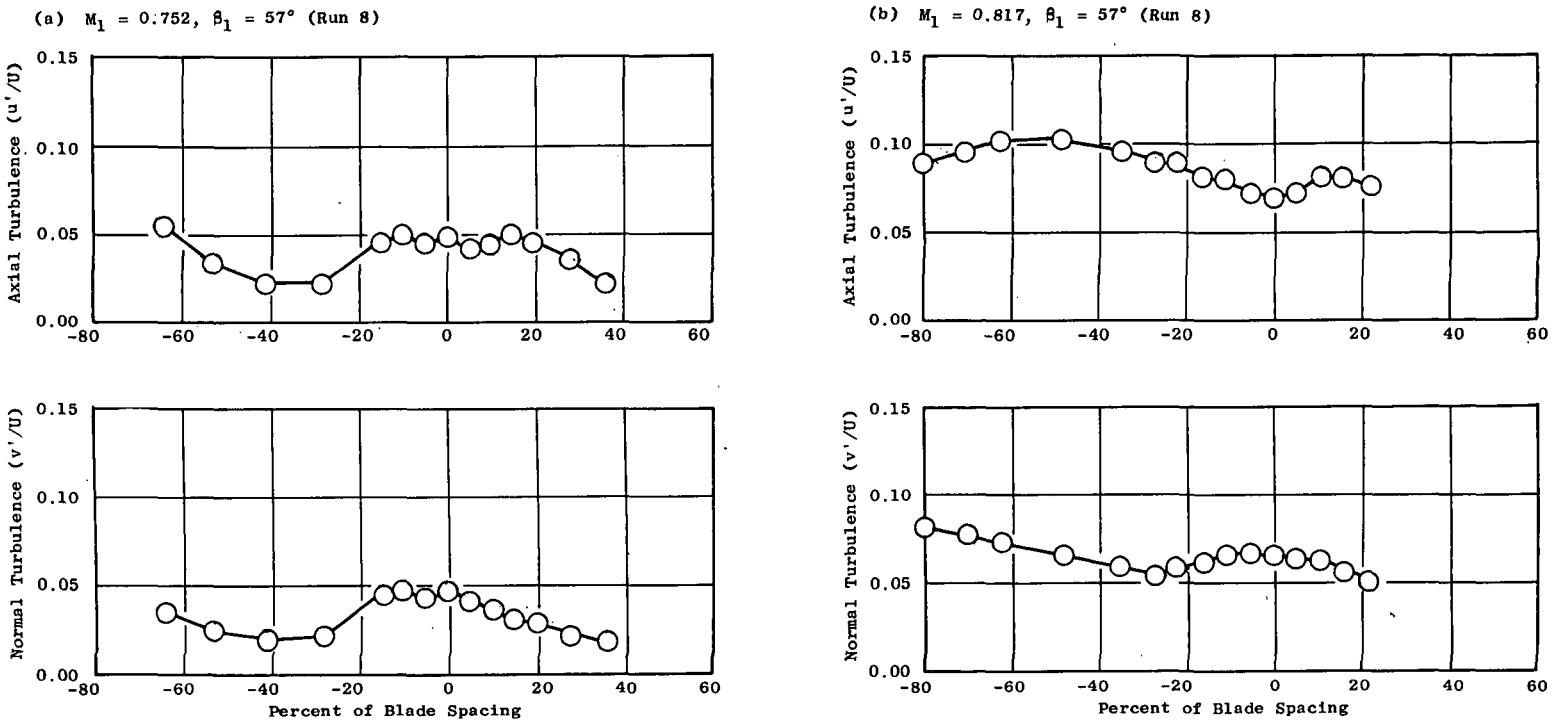


Figure 21. Effect of Inlet Mach Number on Exit Turbulence Profiles, Configuration BL1.

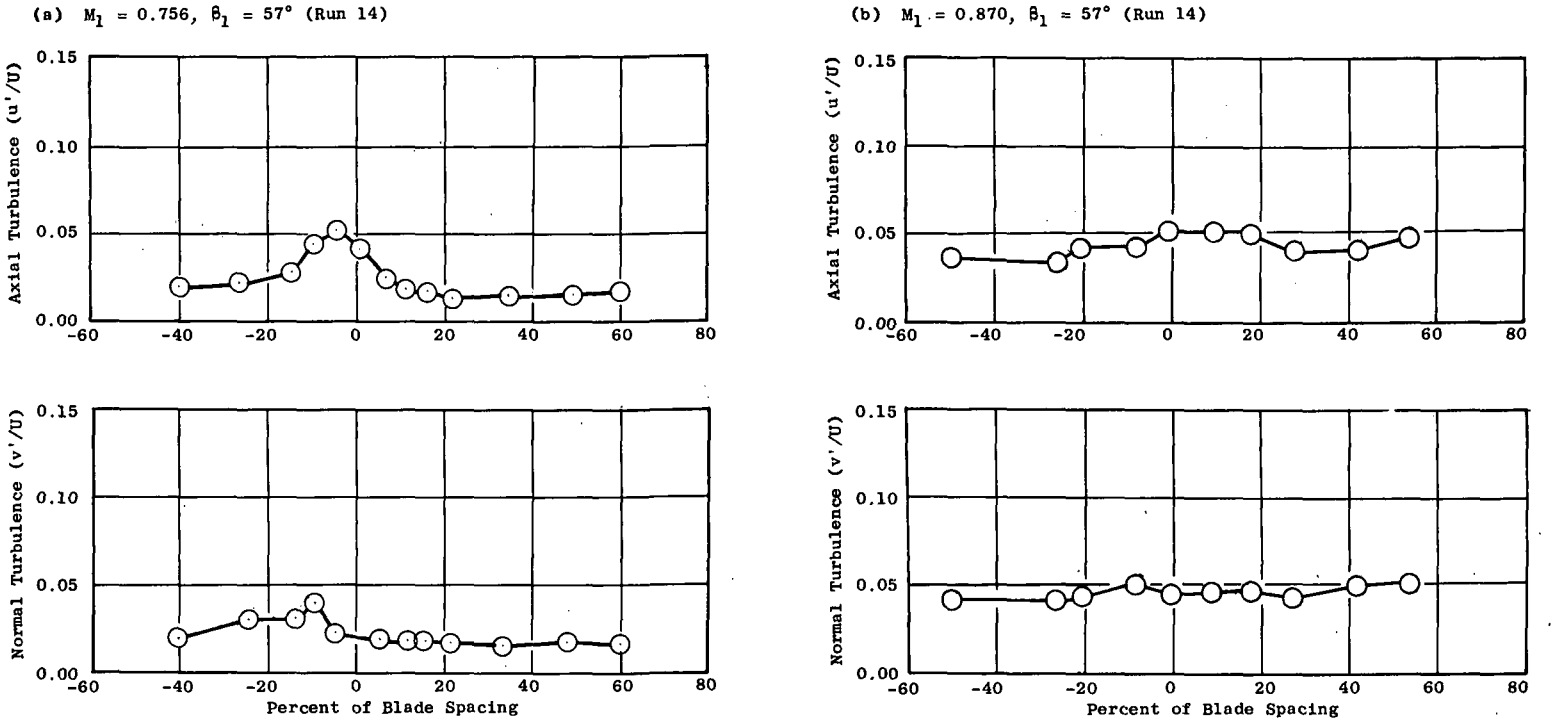


Figure 22. Effect of Inlet Mach Number on Exit Turbulence Profiles, Configuration BL2.

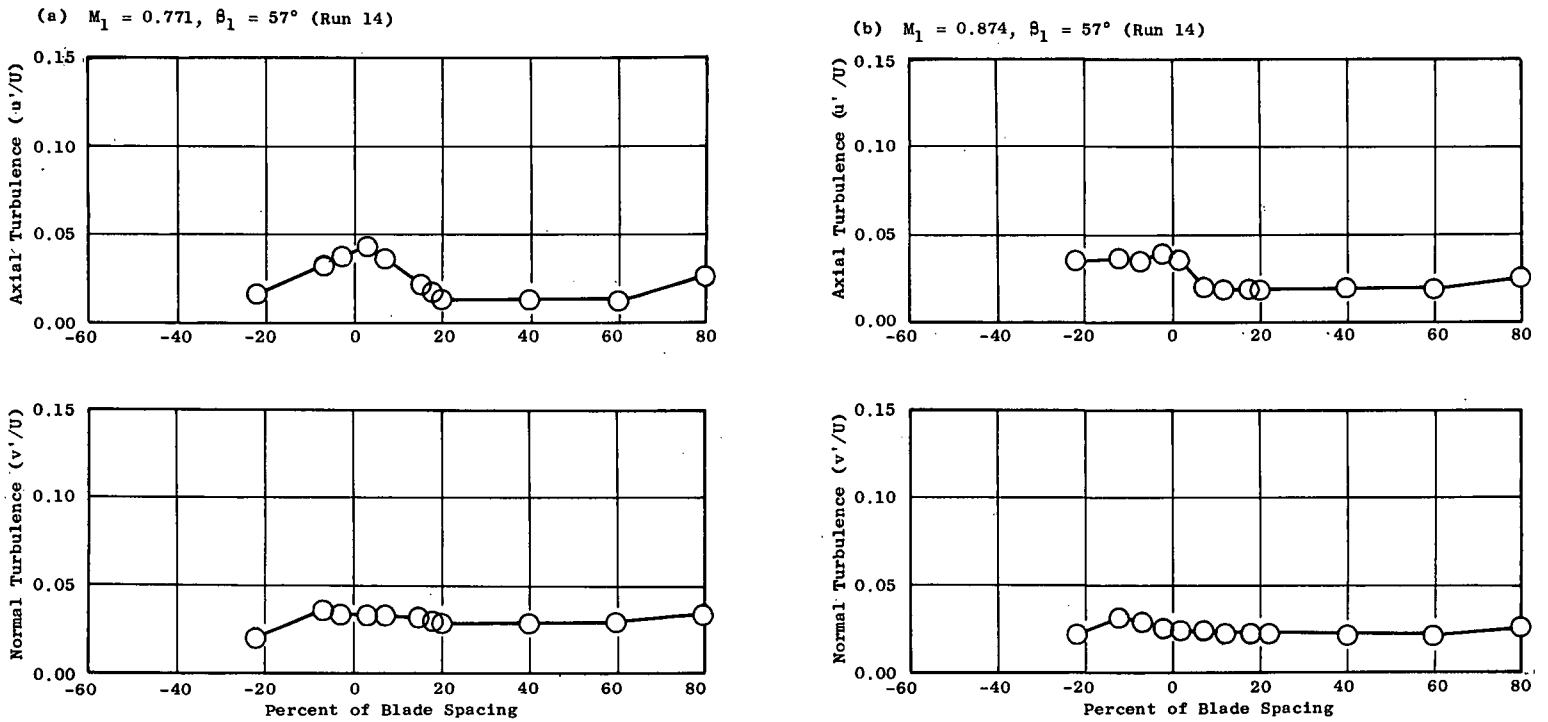


Figure 23. Effect of Inlet Mach Number on Exit Turbulence Profiles, Configuration SR6.

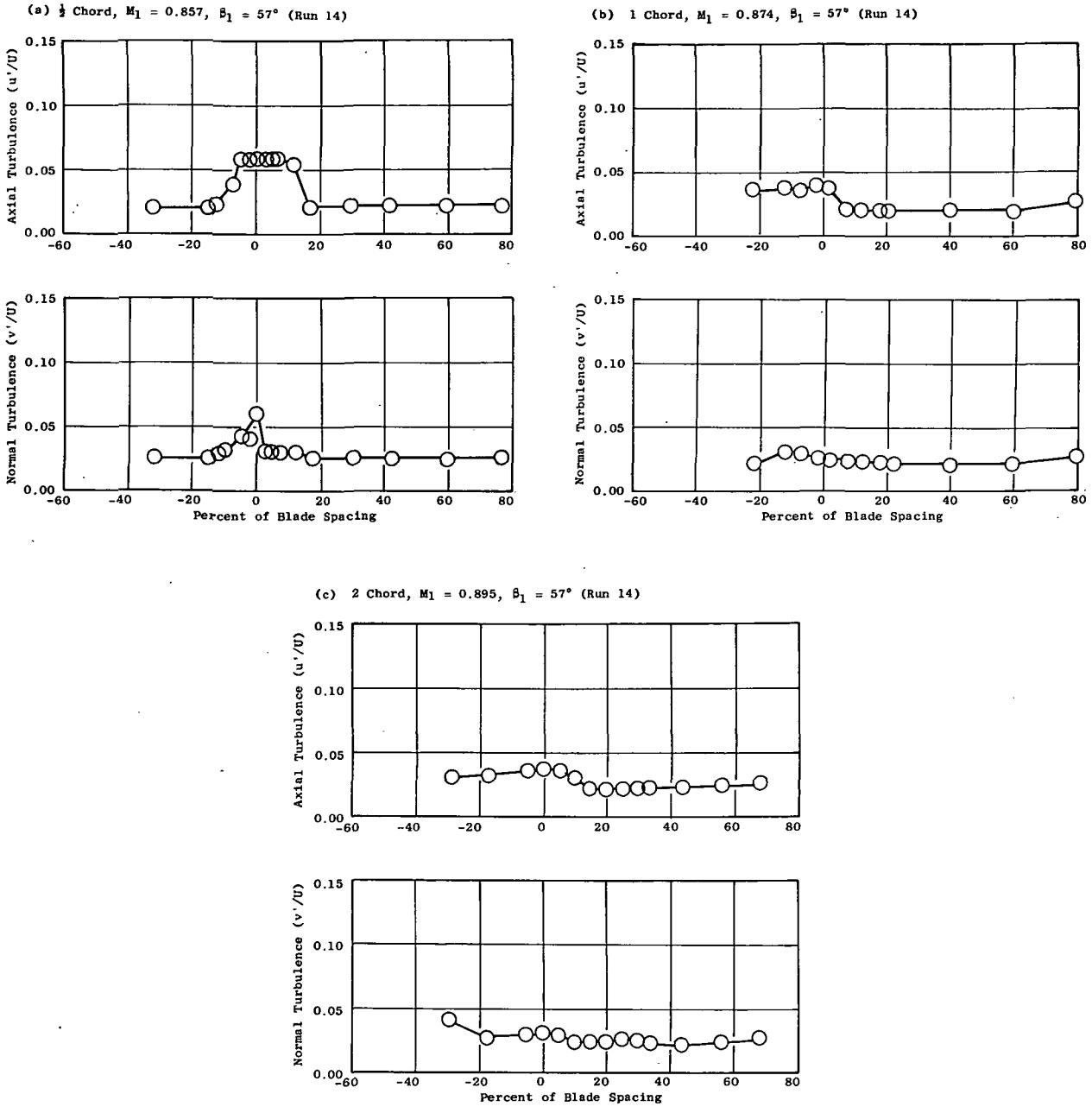


Figure 24. Effect of Traverse Location on Exit Turbulence Profiles, Configuration SR6.

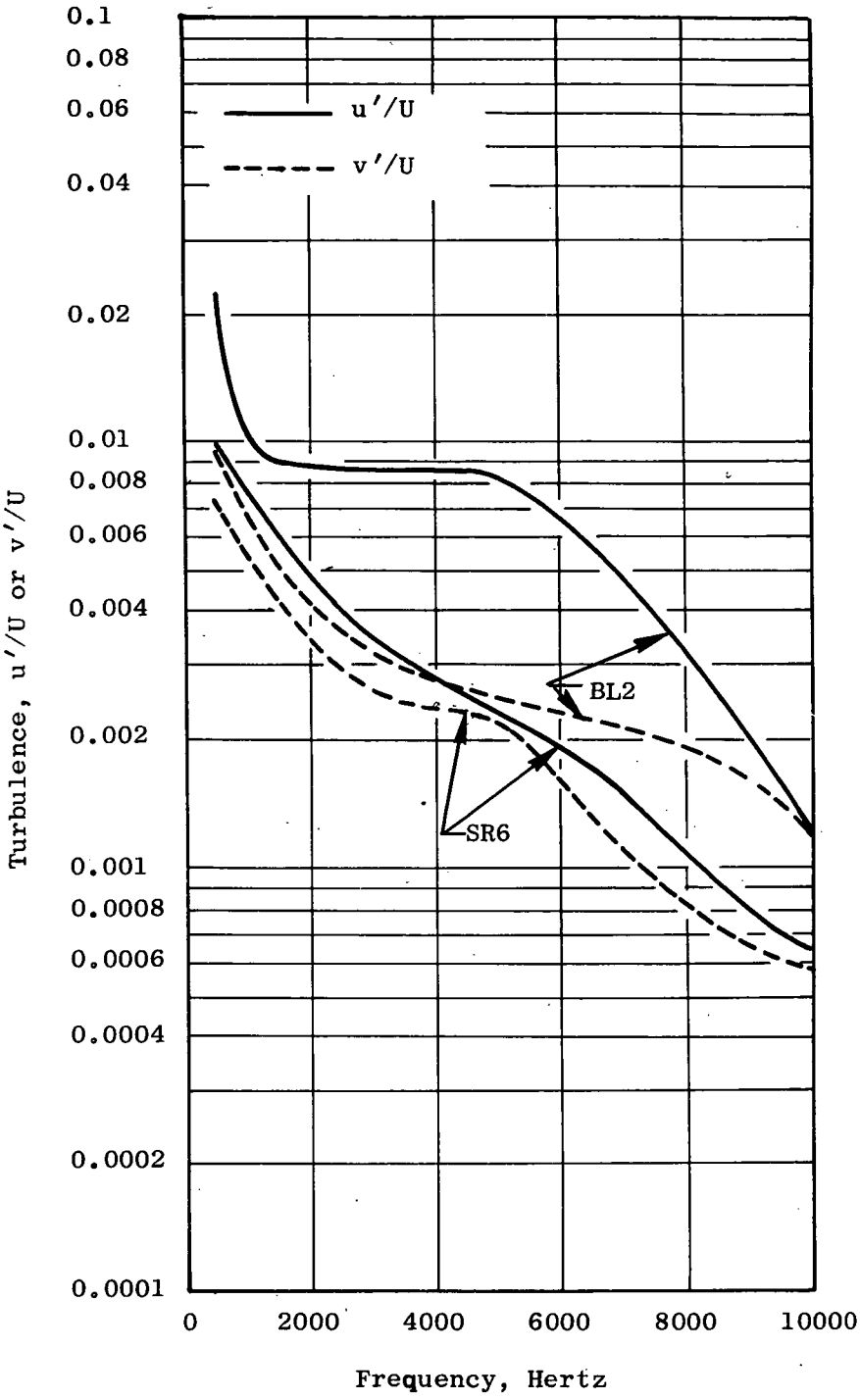


Figure 25. Effects of Serrations on Wake Turbulence Spectrums, Mach = 0.85, $\beta_1$ = 57 Degrees.

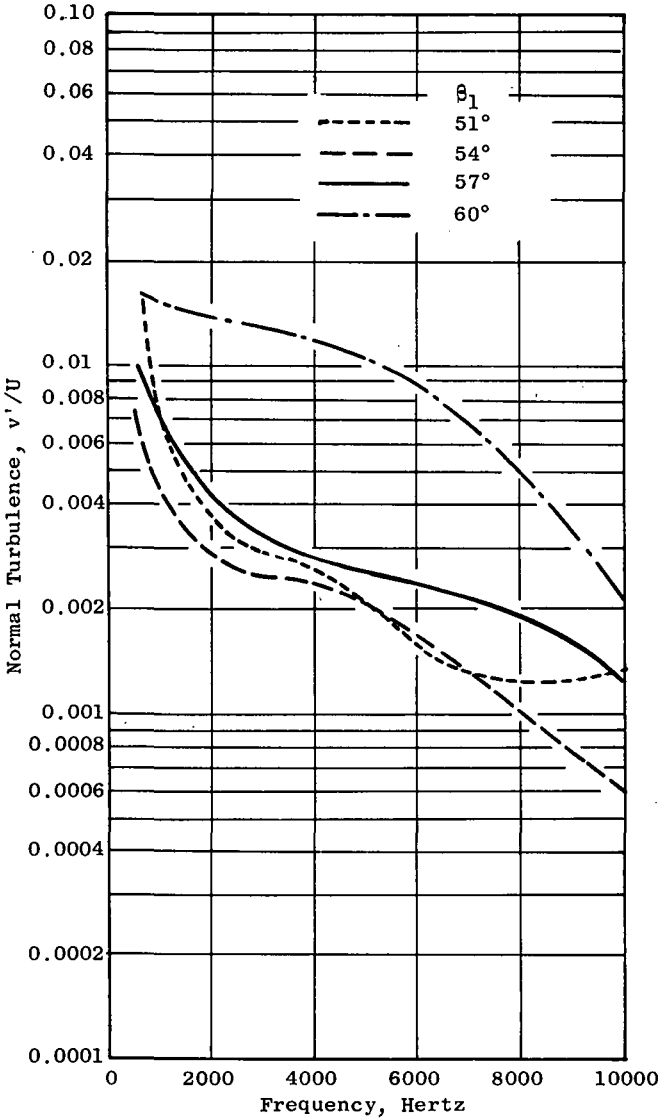


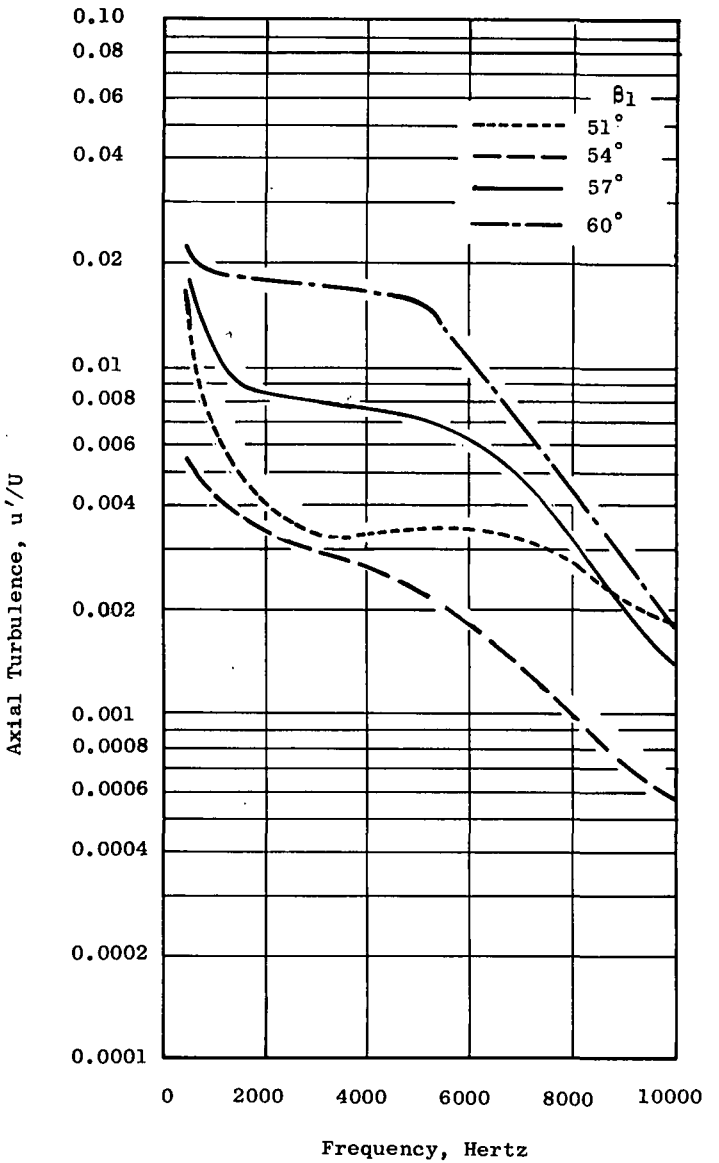


Figure 26. Effects of Inlet Air Angle on Wake Turbulence Spectrums, Configuration BL2, Mach = 0.85.

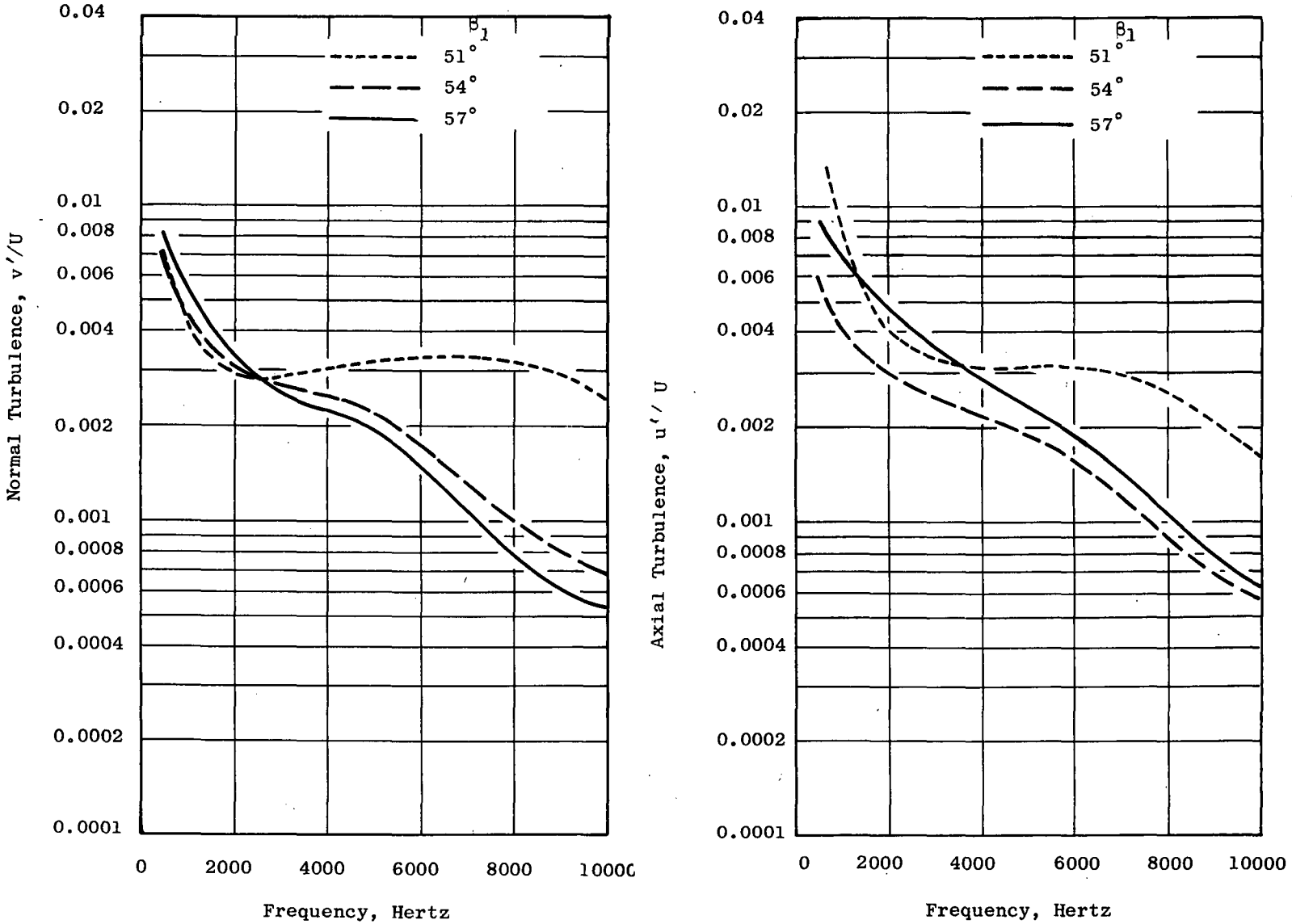


Figure 27. Effect of Inlet Air Angle on Wake Turbulence Spectrums, Configuration SR6, Mach = 0.85.

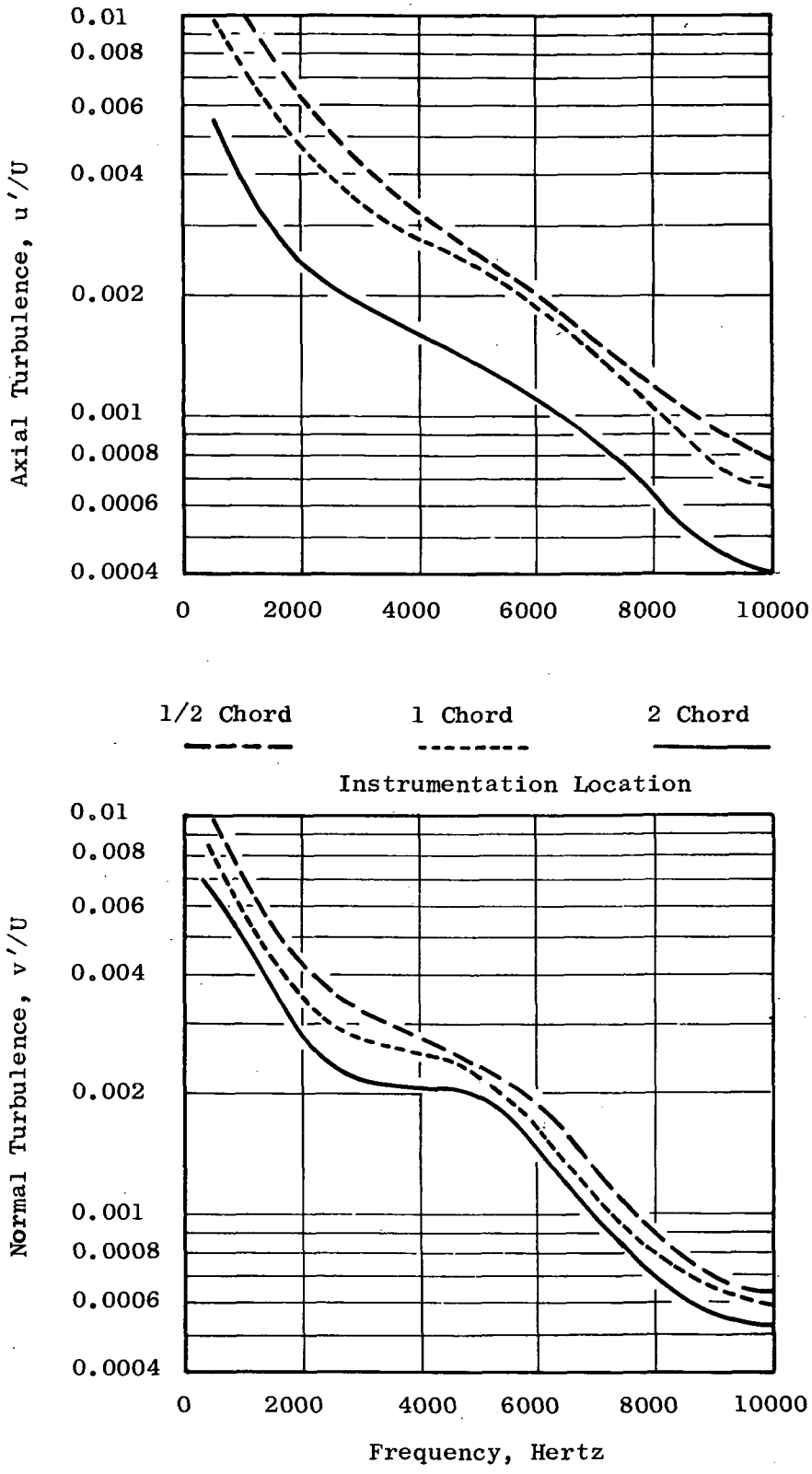


Figure 28. Effects of Measurement Location on Wake Turbulence Spectrums, Configuration SR6, Mach = 0.85, $\beta_1$ = 57 Degrees.

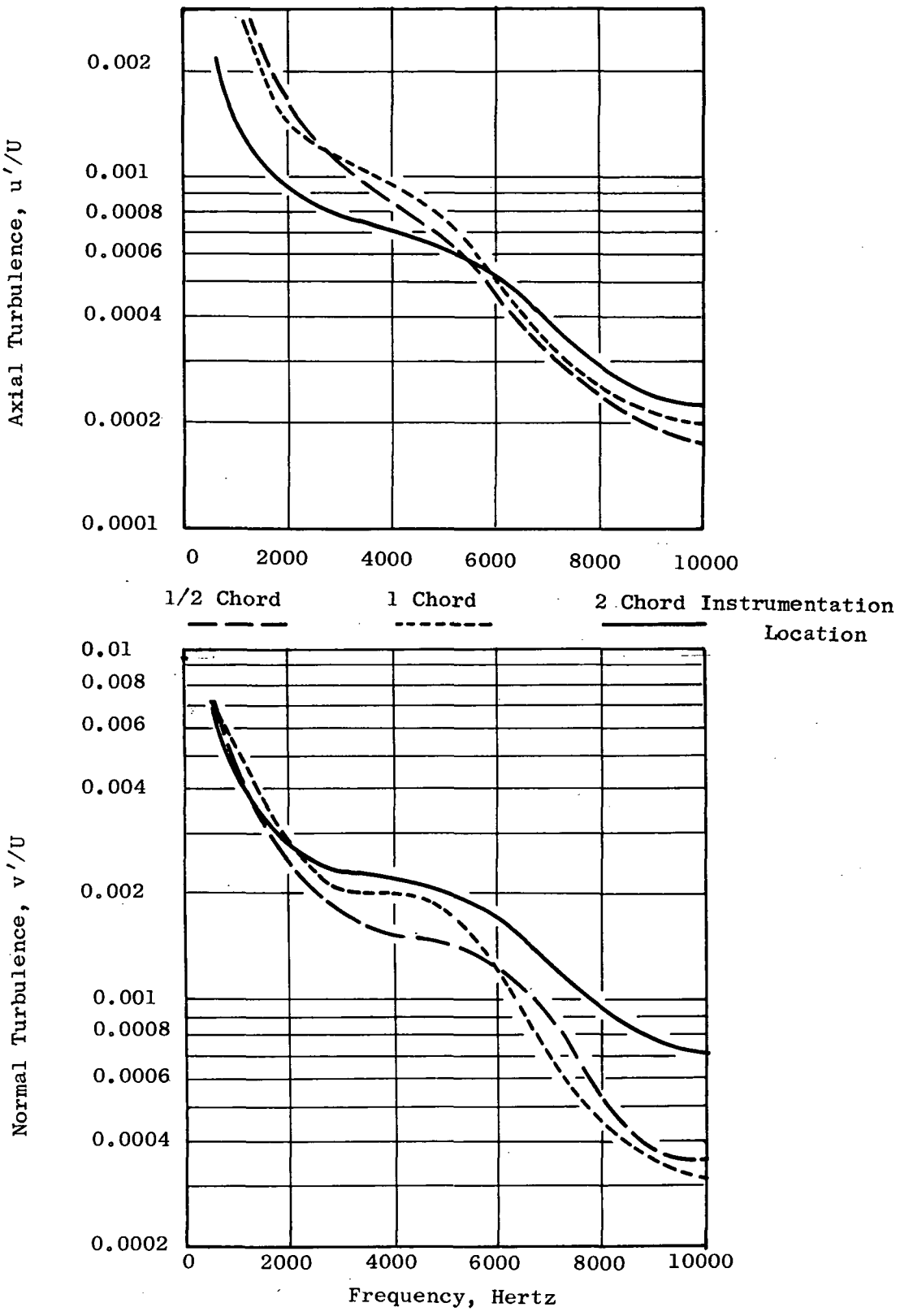


Figure 29. Effects of Measurement Location on Free-stream Turbulence Spectrums, Configuration SR6, Mach = 0.85, $\beta_1$ = 57 Degrees.

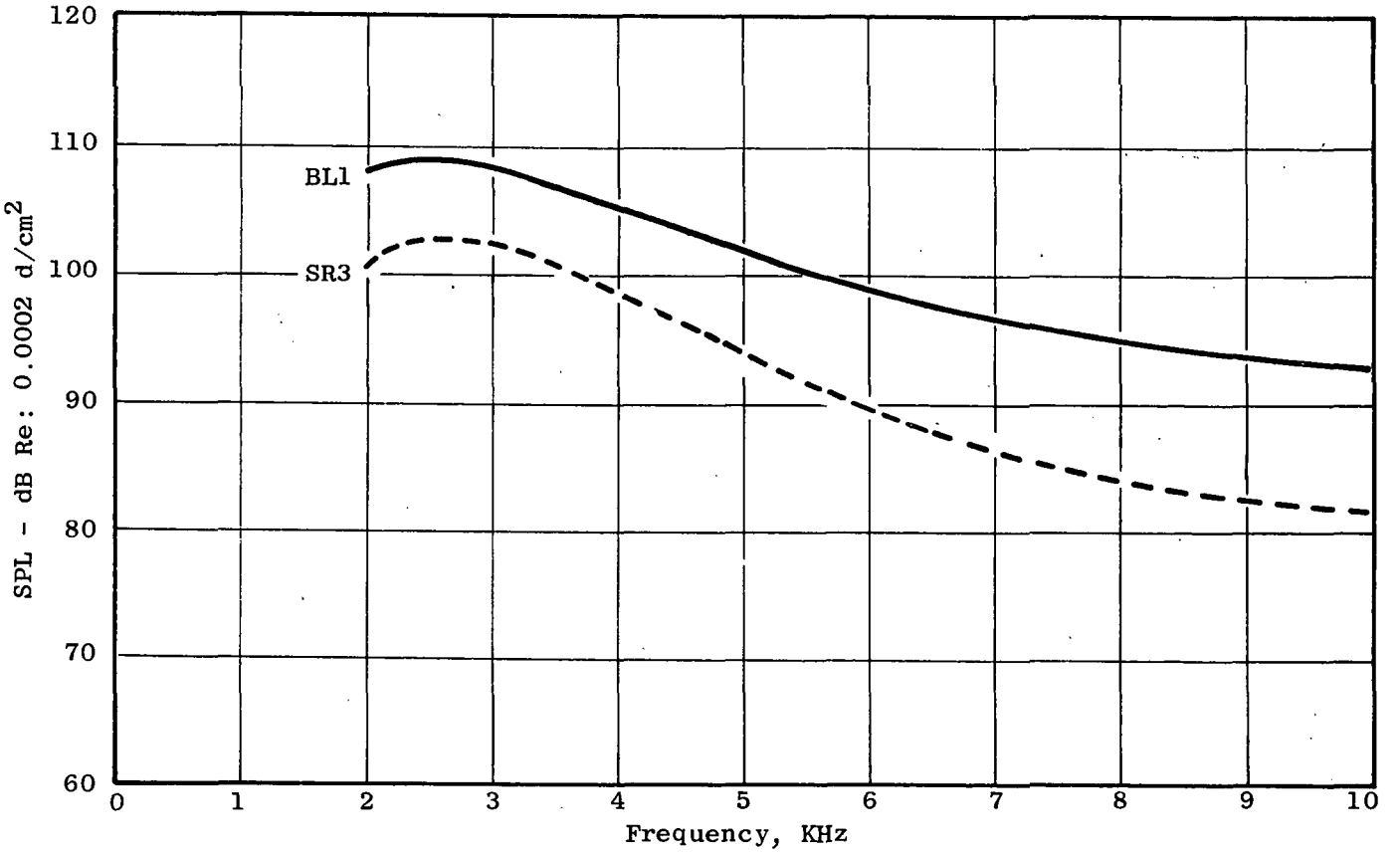


Figure 30. Noise Comparison of BL1 and SR3, Mach = 0.85, $\beta_1$ = 57 Degrees.

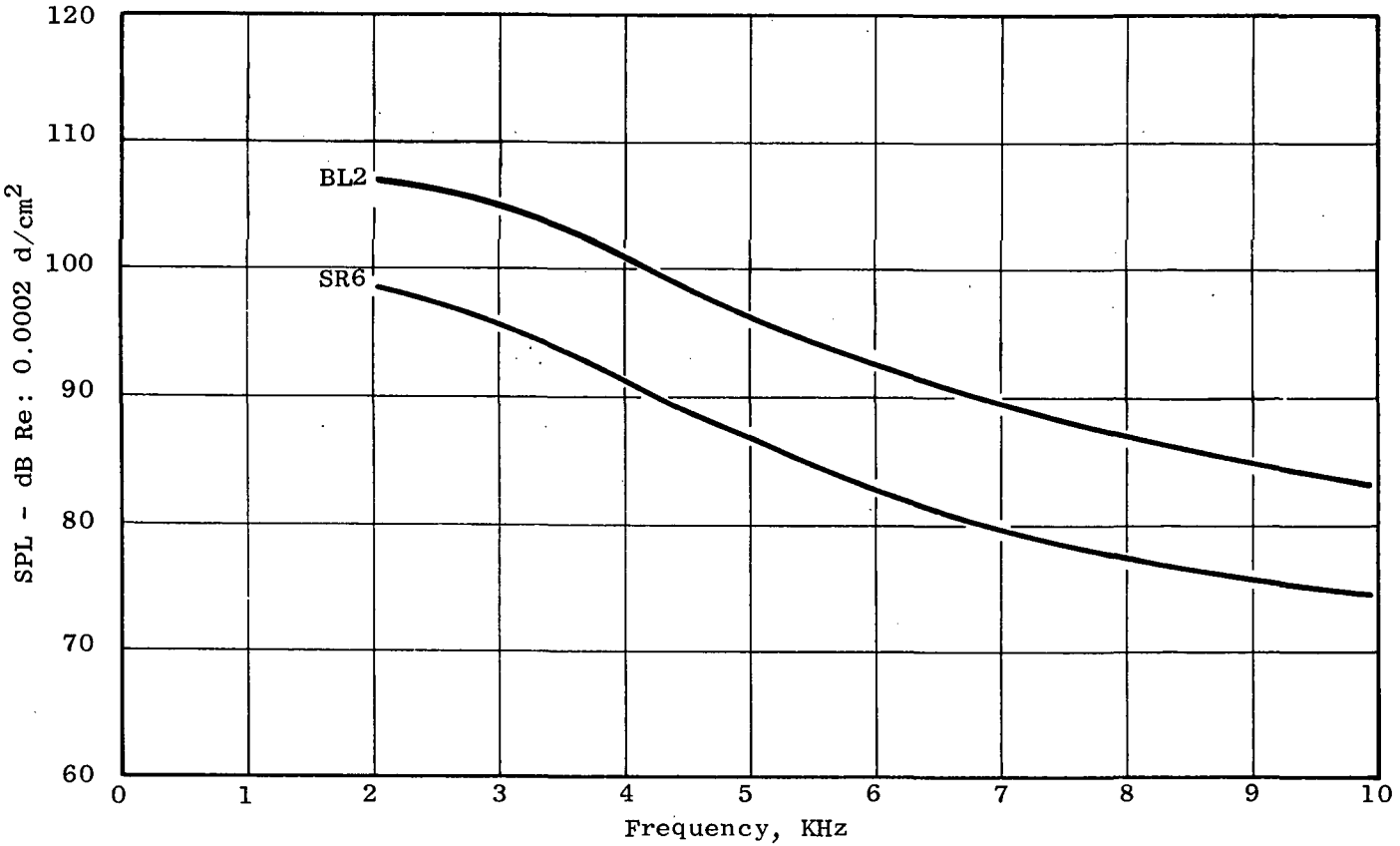


Figure 31. Noise Comparison of BL2 to SR6, Mach = 0.85, $\beta_1$ = 57 Degrees.

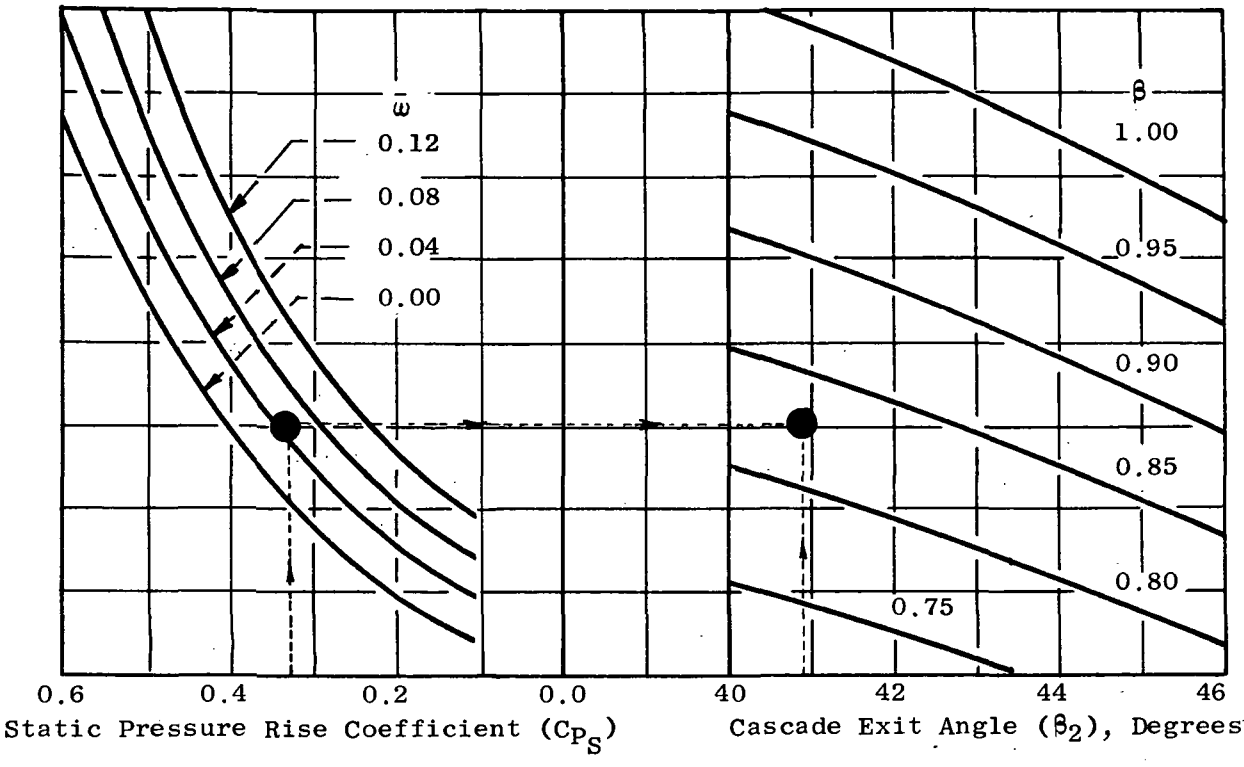


Figure 32. Nomograph of Static Pressure Coefficient at Mach = 0.85, $\beta_1$ = 57 Degrees.

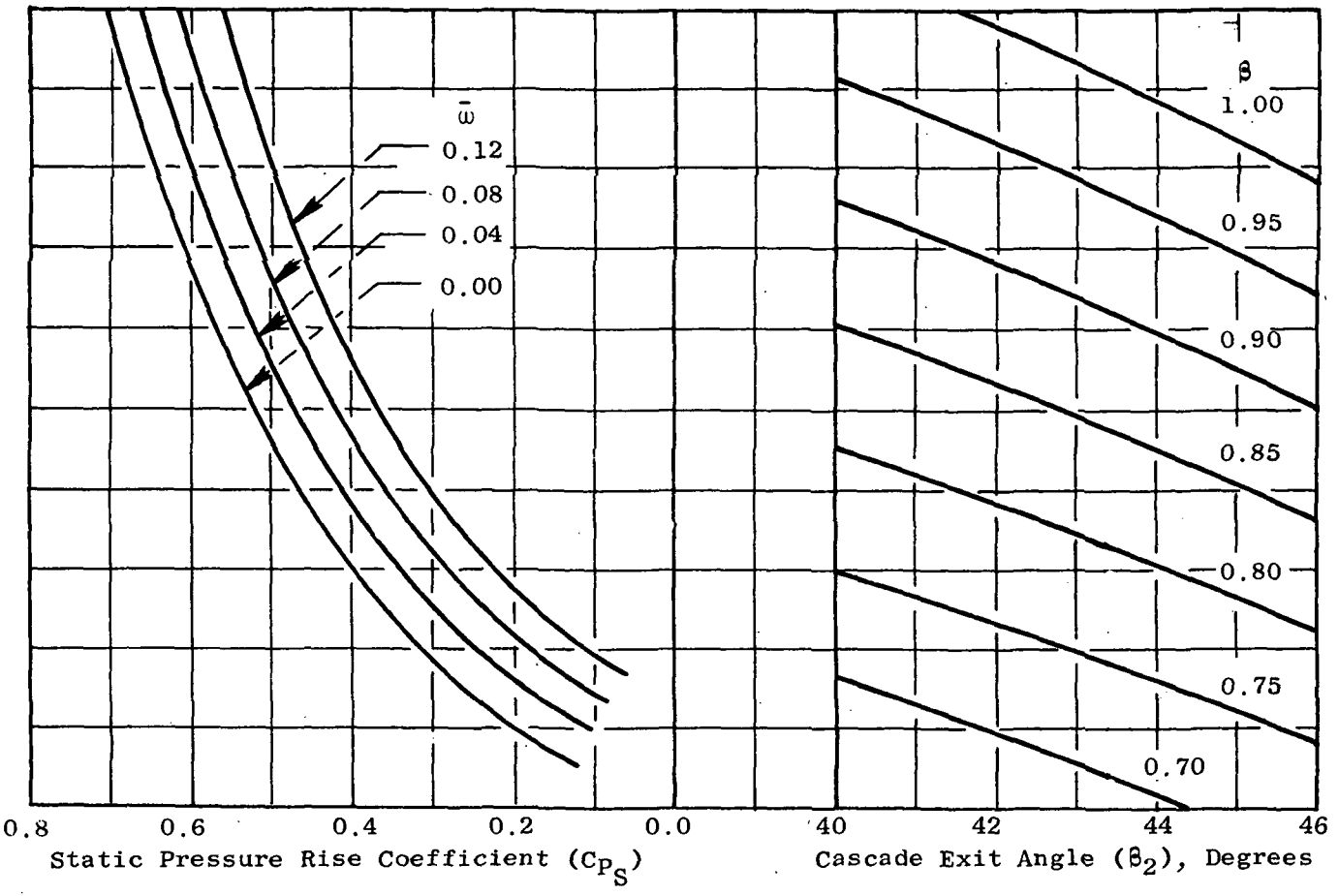


Figure 33. Nomograph of Static Pressure Coefficient at Mach = 0.85, $\beta_1$ = 60 Degrees.

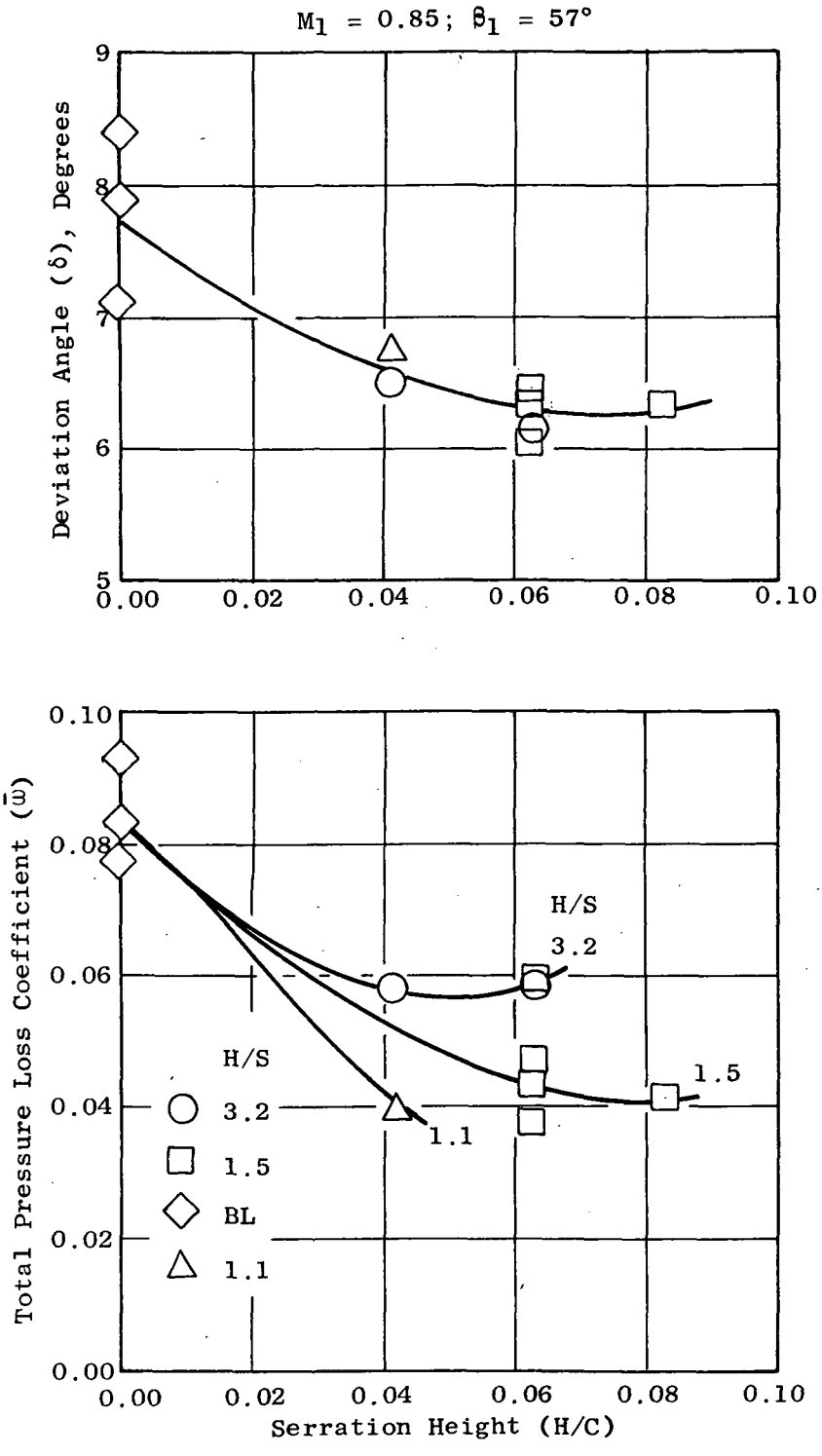


Figure 34. Effects of Serration Geometry on Blade Aerodynamic Performance.

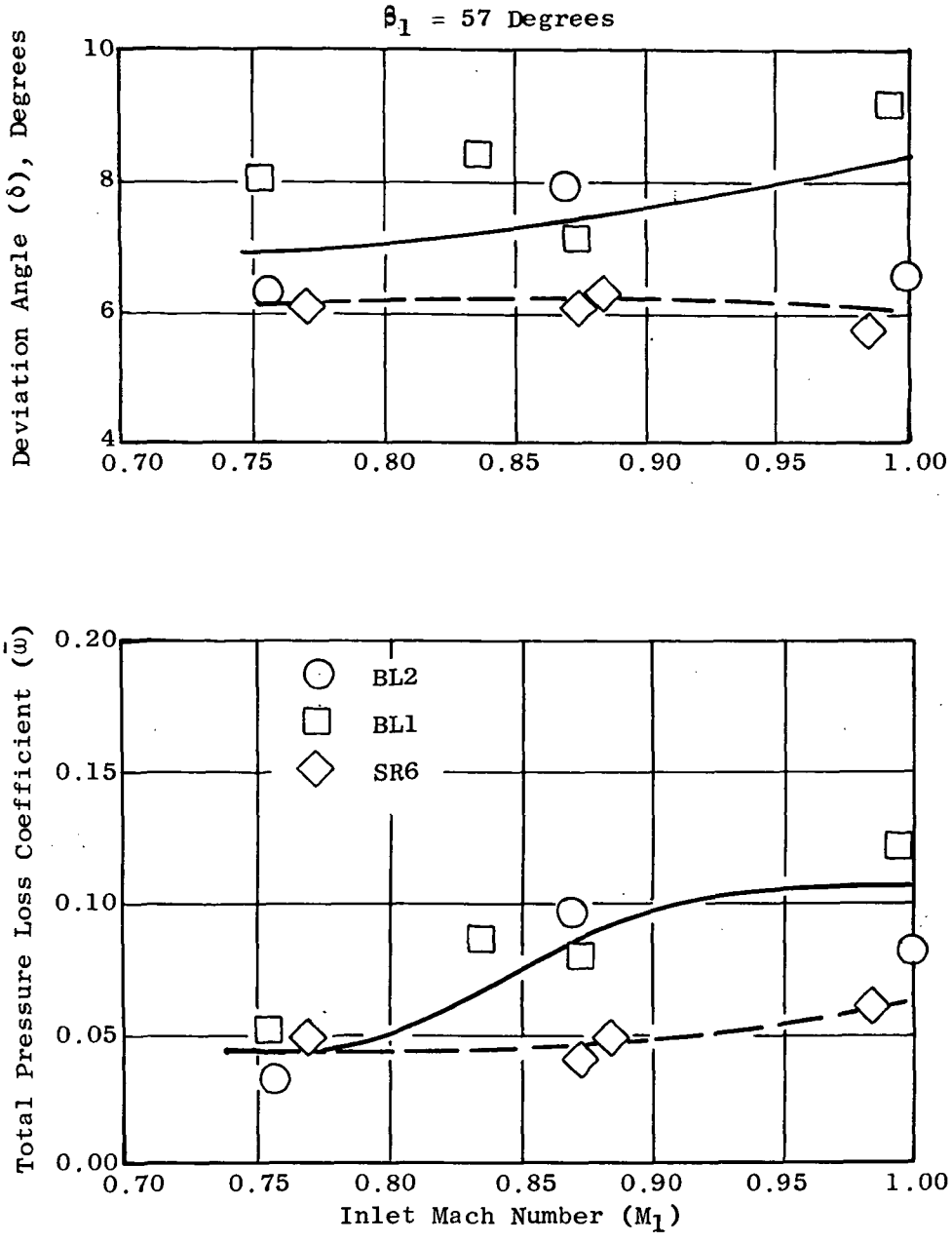


Figure 35. Effects of Serrations on Blade Aerodynamic Performance for a Range of Inlet Mach Numbers.

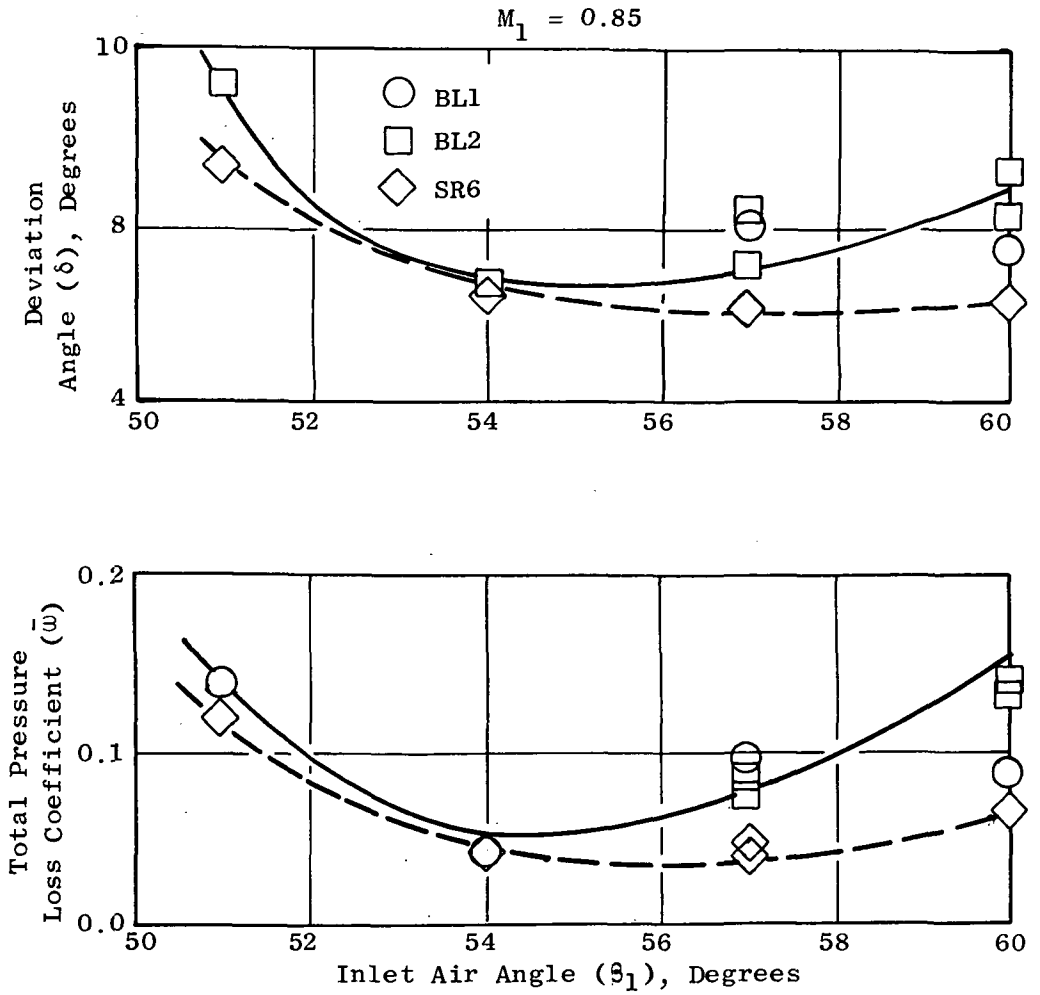


Figure 36. Effects of Serrations on Blade Aerodynamic Performance for a Range of Inlet Air Angles.

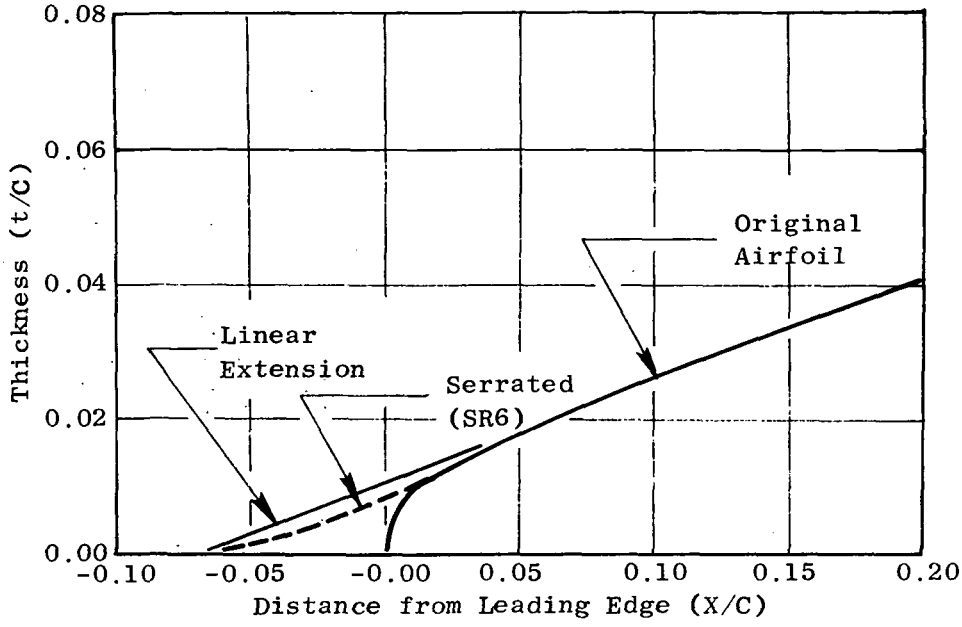


Figure 37. Airfoil Leading Edge Thickness Distriubtions, Showing Effects of Serrated Leading Edge.

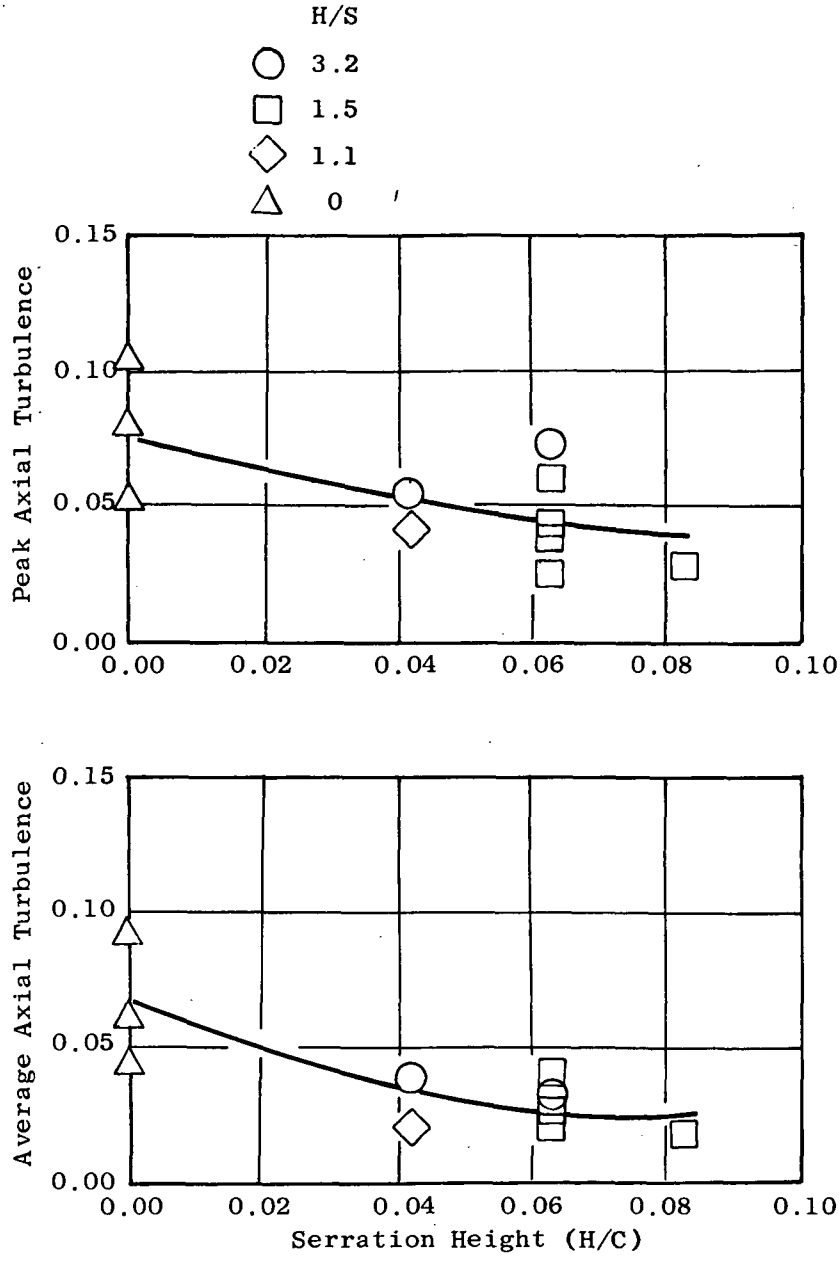


Figure 38. Effects of Serration Geometry on Exit Axial Turbulence Levels, Mach = 0.85, $\beta_1$ = 57 Degrees.

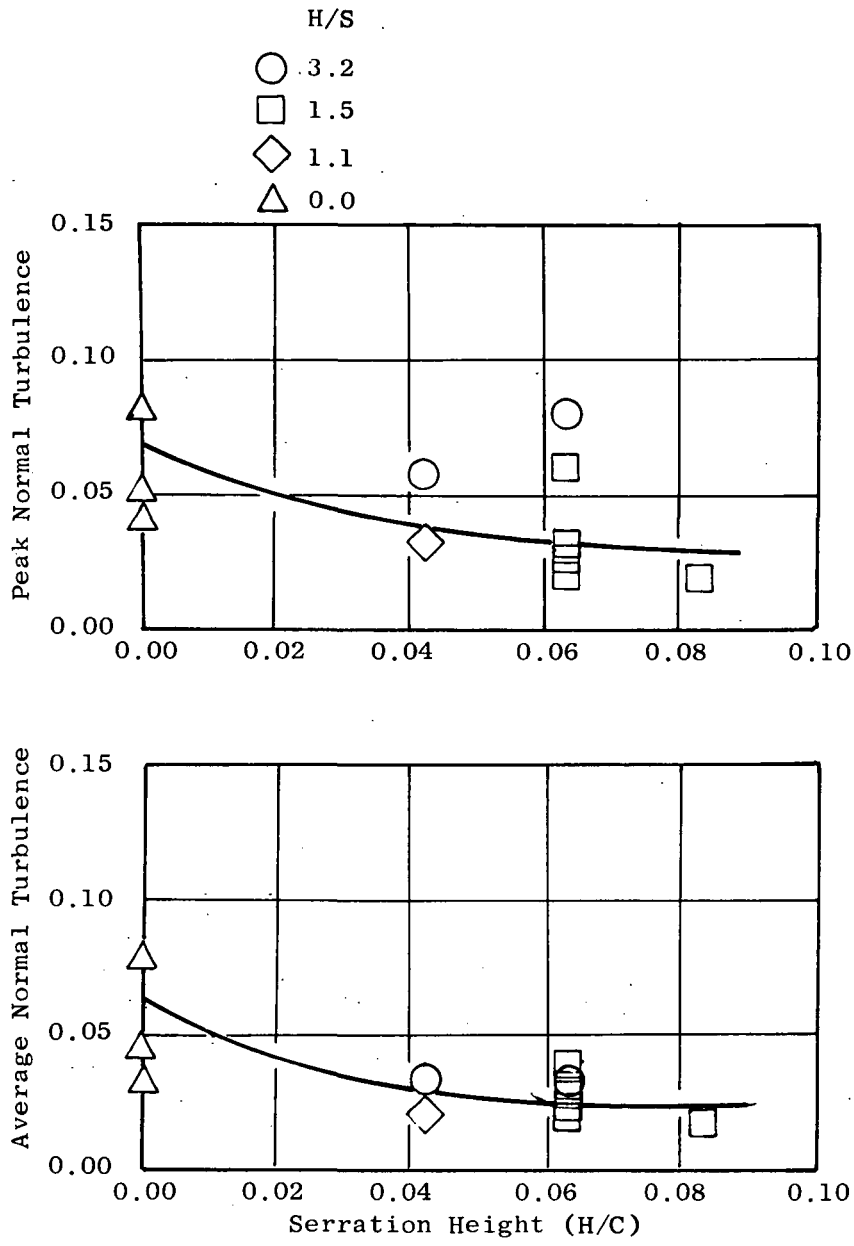


Figure 39. Effects of Serration Geometry on Exit Normal Turbulence Levels, Mach = 0.85, $\beta_1$ = 57 Degrees.

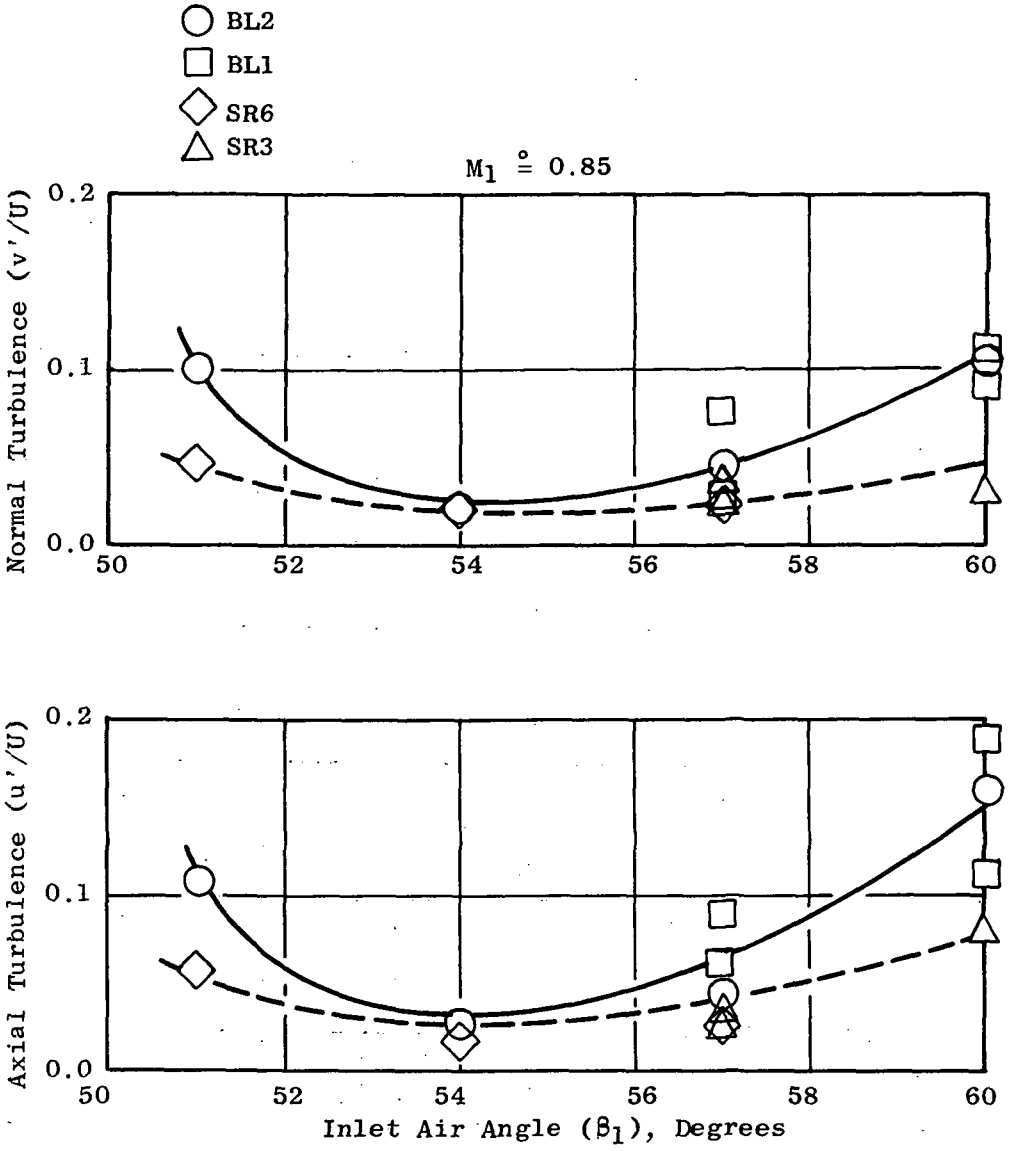


Figure 40. Effects of Serrations on Blade Average Turbulence Levels for a Range of Inlet Air Angles.

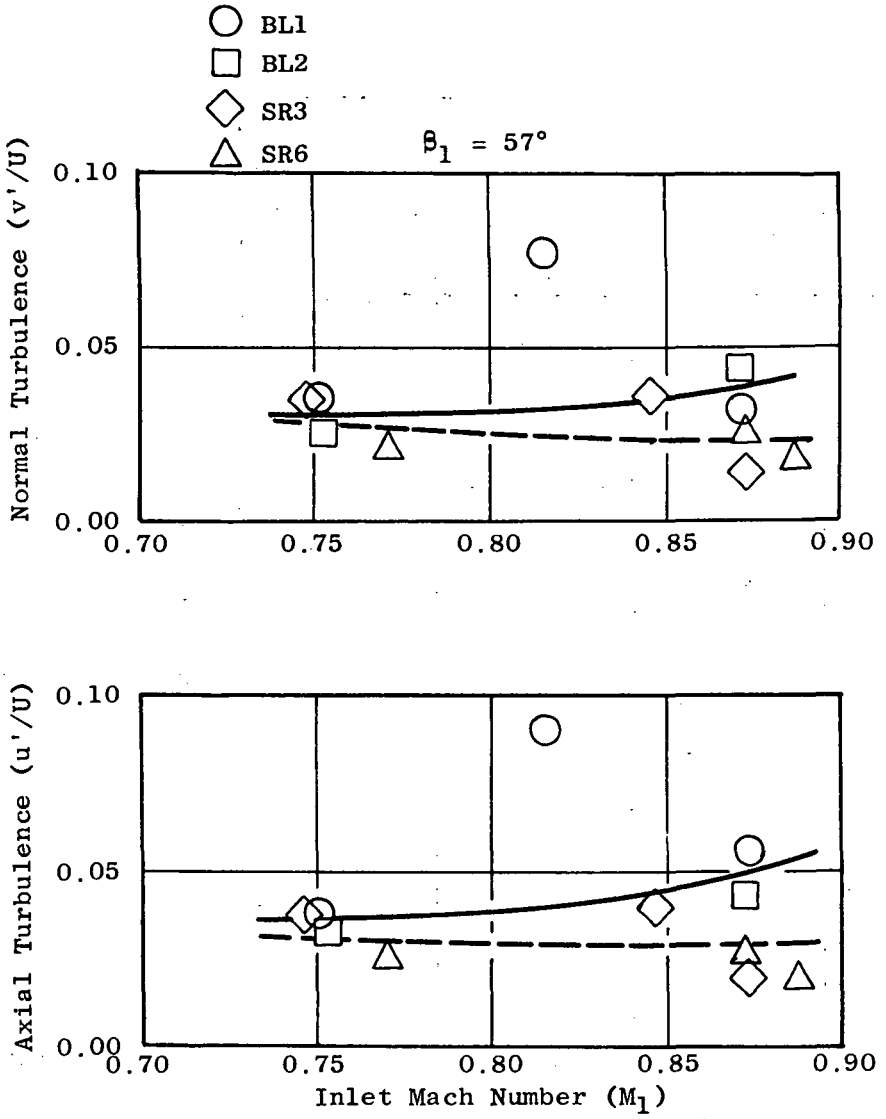


Figure 41. Effects of Serrations on Blade Average Turbulence Levels for a Range of Inlet Mach Numbers.

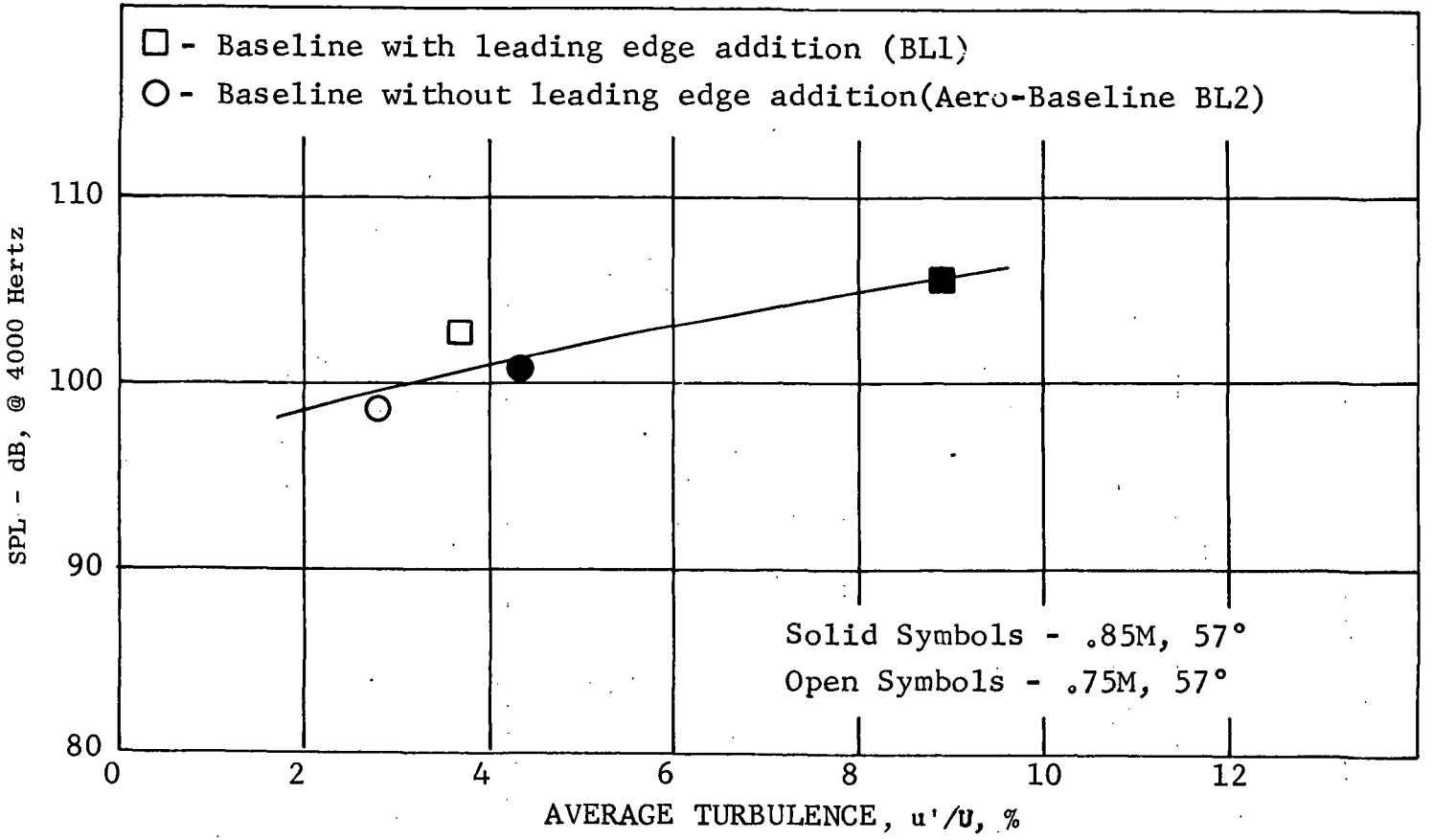


Figure 42. Unserrated Blade Noise Levels at 4000 Hertz.

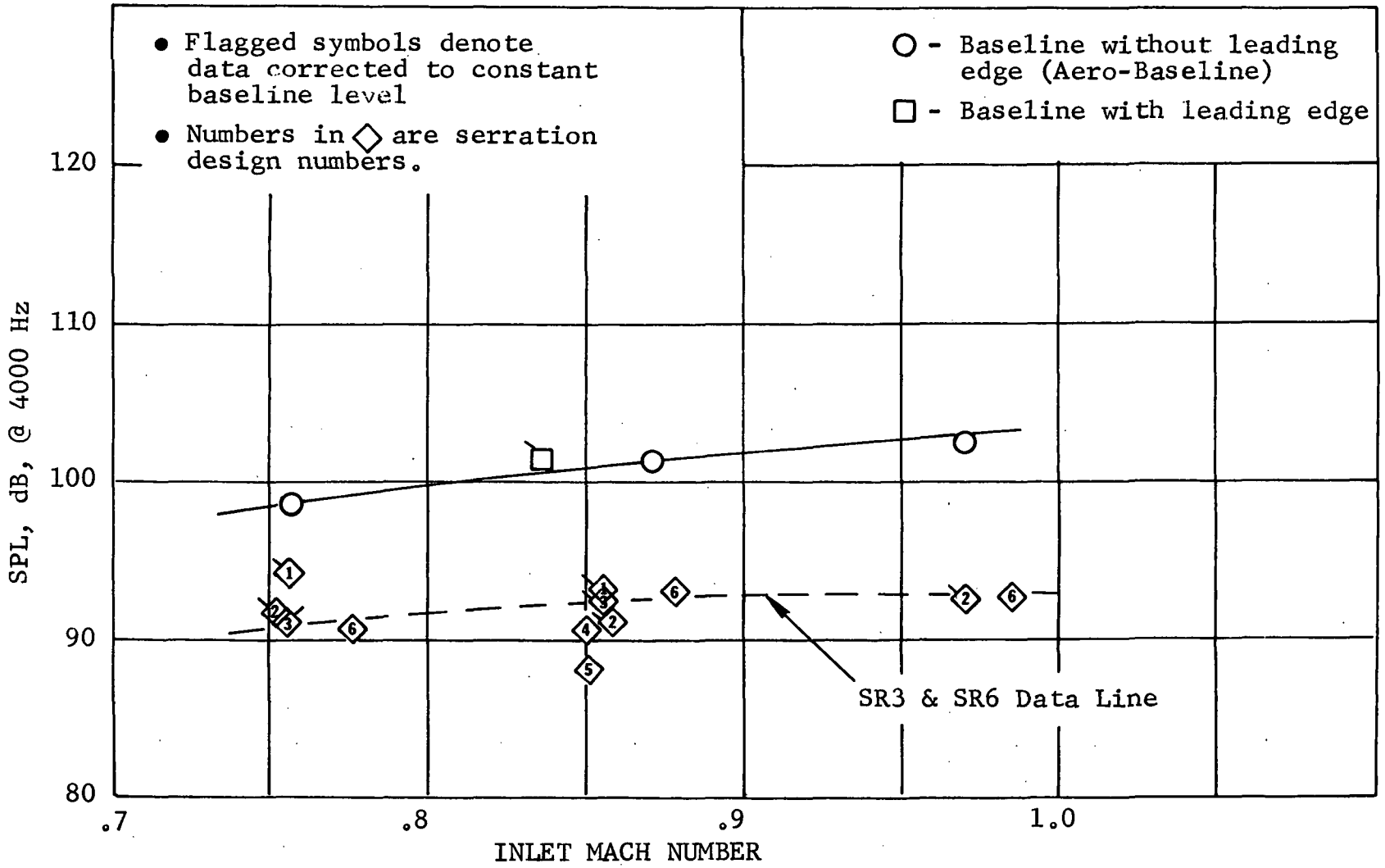


Figure 43. Unserrated and Serrated Blades Measured Noise at 4000 Hertz, $\beta_1$ = 57 Degrees.

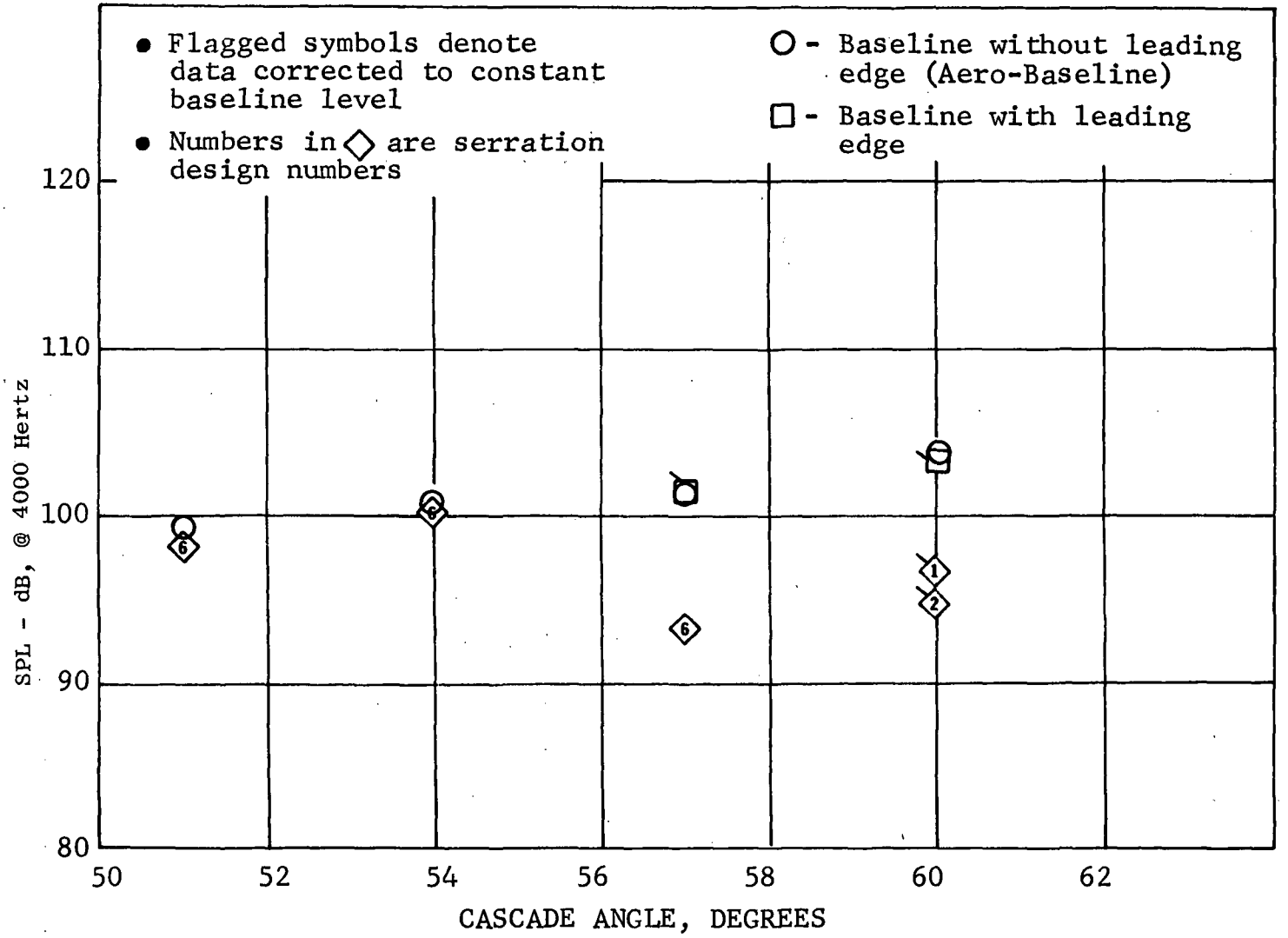


Figure 44. Effect of Cascade Angle on Noise.

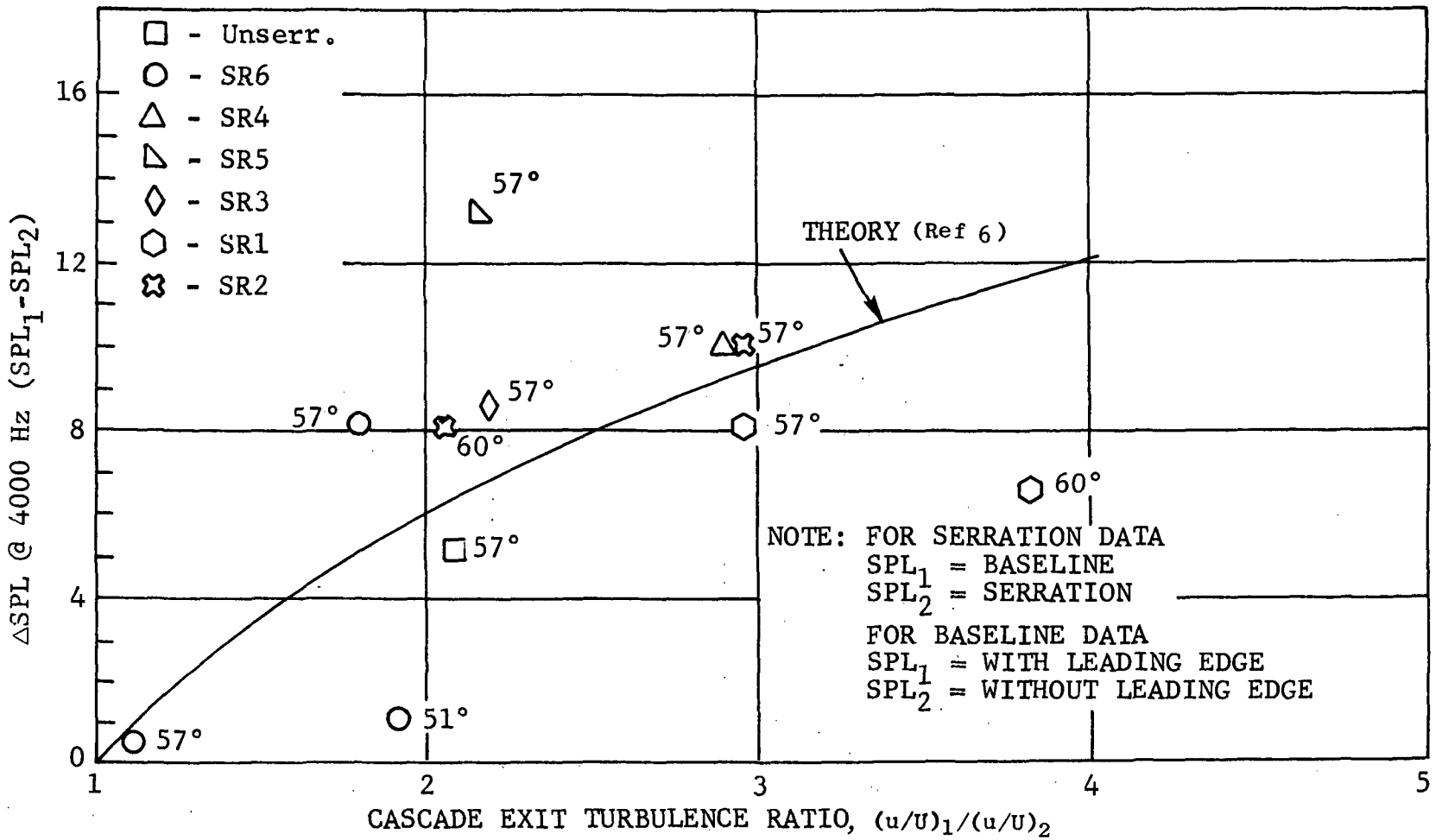


Figure 45. Comparison of Measured Noise Reduction and Theoretical Prediction, Mach = 0.85.

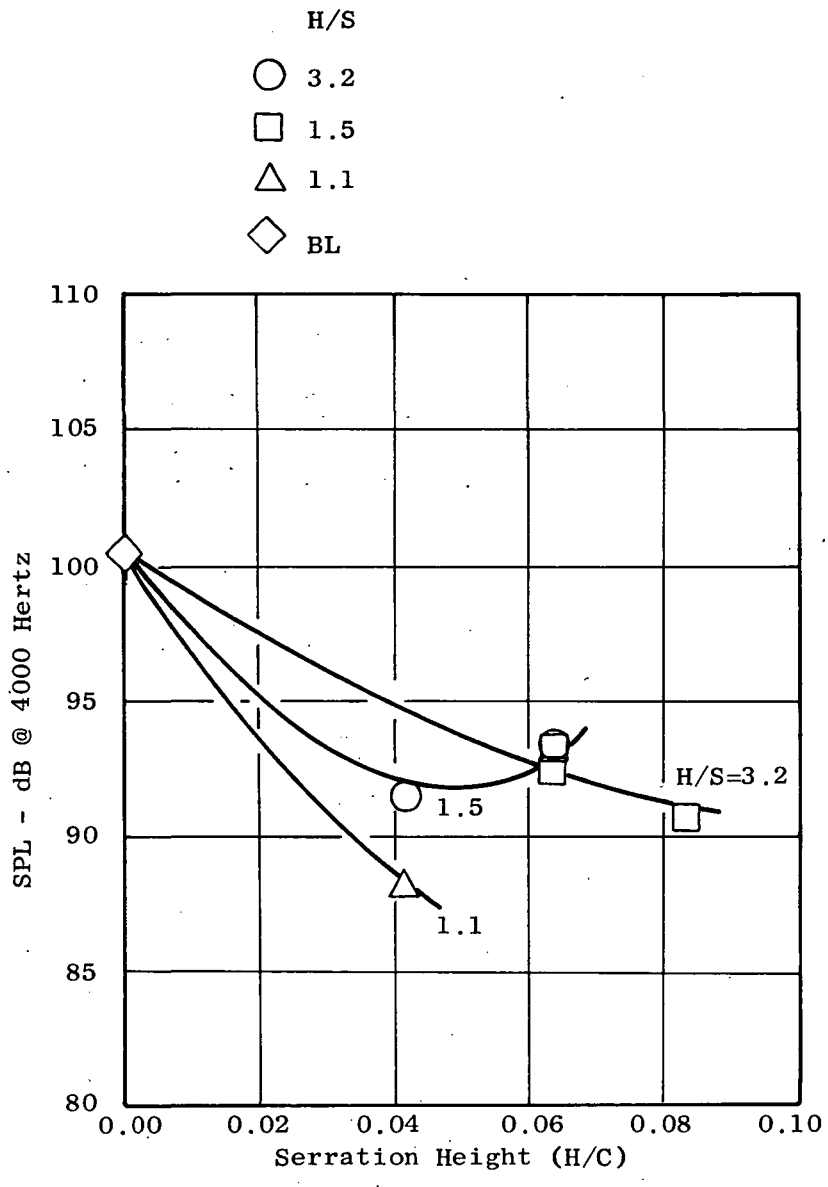


Figure 46. Effects of Serration Geometry on Acoustic Performance.

*"The aeronautical and space activities of the United States shall be conducted so as to contribute . . . to the expansion of human knowledge of phenomena in the atmosphere and space. The Administration shall provide for the widest practicable and appropriate dissemination of information concerning its activities and the results thereof."*

—NATIONAL AERONAUTICS AND SPACE ACT OF 1958

# NASA SCIENTIFIC AND TECHNICAL PUBLICATIONS

TECHNICAL REPORTS: Scientific and technical information considered important, complete, and a lasting contribution to existing knowledge.

TECHNICAL NOTES: Information less broad in scope but nevertheless of importance as a contribution to existing knowledge.

TECHNICAL MEMORANDUMS: Information receiving limited distribution because of preliminary data, security classification, or other reasons. Also includes conference proceedings with either limited or unlimited distribution.

CONTRACTOR REPORTS: Scientific and technical information generated under a NASA contract or grant and considered an important contribution to existing knowledge.

TECHNICAL TRANSLATIONS: Information published in a foreign language considered to merit NASA distribution in English.

SPECIAL PUBLICATIONS: Information derived from or of value to NASA activities. Publications include final reports of major projects, monographs, data compilations, handbooks, sourcebooks, and special bibliographies.

TECHNOLOGY UTILIZATION PUBLICATIONS: Information on technology used by NASA that may be of particular interest in commercial and other non-aerospace applications. Publications include Tech Briefs, Technology Utilization Reports and Technology Surveys.

***Details on the availability of these publications may be obtained from:***

**SCIENTIFIC AND TECHNICAL INFORMATION OFFICE**

**NATIONAL AERONAUTICS AND SPACE ADMINISTRATION**

**Washington, D.C. 20546**